

**Examination of the biocompatibility and anti-microbial
activity of coated dental implants**

By

RADWAN SALEM SADIQ ABDULGADER

A thesis submitted in partial fulfilment of the requirements for the degree of
Magister Scientiae in the Department of Medical Bioscience, University of the
Western Cape.



November, 2016

Supervisor

Professor Thomas K Monsees

Co-Supervisor

Professor Charlene WJ Africa

KEY WORDS

Osseointegration

Biocompatibility

Dental implant coatings

Ti₆Al₄V alloy

Cell morphology

Antimicrobial activity

Cell density

Fluorescence microscopy

Osteosarcoma (SaOS-2) cells

Cell viability



ABSTRACT

Teeth are important to all people for chewing, speech and aesthetics. Tooth decay, periodontal disease and physical trauma or injuries are the main causes of tooth loss. There are different forms of treatment for tooth loss such as dental bridges, removable dentures and dental implants. Dental implants are considered to be better than the other options. They have artificial tooth roots that are placed in the locations of missing teeth. After surgery, osteoblasts attach to the implant and build new bone around the implant in a process known as osseointegration. Titanium alloys (especially Ti₆Al₄V) are the most widely used biomedical materials in dental and orthopaedic implants due to their excellent biocompatibility, good mechanical properties and corrosion resistance. Although Ti₆Al₄V alloy is a favourable material, dental implants can fail (i.e. loosen and eventually fall out). Reasons of dental implant failure are microbial infections, poor surgical execution and biomechanical overloading on the implant surface. Thus, the aim of this study was to evaluate whether specific novel implant coatings could improve the biocompatibility and anti-microbial activity of the standard Ti₆Al₄V alloy. To that end, the cell adhesion, viability and morphology of SaOS-2 (osteoblast-like) cells were investigated after culturing them on samples of Ti₆Al₄V coated with hydroxyapatite, magnesium oxide and either titanium dioxide or silicon carbide. Morphology of cells was visualized using phalloidin-TRITC (for actin fibres) and DAPI (for the nuclei), whereas viability was determined using propidium iodide (dead cells) and calcein-AM (live cells) and all were viewed using fluorescence microscopy. The disc diffusion (Kirby-Bauer) assay was used to determine potential antimicrobial activities of the novel implant coatings against *Candida albicans*, *Streptococcus sanguinis*, *Staphylococcus aureus* and *Escherichia coli*.

Results from this study showed that all novel coatings are biocompatible as they allow the attachment and growth of SaOS-2 cells. However, there were clear differences between the individual coatings. Titanium dioxide-doped surfaces (Sample 3: hydroxyapatite 50W, titanium dioxide 25W, magnesium oxide 25W

coating; and Sample 4: hydroxyapatite 50W, titanium dioxide 25W, magnesium oxide 50W coating) seem to accelerate initial cell adhesion and are thus more favourable than the standard alloy. In contrast, addition of silicon carbide (as in Sample 1: hydroxyapatite 50W, silicon carbide 15W, magnesium oxide 50W coating; and Sample 2: hydroxyapatite 50W, silicon carbide 15W, magnesium oxide 25W coating) had a detrimental effect on biocompatibility.

More specifically, bone cells grown on hydroxyapatite (HAP) 50W, silicon carbide (SiC) 15W, magnesium oxide (MgO) 50W sample did not have proper morphology, whereas cells on hydroxyapatite 50W, silicon carbide 15W, magnesium oxide 25W sample were similar in morphology to cells seeded on the standard alloy, Ti₆Al₄V. Moreover, HAP 50W, SiC 15W, MgO 50W coating and HAP 50W, SiC 15W, MgO 25W coating reduced the cell viability and density compared to the uncoated Ti₆Al₄V. Furthermore, HAP 50W, SiC 15W, MgO 25W coating produced improved cell viability and density compared to HAP 50W, SiC 15W, MgO 50W coating. In this context it seems that the higher the magnesium oxide concentration of the coatings, the worse is its biocompatibility. Cell morphology, viability and density on hydroxyapatite 50W, silicon carbide 15W, magnesium oxide 50W sample were worse compared to the cells cultured on hydroxyapatite 50W, titanium dioxide (TiO₂) 25W, magnesium oxide 50W sample. In addition, hydroxyapatite 50W, silicon carbide 15W, magnesium oxide 25W sample gave poorer results for the cell density, cell viability and cell morphology compared to hydroxyapatite 50W, titanium dioxide 25W, magnesium oxide 25W sample. Consequently, the silicon carbide in the coatings appears to have a negative effect on biocompatibility when compared to the standard alloy. On the other hand, SaOS-2 cells on both hydroxyapatite 50W, titanium dioxide 25W, magnesium oxide 25W sample and hydroxyapatite 50W, titanium dioxide 25W, magnesium oxide 50W sample showed similar morphology, viability and 72 hour cell density to the Ti₆Al₄V alloy. However, after 24 hours the cell densities on HAP 50W, TiO₂ 25W, MgO 25W sample and HAP 50W, TiO₂ 25W, MgO 50W coating were significantly higher than the cell density on Ti₆Al₄V. This indicates faster initial cell attachment on HAP 50W, TiO₂ 25W, MgO 25W

coating and HAP 50W, TiO₂ 25W, MgO 50W coating and might be due to a higher degree of extracellular matrix secretion than by cells grown on Ti₆Al₄V.

Disc diffusion assays demonstrated that none of the microorganisms used showed susceptibility to any of the novel implant coatings tested. Therefore, none of the novel implant coatings showed any proven antimicrobial activity.



DECLARATION

I declare that *Examination of the biocompatibility and anti-microbial activity of coated dental implants* is my own work, that it has not been submitted for any degree or examination in any other university, and that all the sources I have used or quoted have been indicated and acknowledged by complete references.

Radwan Salem Sadiq Abdulgader

Signed:.....

Date: November 2016



PUBLICATIONS

A part of the thesis was submitted for publication:

- Vladescu A, Cotrut CM, Azem FA, Pana I, Braic V, Birlik I, Kiss A, Braic M, Abdulgader R, Booysen R, Monsees TK (2017). Si and Mg doped hydroxyapatite synthesis by magnetron sputtering method for biomedical applications. *Annals of Biomedical Engineering* (Submitted).

A part of the thesis was also presented as posters at the Annual Physiology Society of Southern Africa Conference, 2016:

- Abdulgader R, Booysen R, Vladescu A, Monsees TK (2016). Addition of TiO₂ and MgO improves biocompatibility of hydroxyapatite-coated dental implants. Physiology Society of Southern Africa, 28 August 2016, Cape Town.
- Booysen R, Abdulgader R, Vladescu A, Monsees TK (2016). Adhesion and viability of human osteosarcoma cells on SiC and MgO sputtered hydroxyapatite-coated dental implants. Physiology Society of Southern Africa, 28 August 2016, Cape Town.

DEDICATION

I dedicate this thesis to both my loving mother as well as my wife; for their efforts towards my education, for their unceasing prayers and continuous encouragement. Thank you for giving me the opportunity to prove myself and explore my capabilities.



ACKNOWLEDGEMENTS

Thank you my God for seeing me through the completion of this work and without you nothing is possible.

First and foremost, I would like to thank my supervisor, Prof. Thomas K. Monsees, all my appreciation and admiration that cannot be expressed in mere words for everything that you have done for me academically and personally.

Special thanks to my Co- supervisor, Prof. Charlene Africa, for all her guidance, patience and for supporting me throughout this journey of preparing my thesis.

I would like to express my deepest gratitude to my friend, Mr. Robin Booysen for his excellent guidance, caring and encouragement during my thesis.

I would also like to thank the following persons for their help during the course of this study: Dr. Salem Shalaweh, Dr. Mustafa Drah, Dr. Pedro Abrantes, Mr. Ernest Maboza and Ms. Vanessa Jooste.

Thanks also to my colleagues at the Dental Technology Department of Tripoli University, namely Dr. Dafer Sheibani, Dr. Salah Shcorvo, Dr. Juma Bin Sulaiman and Dr. Fateh Enbia.

More thanks to the rest of the Department of Medical Bioscience, University of the Western Cape, for helping me.

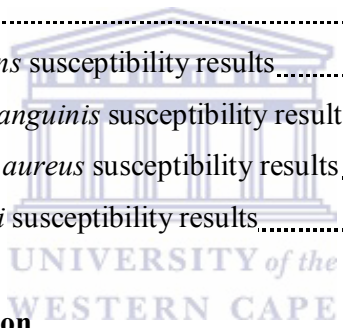
Lastly, warm heartfelt thanks to my mother, my wife, my sons (Mohamed and Ahmed), the rest of my family and my friends.

TABLE OF CONTENTS

	Page
Title page.....	i
Key Words.....	ii
Abstract.....	iii
Declaration.....	vi
Publication.....	vii
Dedication.....	viii
Acknowledgements.....	ix
Table of contents.....	x
List of Tables.....	xiii
List of Figures.....	xiv
List of abbreviation.....	xvi
CHAPTER 1: Introduction.....	1
1.1 Oral cavity.....	1
1.2 Teeth.....	1
1.3 Tooth loss causes.....	2
1.3.1 Tooth decay.....	3
1.3.2 Periodontal disease.....	3
1.3.3 Physical trauma or injury.....	4
1.4 Disadvantages of tooth loss.....	4
1.4.1 Effects on the jaw bone.....	4
1.4.2 Effects on other teeth.....	4
1.5 Treatment for tooth loss.....	5
1.5.1 Dental bridges.....	5
1.5.2 Removable dentures.....	6
1.5.3 Dental implants.....	7
1.6 Dental implantology.....	9
1.6.1 History of dental implant.....	10
1.6.2 Implant materials.....	12

1.6.2.1 Titanium-based alloy.....	12
1.6.2.2 Ceramics.....	15
1.6.2.3 Polymers.....	15
1.6.2.4 Coatings.....	16
1.6.3 Main procedural steps of dental implantation.....	17
1.6.3.1 Stage I Operation (fixture installation and osseointegration).....	17
1.6.3.2 Stage II Operation (abutment connection).....	18
1.6.3.3 Stage III (final prosthesis).....	18
1.7 Potential reasons for dental implant failure.....	19
1.8 Interaction between implant and body.....	19
1.8.1 Osseointegration (Adhesion).....	19
1.8.2 Host response to implants.....	21
1.8.3 Microbial etiology of implant failure.....	24
1.9 Biocompatibility.....	27
1.10 Aims and objectives of this study.....	27
CHAPTER 2: Materials and Methods.....	29
2.1 Stock solutions and buffers.....	29
2.2 Sterilisation of Ti ₆ Al ₄ V samples.....	31
2.3 Sterilisation of cover glass slips coated with PLL.....	31
2.4 Cell culture.....	32
2.4.1 Cell seeding and growth.....	32
2.4.2 Subculturing of cells.....	33
2.4.3 Cell counting.....	33
2.4.4 Freezing cells.....	34
2.5 Osteoblast-based assays.....	34
2.5.1 Fluorescence labeling of actin and nuclei.....	34
2.5.2 Cell Viability assays.....	36
2.6 Microorganism strains and culture conditions.....	37
2.6.1 Preparation of agar plates.....	38
2.6.1.1 Columbia blood agar base.....	38
2.6.1.2 Yeast nitrogen base agar supplemented with glucose.....	38

2.6.2 Gram staining and microscopy.....	39
2.7 Antimicrobial susceptibility testing.....	40
2.7.1 Preparation of microorganism suspensions.....	40
2.7.2 Disc diffusion assay (Kirby-Bauer assay).....	40
2.8 Statistical Analysis.....	41
CHAPTER 3: Results.....	42
3.1 Osteoblast-based assays.....	42
3.1.1 Cell morphology assessment.....	42
3.1.1.1 Cell morphology on PLL-coated glass.....	43
3.1.1.2 Cell attachment on coated Ti ₆ Al ₄ V discs.....	46
3.1.2 Cell viability assay on coated Ti ₆ Al ₄ V discs.....	52
3.2 Microbiology tests.....	65
3.2.1 <i>Candida albicans</i> susceptibility results.....	66
3.2.2 <i>Streptococcus sanguinis</i> susceptibility results.....	68
3.2.3 <i>Staphylococcus aureus</i> susceptibility results.....	70
3.2.4 <i>Escherichia coli</i> susceptibility results.....	72
CHAPTER 4: Discussion.....	75
4.1 Osteoblast-based assays.....	75
4.2 Antimicrobial susceptibility testing.....	81
CHAPTER 5: Conclusion.....	85
CHAPTER 6: References.....	87



LIST OF TABLES

1.1 Mechanical properties of titanium alloys.....	14
2.1 Preparation of stock solutions and buffers.....	29
3.1 Table showing the cell densities calculated from the phalloidin-TRITC and DAPI photomicrographs.....	52
3.2 Table showing the percentage of live and dead cells on the implant samples and controls after 24 hours of cell culture.....	64
3.3 Table showing the percentage of live and dead cells on the implant samples and controls after 72 hours of cell culture.....	64
3.4 Inhibition zone diameters of sample discs against <i>C. albicans</i> , <i>S. sanguinis</i> , <i>S. aureus</i> and <i>E. coli</i>	74



LIST OF FIGURES

1.1 Anatomical structure of a tooth.....	2
1.2 Tooth tilting that was caused by tooth loss.....	5
1.3 The installation of a dental bridge.....	6
1.4 Removable dentures: A) partial denture, B) complete denture.....	7
1.5 The dental implant compared to a natural tooth.....	8
1.6 Dental implants for (A) single and (B) multiple tooth replacement.....	10
1.7 Titanium alloy (Ti ₆ Al ₄ V).....	13
1.8 Overview of dental implantology.....	18
1.9 Illustration of focal contacts in osteoblasts.....	21
3.1 Fluorescence photomicrographs showing the cell morphology of SaOS-2 cells attached to glass discs at various times.....	46
3.2 Fluorescence photomicrographs showing the cell morphology of SaOS-2 cells grown on the implant samples for 24 hours.....	49
3.3 Fluorescence photomicrographs showing the cell morphology of SaOS-2 cells grown on the implant samples for 72 hours.....	51
3.4 Fluorescence photomicrographs of the live/dead cell results of cells cultured on the implant samples or the controls for 24 hours.....	56
3.5 Graph showing the percentage of live or dead SaOS-2 cells 24h after seeding on the implant samples.....	57
3.6 Graph showing the relative live cell density of cells cultured on the implant samples or the controls for 24 hours.....	58
3.7 Fluorescence photomicrographs of the live/dead cell results of cells cultured on the implant samples or the controls for 72 hours.....	61
3.8 Graph showing the percentage of live or dead SaOS-2 cells 72h after seeding on the implant samples.....	62
3.9 Graph showing the relative live cell density of cells cultured on the implant samples or the controls for 72 hours.....	63

3.10 Gram staining photos.....	65
3.11 Photographs of Petri dishes, showing inhibition of <i>Candida albicans</i> growth on YNBG medium in the presence of samples and a control.....	67
3.12 Photographs of Petri dishes, showing inhibition of <i>Streptococcus sanguinis</i> growth on CAB medium in the presence of samples and a control.....	69
3.13 Photographs of Petri dishes, showing inhibition of <i>Staphylococcus aureus</i> growth on CAB medium in the presence of samples and a control.....	71
3.14 Photographs of Petri dishes, showing inhibition of <i>Escherichia coli</i> growth on CAB medium in the presence of samples and a control.....	73



LIST OF ABBREVIATIONS

Al	Aluminium
Al₂O₃	Aluminum Oxide
ATCC	American Type Cell Culture
BSA	Bovine Serum Albumin
C	Negative Control
<i>C. albicans</i>	<i>Candida albicans</i>
Ca₃(PO₄)₂	Tricalcium Phosphate
CAB	Columbia Agar Base
CaCl₂	Calcium Chloride
Calcein-AM	Calcein Acetoxymethyl Ester
CO₂	Carbon Dioxide
CXM	Cefuroxime
DAPI	4',-6-diamidino-2-phenylindole dihydrochloride
DMSO	Dimethylsulphoxide
<i>E. coli</i>	<i>Escherichia coli</i>
ECM	Extracellular Matrix
EDTA	Ethylene Diamine Tetra Acetic acid
FBS	Fetal Bovine Serum
FCA	Fluconazole
HAP	Hydroxyapatite
HSCs	Hematopoietic Stem Cells
KCl	Potassium Chloride
M	Molar
McF	McFarland Standard
Mg	Magnesium
MgCl₂	Magnesium Chloride
MgO	Magnesium Oxide
mM	Millimolar
MSCs	Mesenchymal Stem Cells
NaCl	Sodium Chloride

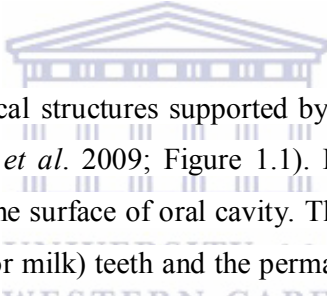
PBS	Phosphate Buffered Saline
PC	Positive Control
PI	Propidium Iodide
RGD	Arginylglycylaspartic acid group
RO	Reverse Osmosis
RT	Room Temperature
<i>S. aureus</i>	<i>Staphylococcus aureus</i>
<i>S. sanguinis</i>	<i>Streptococcus sanguinis</i>
SaOS-2	Osteosarcoma Cells
Si	Silicon
Si₃N₄	Silicon Nitride
SiC	Silicon Carbide
SiO₂	Silicon Dioxide
SN	Sensititre Nephelometer
Ti	Titanium
TiO₂	Titanium Dioxide
TRITC	Tetramethylrhodamine isothiocyanate
TritonX-100	4-(1,1,3,3-Tetramethylbutyl) phenyl-polyethylene glycol, t-Octylphenoxypolyethoxyethanol, Polyethylene glycoltert-octylphenyl ether
UV	Ultraviolet
V	Vanadium
v/v	Volume to volume
YNBG	Yeast nitrogen base agar

CHAPTER 1: Introduction

1.1 Oral cavity

The oral cavity consists of the mouth, tongue, teeth, gingiva (gums), palate, the palatine tonsils, and the ducts of the salivary glands; which work together to aid in digestion and ingestion (Gray *et al.* 2005; Carey *et al.* 2009). Furthermore, the oral cavity has a very unique environment which microorganisms (including pathogens) have easy access to (Dale and Fredericks, 2005), and acts as a portal of entry for microbes to the rest of the body via the epithelium of the gastrointestinal tract (Dale and Fredericks, 2005). There are more than 500 species of bacteria in the human oral cavity that interact with oral tissues (Bik *et al.* 2010; Ali and Tanwir, 2012). All oral microorganisms also have systems for combating competing microorganisms and potential pathogens (Marcotte and Lavoie, 1998).

1.2 Teeth



The teeth are hard conical structures supported by the alveolar bone of the upper and lower jaws (Carey *et al.* 2009; Figure 1.1). In addition, the teeth constitute approximately 20% of the surface of oral cavity. There are only two types of teeth, namely the deciduous (or milk) teeth and the permanent teeth. Milk teeth appear in the oral cavity between the ages of 6 months and 2.5 years (Gray *et al.* 2005; Carey *et al.* 2009; Nelson and Ash, 2010). There are 10 milk teeth in each jaw, which are the central incisor, lateral incisor, canine, first molar and second molar. The permanent teeth start to appear in the oral cavity at the age of 6 years, and they replace the deciduous teeth by approximately 12 years. There are 16 permanent teeth in each jaw of adults, namely the central incisors, lateral incisors, canines, first molars, second molars, third molars, first premolars, second premolars (Gray *et al.* 2005; Carey *et al.* 2009; Nelson and Ash, 2010).

Generally, the primary role of teeth is mastication (to cut the food by the anterior teeth, or to grind the food by the posterior teeth) (Nelson and Ash, 2010). Furthermore, the teeth play roles in speech (phonetic of some letters), and improving the aesthetic appearance of the face (Nelson and Ash, 2010).

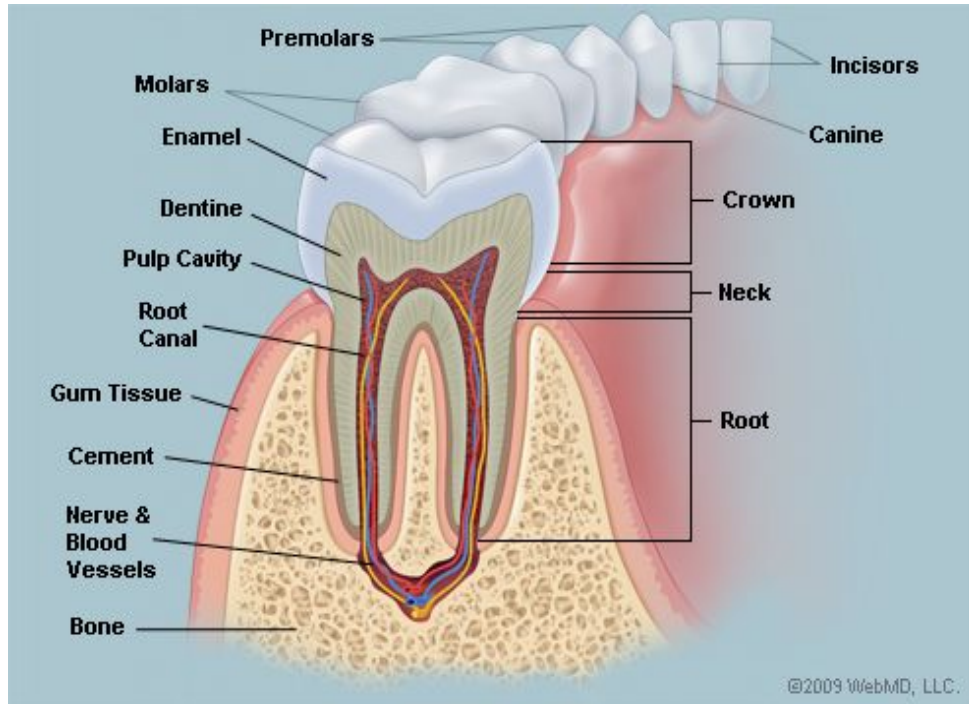


Figure 1.1: Anatomical structure of a tooth: the crown is the part of the tooth which is covered by enamel, and exposed to the mouth. The cervix (neck) is the junction between the crown and the root. The root is the part of the tooth which is covered by cementum; the tooth may have a single root or multiple roots. The apex of the root is the end of the terminal part of the root (www.webmd.com).

1.3 Tooth loss causes

There are several reasons for tooth loss such as tooth decay, periodontal disease, physical trauma or injury (Zha, 2011; Pektaş, 2012). Loss of natural dentition varies from patient to patient. Furthermore, complete loss of natural dentition is termed edentulism, while loss of some teeth is called partial edentulism (Pektaş, 2012).

1.3.1 Tooth decay

Tooth decay results from the growth and action of various endogenous bacteria on the tooth surface, as well as around the base of teeth. When one eats foods high in carbohydrates and sugars, plaque bacterial metabolism produces different organic acids (Pektaş, 2012; West and Joiner, 2014) which accumulate in the oral cavity and reduce the oral pH, causing demineralization of tooth enamel (Pektaş, 2012; West and Joiner, 2014). Consequently, the teeth become weakened and the enamel fractures, forming cavities which cause tooth loss (Pektaş, 2012; West and Joiner, 2014).

1.3.2 Periodontal disease

Periodontitis is considered to be one of the primary causes of tooth loss. It is an inflammatory reaction of the tissues surrounding the teeth and is very common in both civilized and primitive communities (Akcali *et al.* 2013). The gum inflammation leads to an erosion of the fibrous connective tissue of the gum causing gingivitis (Pihlstrom *et al.* 2005; Akcali *et al.* 2013). When the alveolar bone becomes involved and is destroyed, the gum recedes and the roots of the teeth become exposed, and subsequently fall out (Pihlstrom *et al.* 2005). This form of periodontal disease is referred to as periodontitis (Kim and Amar, 2006; Pektaş, 2012).

Many factors lead to tooth loss and gingival inflammation such as being older than 35 years, smoking, poor oral hygiene, psychological stress, hypertension, diabetes, bleeding of the gums, and natural bone loss (Pektaş, 2012; Akcali *et al.* 2013; Natto *et al.* 2014).

1.3.3 Physical trauma or injury

According to Glendor (2009), traumatic dental injuries are classified as intentional injuries, such as in fighting, and unintentional injuries, such as in traffic accidents.

1.4 Disadvantages of tooth loss

Tooth loss results in an empty space in the jaw. If left untreated, with time the gap in the mouth will cause various problems for the host.

1.4.1 Effects on the jaw bone

At the site of the missing tooth, there is no transfer of forces between the jaws (Bodic *et al.* 2005). Osteoblasts are responsible for the formation of new bone, whereas osteoclasts are responsible for the resorption of bone. Mechanical forces from chewing stimulate the bone cells (osteoblasts and osteoclasts) to maintain healthy jaw function (Bodic *et al.* 2005). Without the mechanical forces on the jaw, there will be resorption of the jaw bone, which is chronic and irreversible (Bodic *et al.* 2005). Therefore, once a tooth falls out, the main catalyst that triggers bone formation is absent (Pektaş, 2012). Hence, the loss of all teeth leads to complete bone loss and deformation of the jaw shape (Pektaş, 2012).

1.4.2 Effects on other teeth

When tooth loss occurs, two things happen: firstly, the alveolar bone in the socket of lost tooth becomes resorbed, and secondly the bone that surrounds the roots of the functional opponent tooth distorts (Craddock, 2010; Pektaş, 2012). According to Craddock (2010), the functional opponent tooth undergoes eruptive movements. Moreover, the teeth adjacent to the edentulous space will tip and drift towards the gap in the mouth (Craddock, 2010; Figure 1.2).

There are other consequences of tooth loss such as speech problems and problems with the aesthetics of the face (Pektaş, 2012). In addition, as more teeth are lost, chewing becomes more difficult which can potentially lead to malnutrition (Pektaş, 2012).

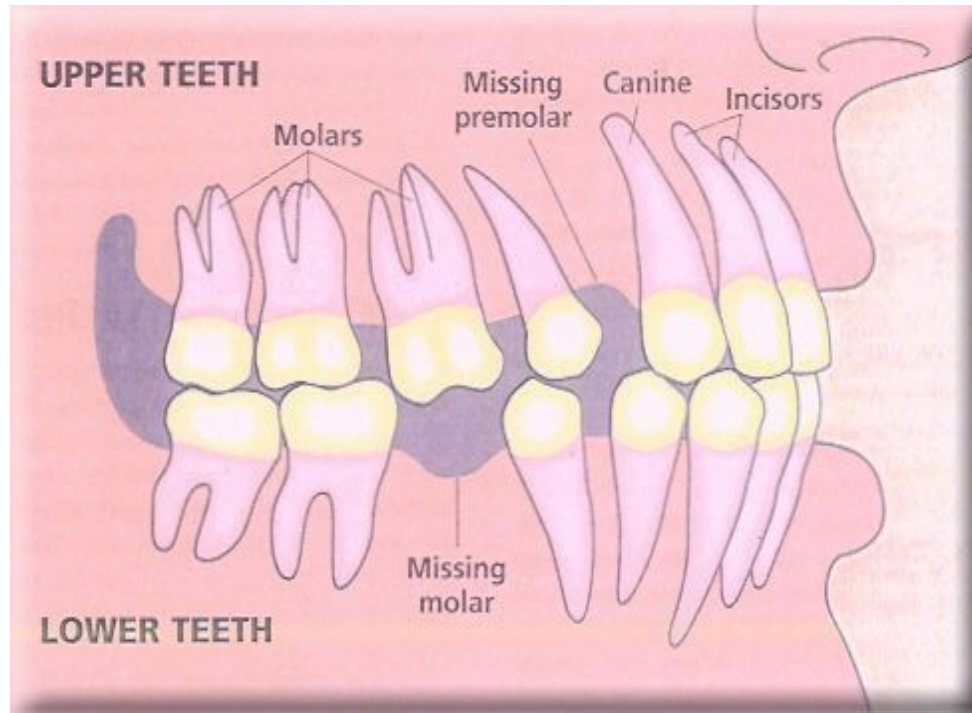


Figure 1.2: Tooth tilting that was caused by tooth loss (www.rydedentalcare.com.au).

1.5 Treatment for tooth loss

For the treatment of tooth loss there are a variety of modern techniques as discussed below.

1.5.1 Dental bridges

A dental bridge consists of artificial teeth that are fitted inside the gap (of the missing tooth) and crowns (of adjacent teeth). The bridge consists of three parts that are connected to each other; namely the anterior crown, the posterior crown and the pontic (see Figure 1.3). Thus, bridges are used to compensate for the loss of one or more teeth by joining an artificial tooth permanently to adjacent teeth or dental implants (Pektaş, 2012).

The advantages of the dental bridges include convenience, improved aesthetics of the face, ease of chewing, ease of speech, stabilizing the natural teeth, a cheaper price (compared to dental implant) and ease of installation. On the other hand, there

are many disadvantages of dental bridges. For example, bone resorption may occur because no force is transmitted through the pontic to the jaw bone (Pektaş, 2012).

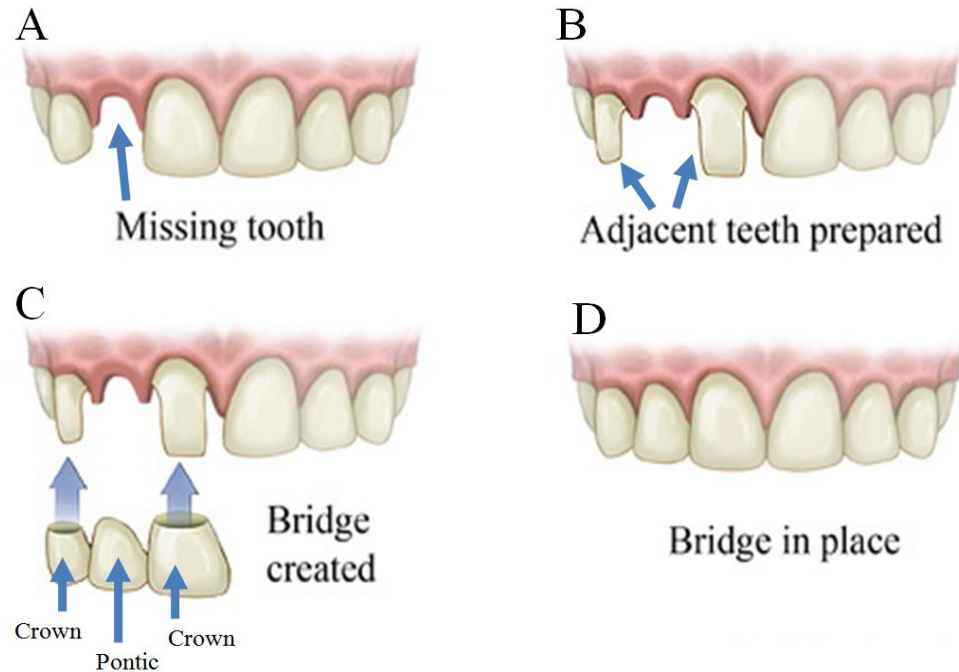


Figure 1.3: The installation of a dental bridge ([adapted from www.sweetwatersmile.com](http://www.sweetwatersmile.com)).

UNIVERSITY OF
WESTERN CAPE

1.5.2 Removable dentures

There are two types of removable dentures: removable partial and complete dentures. Partial dentures are synthetic teeth connected to a piece of plastic (acrylic) that resembles the gums (see Figure 1.4A) (Pektaş, 2012). The partial denture is held in place by metal wire structures that connects the denture to the remaining teeth in the mouth (Pektaş, 2012). Just like the bridge, partial dentures also compensate for tooth loss and stabilize the teeth adjacent to the gap in the mouth (Pektaş, 2012).

Complete dentures are used to treat edentulous patients. Complete dentures cover the whole upper or lower jaw (or both) (see Figure 1.4B). As with partial dentures, complete dentures have artificial teeth installed on a plastic base that resembles the gums (Pektaş, 2012). The advantages of removable dentures are that no surgery is required, they are aesthetically pleasing, and they are relatively cheap. However,

the denture may be uncomfortable at times, it makes the patient more susceptible to oral infections and it is not a permanent solution as it has to eventually be replaced.

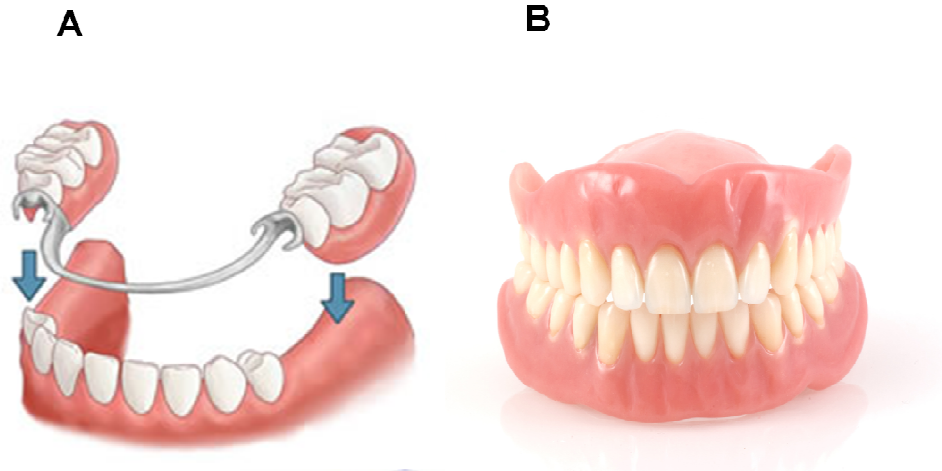


Figure 1.4: Removable dentures: A) partial denture, B) complete denture
(www.painlesspetdentist.com; www.studiodentisticobizioli.it).

1.5.3 Dental implants

Dental implants are synthetic tooth roots that are surgically placed in the locations of missing teeth (see Figure 1.5) (Duraccio *et al.* 2015; Zhang and Zheng, 2015). These roots are connected to an artificial tooth to restore the oral cavity's function of mastication, *inter alia*. Dental implants are a better treatment for tooth loss than dentures and dental bridges, because they are strong, resemble natural teeth and they are durable (Zhang and Zheng, 2015). Dental implantology has a high success rate, which is good for the patient (Al-Makki, 2006; Zhang and Zheng, 2015).

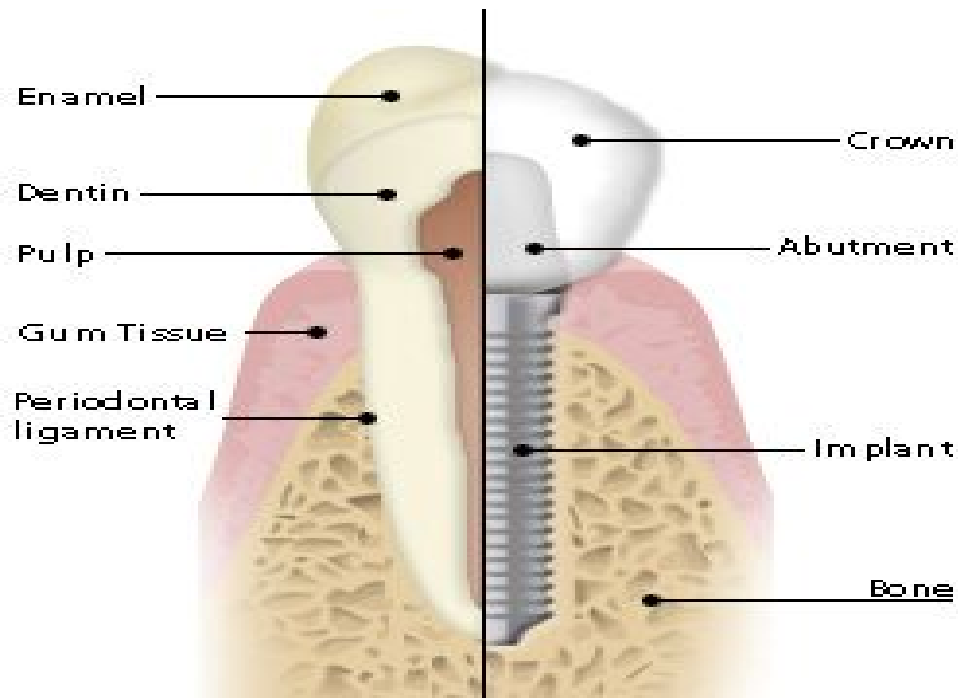


Figure 1.5: The dental implant compared to a natural tooth (www.gratefuldental.com).

A dental implant prosthesis consists of three parts; namely the implant, the abutment and the crown. The abutment (the upper part of the dental implant) adjoins the implant where it protrudes to the oral cavity, above the gum line (Pektaş, 2012; Monsees, 2016). The crown of the dental implant (false tooth) is fitted over the abutment (Pektaş, 2012).

The benefits that dental implants have over other treatments of tooth loss are considerable. Dental implants conserve the alveolar ridges, reduce fragile bone loss after extraction, they provide an improved appearance, convenience, easier eating, improved oral health, improved speech, and are more durable than the alternatives (Al-Makki, 2006; Pektaş, 2012). Additionally, dental implants are more comfortable than removable dentures (Elisa, 2011; Pektaş, 2012). Nonetheless, dental implants do have disadvantages; they permit the easy bacterial invasion of the gingival surface, which may lead to the dissolution of tooth bone. Due to the fact that dental implants provide an interface for the forces on the crown to be transmitted to the bone, they prevent the shrinkage of the alveolar bone, as in the natural tooth case. Thus, the necessary stimulation for bone regeneration not

existing in dental bridge applications is maintained which preserves the bone shape (Pektaş, 2012).

1.6 Dental implantology

Dental implantology is the process of replacing natural teeth roots by implanting synthetic roots of biomaterial into the upper or lower jaw bone. The artificial root remains as a protruding part of the transplant (outside the jaw bone through the gums), where it is used for the installation of false crowns or dentures.

Dental implants have the advantages of stimulating bone formation and the healing process, providing better stability between the bone and the implant surface (which was established by a greater contact area during the healing process) and providing a surface structure which maintains the blood clot (Karamian *et al.* 2014). The best option in dental implants is the use of titanium because this metal is acceptable by vital tissue. The bone cells grow completely around the titanium implant surface and make them able to withstand the functions of natural teeth effectively (Brånemark, 1983; Oshida *et al.* 2010). In addition, dental implants can be used to compensate for one tooth, several teeth or the full mouth (see Figure 1.6) (Kim *et al.* 2011; Duraccio *et al.* 2015).

Dental implants are considered superior to the older techniques such as partial or complete removable dentures and dental bridges (Pektaş, 2012; Misch, 2014).

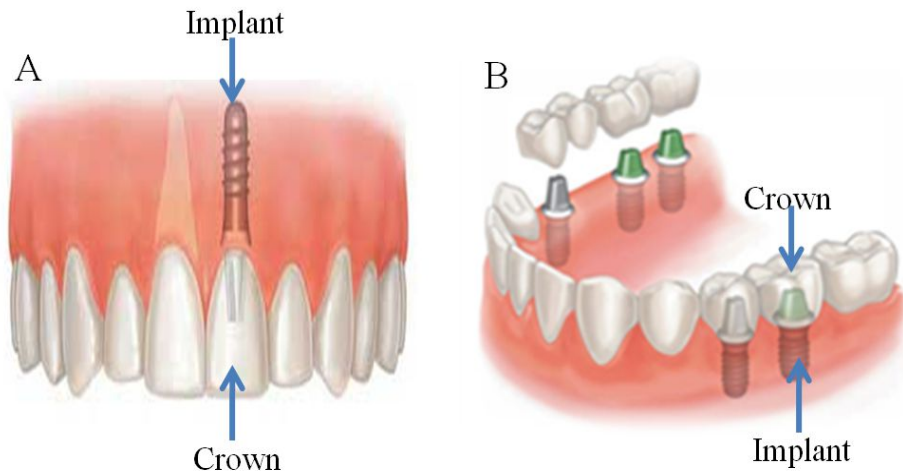


Figure 1.6: Dental implants for (A) single and (B) multiple tooth replacement
 (adapted from www.bournedentalpractice.co.uk; www.dentalimplantcostarica.com).

Dental implant failure rates between 6% and 11% have been reported (Kim *et al.* 2011). Failure of dental implant osseointegration is usually due to one of the following: poor bone quality, excessive loading (when one bites on the implant harder than the bone can withstand), implant fractures, insufficient initial stability and loosening or fracture of the screw (Han *et al.* 2002). Moreover, clinical success rate of the use of implants is most closely related to the bone formation on the endo-osseous implant surface, this process is known as osseointegration (Brånemark, 1983, Brånemark *et al.* 2001; Davies, 2003; Duraccio *et al.* 2015).

1.6.1 History of dental implant

The history of dental implant extends to the era of the pharaohs (since approximately 1700 BC), where they excelled at the transplantation of animal teeth or artificial teeth carved from ivory into the human jaw (Linkow, 2010; Pektaş, 2012). Continued attempts were made by many ancient civilizations (such as the Egyptians, Chinese, Greeks, Babylonians, Indians, Etruscans, Romans, Assyrians and Arabs) to use transplantation procedures and devices (Linkow, 2010; Pektaş, 2012; Duraccio *et al.* 2015).

Archeologists, in 1931, found a woman's mandible of Mayan origin having teeth with pieces of sea shell placed in the location of missing teeth (Linkow, 2010, Pektaş, 2012).

In 1700s, people donated their teeth to replace the missing teeth of rich people in exchange for a fee. Nevertheless, immune system reactions prevented the adaptation of alien materials (Linkow, 2010, Pektaş, 2012).

In the 19th century, people assumed that precious materials would be well tolerated by biological tissues; and thus platinum, gold, silver and other metal alloys were used as implant materials. This led to extremely poor longevity of the implant, because these metals were toxic, showed poor mechanical properties, and were not biocompatible, etc (Linkow, 2010; Pektaş, 2012).

In 1913, Greenfield was considered the first to describe the process of dental implants in scientific references. In 1952, the modern breakthrough in terms of research and studies began at the hands of the Swedish Professor Per-Ingvar Brånemark. While studying bone healing and regeneration around a titanium chamber, he discovered that titanium metal reacts well with body tissues, as well as permitting bone formation around the metal implant surface (osseointegration) (Brånemark, 1983; Brånemark *et al.* 2001; Pektaş, 2012; Duraccio *et al.* 2015). Since then, modern techniques emerged for dental implants, all of which contributed to confirming the biocompatible properties of titanium. Recently, after success from laboratory and clinical studies, dental implants can be considered the ideal replacement for missing teeth (Elisa, 2011; Pektaş, 2012).

In 1965, the first titanium dental implant was intentionally fitted into a human volunteer. Later, in 1967, Leonard Linkow introduced a titanium blade-form implant which provided some mechanical stability, and was compatible with both complete and partial dentures (Linkow, 2010; Pektaş, 2012).

During the 1970s, researchers conducted many experiments to find the best geometric designs for titanium dental implants. Some of the implant designs include the titanium plasma sprayed implants (implants that were coated with titanium at high temperatures and were quickly set) and *intra mobil zylinder* implants (a special shock-absorbing implant that stimulates the periodontal ligament) (Pektaş, 2012; Abraham, 2014). Also in the 1970s, Bränemark established the hollow titanium screw implants which proved to be better than earlier implant designs (Pektaş, 2012).

1.6.2 Implant materials

Modern implant materials are chosen for their excellent characteristics such as good biocompatibility, corrosion resistance, non-carcinogenicity, strength, non-toxicity, mechanical properties, non-inflammatory, non-allergenicity, chemical stability, low elastic modulus, biofunctionality for its lifetime in the host body, etc. Currently, there are three types of dental implant materials that are used; namely, metal (mostly titanium based alloys), ceramics and polymers (Muddugangadhar *et al.* 2011; Patel and Gohil, 2012; Malhotra *et al.* 2014; Osman and Swain, 2015).

1.6.2.1 Titanium-based alloy

Titanium alloys are mixtures of titanium and other elements for example, the Ti_6Al_4V contains 4% vanadium and 6% aluminium (see Figure 1.7) (Elias *et al.* 2008; Özcan and Hämmerle, 2012; Felgueiras, 2014; Osman and Swain, 2015). Titanium does not cause negative reactions in the human body; it is not toxic and is suitable for osseointegration (Duraccio *et al.* 2015).

Newly developed pure titanium (Ti) and its alloys (especially Ti_6Al_4V) have become the most popular biomedical materials, as well as widely used in dental and orthopedic implants (Muddugangadhar *et al.* 2011; Özcan and Hämmerle, 2012; FadI-allah *et al.* 2013; Strnad and Chirila, 2015). In addition, Ti_6Al_4V receives most attention due to its high specific strength, low density, chemical stability, high tensile strength, good resistance to corrosion, excellent mechanical properties, low elastic modulus (approximately 100-110 GPa), hypoallergenicity and good

biocompatibility (non-toxic and not rejected by the human body) compared with other metallic biomaterials. (Soboyejo *et al.* 2002; Liu *et al.* 2004; Majumdar *et al.* 2008; Gallardo-Moreno *et al.* 2009).



Figure 1.7: Titanium alloy (Ti_6Al_4V) (www.vsmmpo-tirus.co.uk).

The mechanical properties of pure titanium and selected titanium alloys are displayed in Table 1

Table 1.1: Mechanical properties of titanium alloys (from Elias *et al.* 2008; Felgueiras, 2014; Duraccio *et al.* 2015; Osman and Swain, 2015).

Material (Alloy)	Modulus (Gpa)	Yield strength (σ_y)	Tensile strength (UTS) (Mpa)	Elongation (%)
Pure Ti - Grade 1	103	170	240	24
Pure Ti - Grade 2	103	275	345	20
Pure Ti - Grade 3	103	380	450	18
Pure Ti - Grade 4	104	485	550	15
Ti-6Al-4V ELI (Mill annealed)	101–110	795 – 875	860 – 965	10 –15
Ti-6Al-4V (Annealed)	110 – 114	825 – 869	895 – 930	6 –10
Ti-15Zr 4Nb-2Ta-0.2Pd	94 – 99	693 – 806	715 – 919	18 – 28
Ti-6Al-7Nb	114	880 – 950	900 – 1050	8 –15
Ti-5Al 2.5Fe	112	895	1020	15

Modulus: a measure of the stiffness of the metal. Yield strength: a measure of the ability of the metal to withstand repetitive loading (without permanently changing shape). Tensile strength: a measure of the metal’s ability to withstand an elongating force. Elongation: the percentage of change in the metal’s length before it fractures.

1.6.2.2 Ceramics

Ceramics are compounds of metallic and nonmetallic elements such as aluminum oxide (Al_2O_3), hydroxyapatite ($\text{Ca}_{10}(\text{PO}_4)_6(\text{OH})_2$), silicon dioxide (SiO_2), silicon carbide (SiC), silicon nitride (Si_3N_4), tricalcium phosphate ($\text{Ca}_3(\text{PO}_4)_2$), and are often used for manufacturing dental implants (Thamaraiselvi and Rajeswari, 2004; Eslami *et al.* 2010; Pektaş, 2012).

Ceramics often have desirable characteristics, such as hardness, improved biocompatibility, antibacterial activities, good physical properties, ease of application; they are chemically inert and are good insulators. Additionally, ceramics can withstand harsher conditions than metals and polymers, but they are very brittle (Malhotra *et al.* 2014).

Zirconium oxide is a modern material used for dental implants due to its good qualities, such as low plaque affinity, good mechanical properties, biocompatibility and aesthetic appearance (Özkurt and Kazazoğlu, 2011; Saini *et al.* 2015).

1.6.2.3 Polymers

Polymers such as polyamide, polyurethane and polyoxymethylene have been used as dental materials, for other implants, sealants, synthetic materials, tooth restoratives, encapsulants, extracorporeal devices, dressings and cements (Bang Lee *et al.* 2000; Pektaş, 2012). Polymers provide dental implants that can imitate the tiny elastic movements of natural teeth (Bang Lee *et al.* 2000; Pektaş, 2012). Furthermore, the studies on polymer use have evolved to investigating their elastic properties for use in implants (Pektaş, 2012).

Polymeric biomaterials have significant advantages when compared with metal or ceramic materials including ease of secondary processability, reasonable cost, ease of manipulation (to produce various shapes), and wide availability (with required physical and mechanical properties) (Bang Lee *et al.* 2000; Saini *et al.* 2015).

1.6.2.4 Coatings

Coatings are used to improve the implant material properties. Recently, research has started depositing coatings onto Ti₆Al₄V alloy, because it is the most widely used implant material. Moreover, the most used bioactive coating is hydroxyapatite (HAP) due to its chemical similarity to bone and teeth (Al-Sanabani *et al.* 2013; Boyd *et al.* 2015). According to Boyd *et al.* (2015), there are various elements and compounds, such as Mg and Si, which are also found in healthy bone. These elements and compounds can be incorporated into HAP to imitate bone chemistry. On the other hand, hydroxyapatite has poor physical properties such as a high dissolution rate in human fluids. HAP-based implants are also difficult to handle during surgery due to low mechanical integrity and could be damaged during the surgery procedure of some medical devices which are placed by press-fitting or screwing (Fulmer *et al.* 2002; Chen *et al.* 2014).

It has been shown that the mechanical properties of hydroxyapatite can be improved by silicon (Si) addition but the dissolution rate and osseointegration remained close to the undoped HAP (Vladescu *et al.* 2014). Furthermore, it is thought that the addition of the Mg into the Si-doped hydroxyapatite may combine the mechanical properties of HAP+Si coatings with the good osseointegration capability of Mg (Revilla-L'opez *et al.* 2016). Improvement of HAP properties is also possible by introducing TiO₂ on HAP coating. This was demonstrated by Lee and Koshizaki (2008) by creating a nano-structured hydroxyapatite (HAP)/TiO₂ composite on commercially pure titanium using the co-sputtering technique.

Therefore, our cooperation partner, Dr. eng. Alina Vladescu (National Institute for Optoelectronics, Magurele, Romania) is trying to reduce inter alia the dissolution rate of HAP by adding different compounds (e.g. silicon carbide, magnesium oxide and titanium dioxide) to HAP coatings. In addition, these compounds are also tested for potential improvement of other mechanical or physico-chemical properties of hydroxyapatite, such as corrosion resistance, hardness, elasticity, and surface roughness. To that end, Dr. Vladescu has prepared novel coatings (a hydroxyapatite 50W, silicon carbide 15W, magnesium oxide 50W coating, a hydroxyapatite 50W,

silicon carbide 15W, magnesium oxide 25W coating, a hydroxyapatite 50W, titanium dioxide 25W, magnesium oxide 25W coating and a hydroxyapatite 50W, titanium dioxide 25W, magnesium oxide 50W coating) to be tested for their effects on biocompatibility in this thesis.

1.6.3 Main procedural steps of dental implantation

1.6.3.1 Stage I Operation (fixture installation and osseointegration)

After administration of local anesthesia, a simple incision is made in the gum, at the location of the lost natural tooth/teeth root(s). A hole is drilled in the bone (in that place) using a special drill bit; this hole must be proportionate in shape and size to the implant. Thereafter, the implant is placed in the bone (hole) and a metal cover is then also put into place. Lastly, the gums are sutured and allowed to heal (Nippon dental university department of oral implantology, 1994; Zha, 2011).

The next step of the implant procedure is the process of bone cell (from the jaw bone) adhesion to the titanium implant surface (osseointegration). This process needs a period of almost 3 months and 6 months to complete in the mandible and maxilla, respectively. Osseointegration is the most important stage in implantology; the success rate of the procedure depends on the patient's care and their adherence to the recommendations of the surgeon. After the osseointegration period, an X-ray image is taken to confirm the adhesion, as well as the stability of the implant.

1.6.3.2 Stage II Operation (abutment connection)

Once bone adhesion is confirmed, the patient is given a local anesthetic and given a simple slit in the gum to expose the implant and remove the metallic implant cover. Finally, the second part of the implant (abutment), which starts from the bone level, is put into place (Nippon dental university department of oral implantology, 1994; Zha, 2011).

1.6.3.3 Stage III (final prosthesis)

After the gums heal from the second stage, impressions and measurements are taken of the mouth, and sent to the laboratory to construct the final crowns or bridges. The crowns/bridges should preferably be made of zirconium covered with porcelain, because it provides the best aesthetics and are suitable for implants (Nippon dental university department of oral implantology, 1994; Zha, 2011); see Figure 1.8.

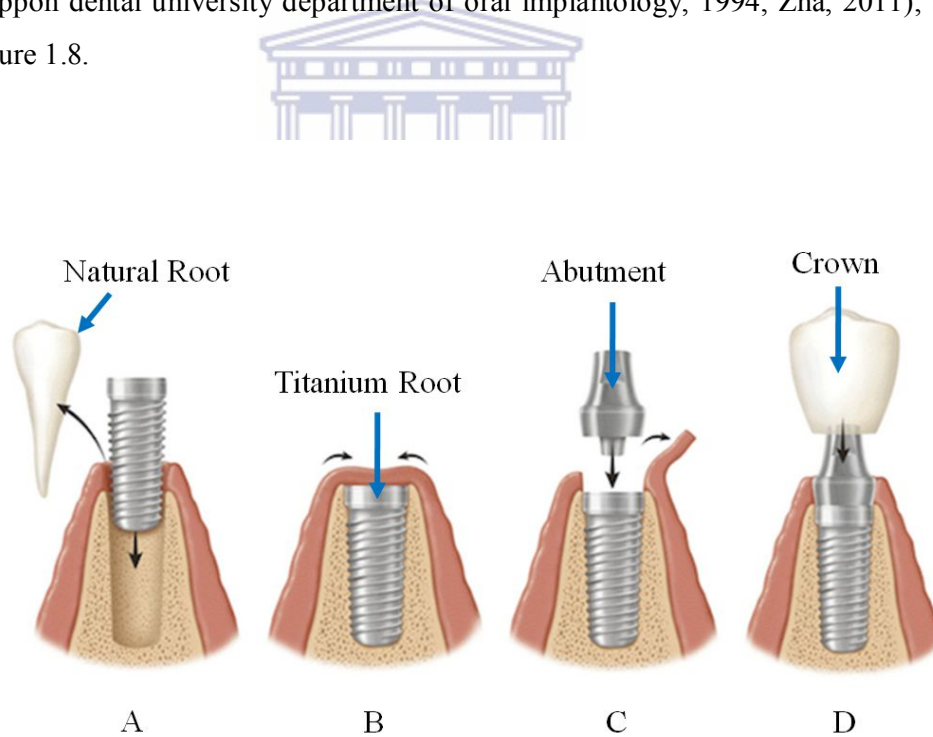


Figure 1.8: Overview of dental implantology. (A) Stage I Operation (Fixture Installation and osseointegration), (B) Stage II Osseointegration, (C) Stage II Operation (Abutment Connection), (D) Stage III (Final Prosthesis) ([adapted from www.bethesdadentalimplantcenter.com](http://www.bethesdadentalimplantcenter.com)).

1.7 Potential reasons for dental implant failure

Risk factors for dental implant failure include poor bonding of titanium implants to bone cells and tissues; loosening of screw; smoking; poor surgical execution; poor bone quality; poor implant quality; advanced age; poor treatment planning; biomechanical overloading; microbial infection on the implant material surface; bad chewing habits; increased morbidity; systemic diseases; implant location; poor fundamental stability; poor oral hygiene and fracture of implants (Porter and Von Fraunhofer, 2005; Javed and Romanos, 2010; Sakka *et al.* 2012). All of these factors can contribute to inflammation and/or bone loss and/or hampered wound healing, which ultimately leads to implant failure (Sakka *et al.* 2012).

1.8 Interaction between implant and body

1.8.1 Osseointegration (Adhesion)

Osseointegration is the growth of bone cells and formation of the structural and functional interface, directly between living bone cells and the titanium implant surface that can provide support for the prosthesis, without any intervening soft tissue (Pye *et al.* 2009; Nandal *et al.* 2014; Kim *et al.* 2015; Monsees, 2016). Titanium has a greater ability to facilitate osseointegration than other metals, and it can also transfer occlusal forces directly to the bone (Yoshinari *et al.* 2002). The concept of osseointegration was introduced by Brånemark in the mid 1960s. An implant is considered as osseointegrated when there is no relative movement between the bone and the implant (Jayesh and Dhinakarsamy, 2015; Strnad and Chirila, 2015).

Osseointegration depends (in the field of dentistry) on an understanding of the compensatory capacities of hard and soft tissues, and the period of healing. Clinically, osseointegration is a process by which an asymptomatic (without any adverse effects to the patient's health) installation of a rigid alloplastic material is achieved and maintained in the bone during functional loading use. Anatomically, the bone healing process and factors which provide osseointegration can be improved by increasing bone implant contact (Brånemark, 1983). However, osseointegration, also known as coupling, is a continuous procedure which is under

the control of both osteoblasts and osteoclasts (Martin and Sims, 2005; Chug *et al.* 2013; Macha *et al.* 2014).

The attachment of osteoblasts to the implant surface is essential for successful osseointegration (Monsees *et al.* 2005; Ballo *et al.* 2011; Kim *et al.* 2015). According to Greenwood and Murphy-Ullrich (1998), cell adhesion is a three-step process. The first step is cell attachment, this is followed by cell spreading, and the final step is the formation of focal adhesion points and actin fibers (Monsees *et al.* 2005).

The nearest attachment locations between the osteoblast and implant surface are called focal contacts (Anselme, 2000). Moreover, focal contacts (adhesion plaques) tend to form at the front edge of moving osteoblasts (Monsees *et al.* 2005). The focal contacts are made up of many cytosolic proteins, such as tensin, paxillin, and vinculin; as well as the transmembrane proteins known as integrins (Anselme, 2000). Vinculin is used as a relay and connection between actin fibers (cytoskeleton) and the integrins (Anselme, 2000; Monsees *et al.* 2005; Monsees, 2016); see Figure 1.9. Thus, cellular probes for vinculin can serve as markers for the focal contacts of osteoblasts (Monsees *et al.* 2005).

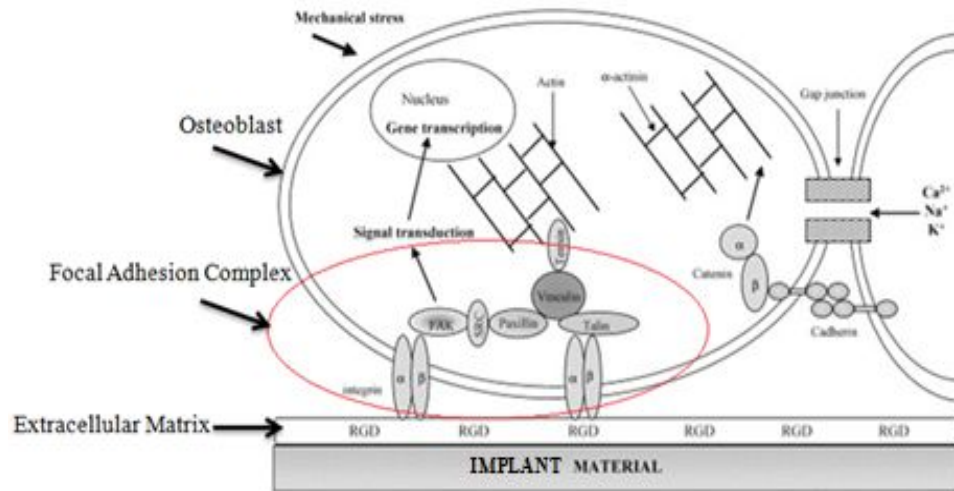


Figure 1.9: Illustration of focal contacts in osteoblasts (adapted from Anselme, 2000). RGD: arginine - glycine- aspartic acid group, which is found the extracellular matrix proteins.

1.8.2 Host response to implants

According to Özcan and Hämmerle (2012), bone cell attachment to a titanium implant surface is an important initial step in the bone's response to the implant. Ideally, the bone cells should grow into, and fill the gap between the implant and the bone tissue within the three-six month healing period. The success rate of titanium implantation depends on wound healing and bone formation (Boyan *et al.* 1998; Shibata and Tanimoto, 2015). Moreover, new bone formation around the titanium implant needs precursors of osteoblasts, production of the osteoid (extracellular matrix), and calcification of the osteoids (Boyan *et al.* 1998).

Bone remodeling is carried out by basic multicellular units (BMUs, also known as bone remodeling units), made up of osteoclasts and osteoblasts (Clarke, 2008; Matsuo and Irie, 2008; Kini and Nandeesh, 2012; Weatherholt *et al.*, 2012). Osteoclasts are bone cells that are derived from hematopoietic stem cells (HSCs); they resorb bone, are multinucleated and are larger than osteoblasts (Kini and Nandeesh, 2012; Weatherholt *et al.* 2012). On the other hand, osteoblasts are also bone cells, but are derived from mesenchymal stem cells (MSCs); they form new bone, are mononucleated and are smaller than osteoclasts (Kini and Nandeesh, 2012; Weatherholt *et al.* 2012). Additionally, osteocytes are another group of bone

cells that are derived from osteoblasts, during bone formation (Matsuo and Irie, 2008; Kini and Nandeesh, 2012). Osteocytes are permanent residents of all bone; unlike osteoclasts and osteoblasts, which are only temporarily active in bone remodeling at any given location.

Osteocytes are sensitive to bone damage, low blood calcium levels, low bone loading, etc. and, once this is detected, the osteocytes undergo apoptosis (Matsuo and Irie, 2008). According to Matsuo and Irie (2008), osteocytes may send signals to the osteoclasts, during the apoptotic process, which attract osteoclasts to the damaged site and initiate bone resorption. On the other hand, during bone health, osteocytes might send inhibitory signals to osteoclasts to prevent bone resorption (Matsuo and Irie, 2008). After osteocyte apoptosis, osteocytes die and are unable to send inhibitory signals to the osteoclasts; thus, osteoclasts can resorb the bone tissue (Matsuo and Irie, 2008).

Bone remodeling can only occur if osteoblasts and osteoclasts communicate with one another, in a process called coupling (Clarke, 2008; Matsuo and Irie, 2008; Kini and Nandeesh, 2012; Weatherholt *et al.* 2012). Coupling acts to control the entire process of bone remodeling. However, different authors suggested various ideas for the specifics of the coupling process (Clarke, 2008; Matsuo and Irie, 2008; Kini and Nandeesh, 2012; Weatherholt *et al.* 2012).

According to Clarke (2008), during bone resorption, osteoclasts produce hydrogen ions and enzymes, such as cathepsin K, which help to dissolve the mineral components of the bone matrix and to digest the proteinaceous bone matrix, respectively. Consequently, calcium is released from the bone matrix, leading to a local high calcium concentration (Matsuo and Irie, 2008). Osteoclasts send signals to the osteoblasts precursors to undergo osteoblastogenesis (Matsuo and Irie, 2008). Additionally, osteoclasts undergo apoptosis in response to the high calcium levels (Matsuo and Irie, 2008).

Osteoblasts initiate the process of building new bone; this process takes longer than bone resorption, taking approximately three months, compared to three weeks for resorption (Matsuo and Irie, 2008). Firstly, osteoblasts produce specific proteins, such as type I collagen and osteocalcin, which are used to make the bone matrix; the unmineralized bone is called the osteoid (Weatherholt *et al.* 2012). Thereafter, osteoblasts produce other types of proteins, such as alkaline phosphatase, which is used for bone mineralization (Weatherholt *et al.* 2012). At the final stage of new bone formation, osteoblasts become trapped within the bone matrix. When the osteoblasts become trapped, they are considered to be osteocytes (Kini and Nandeesh, 2012; Weatherholt *et al.* 2012).

In summary, bone remodeling depends on three types of bone cells, namely osteocytes, osteoclasts and osteoblasts. Osteocytes sense the state of bone, and communicate with osteoclasts to resorb old bone when needed. Thereafter, osteoclasts resorb the old bone by secreting hydrogen ions and specific enzymes. Finally, osteoblasts form new bone by secreting specific proteins that produce the osteoid and allow bone mineralization.

There are some undesirable conditions that lead to the cessation of osseointegration; such as strong biting before the healing period is complete and small movement of the implant (Shibata and Tanimoto, 2015).

The interface between bone tissue and the implant surface is rich in glycosaminoglycans, as well as noncollagenous proteins, amongst others. Studies have shown that new bone starts growing directly from the titanium implant surface and spreads outwards. Additionally, the new bone (growing from the titanium implant) spreads faster than the bone that grows towards the implant. Nonetheless, the events at the interface between the bone tissue and the titanium implant are still under investigation (Shibata and Tanimoto, 2015).

1.8.3 Microbial etiology of implant failure

The human mouth has an appropriate environment for the colonization and growth of microorganisms (Marcotte and Lavoie, 1998). This is because the oral cavity is warm, moist and receives a lot of food.

Many studies have demonstrated how microorganisms can lead to dental implant failures (Wood and Vermilyea, 2004; Pye *et al.* 2009; Elashi, 2015). These microorganisms include *Candida* species (e.g. *Candida albicans*), Streptococci (e.g. *Streptococcus sanguinis*), Staphylococci (e.g. *Staphylococcus aureus*) and enteric bacteria (e.g. *Escherichia coli*) (Pye *et al.* 2009; Elashi, 2015; Monsees, 2016). Microbial infection, during the surgical process, is a major cause of osseointegration failure, which ultimately leads to implant failure (Kargupta *et al.* 2014; Monsees, 2016).

Candida albicans (*C. albicans*) is a dimorphic fungus, which causes candidiasis (Kabir *et al.* 2012; Meng, 2014; Elashi, 2015). Candidiasis usually occurs in either the oral cavity (called oral thrush) or the genital tract (called vaginal thrush in females and candidal balanitis in males) (Kabir *et al.* 2012; Mayer *et al.* 2013). Thrush and candidal balanitis present as white spots at the appropriate locations (Kabir *et al.* 2012). *Candida albicans* is used globally as a model oral fungus for investigating the potential antimycotic properties of various samples. Hence, *Candida albicans* was also used in this thesis to test the potential antifungal properties of the sample coatings.

Streptococcus sanguinis (*S. sanguinis*) is a Gram positive bacterium, which is coccus-shaped (ball shaped) and facultatively anaerobic (Chowdhury *et al.* 2014). *S. sanguinis* is usually present in dental plaque and causes dental cavities and endocarditis (Chowdhury *et al.* 2014). When a surgeon makes an incision in the gum for implantology, *S. sanguinis* can potentially enter the blood and travel to the heart, where it may cause endocarditis a condition which can be fatal to the patient. Thus, *S. sanguinis* was used as a model to determine the antibacterial potential of the selected samples (hydroxyapatite 50W, silicon carbide 15W, magnesium oxide

50W sample, hydroxyapatite 50W, silicon carbide 15W, magnesium oxide 25W sample, hydroxyapatite 50W, titanium dioxide 25W, magnesium oxide 25W sample and hydroxyapatite 50W, titanium dioxide 25W, magnesium oxide 50W sample).

Staphylococcus aureus (*S. aureus*) is another Gram positive bacterium, which is also coccus-shaped (ball shaped) and facultatively anaerobic (Leung, 2008; Atbayga, 2013). *S. aureus* is part of the natural flora of the nasal cavity and skin (Atbayga, 2013). *S. aureus* can cause various opportunistic infections, such as gastroenteritis and skin infections (Ladhani *et al.* 2004). Additionally, the nose and oral cavity are linked to each other via the pharynx, and postnasal drip can inoculate the mouth with *S. aureus*. For these reasons, *S. aureus* was also chosen to ascertain the potential antibacterial effects of the selected samples (hydroxyapatite 50W, silicon carbide 15W, magnesium oxide 50W sample, hydroxyapatite 50W, silicon carbide 15W, magnesium oxide 25W sample, hydroxyapatite 50W, titanium dioxide 25W, magnesium oxide 25W sample and hydroxyapatite 50W, titanium dioxide 25W, magnesium oxide 50W sample).

Escherichia coli (*E. coli*) is a Gram negative bacterium, which is rod-shaped and facultatively anaerobic (Atbayga, 2013; Elashi, 2015). *E. coli* is part of the natural flora of the colon and is internationally used as an indicator of fecal contamination (Atbayga, 2013). *E. coli* can cause many different infections, such as gastroenteritis and urinary tract infections (Elashi, 2015). Additionally, *E. coli* infections typically occur due to unsanitary practices, such as not washing hands after using the toilet or before eating (Elashi, 2015). Consequently, *E. coli* could inoculate the mouth and may cause an infection that can ultimately lead to an implant failure.

There are three different groups of microbial infections; namely superficial immediate infections, deep immediate infections and deep late infections (Costa *et al.* 2011; Kargupta *et al.* 2014). In addition to simple infections, biofilms complicate implantology further. The microorganisms in the mouth have the capability for biofilm formation. Additionally, biofilms can colonize practically any material (e.g. metals, ceramics and polymers), including medical devices (Costa *et*

al. 2011). The potential infections from dental implant surgery may require implant removal, amongst others, which is highly inconvenient for the patient (Costa *et al.* 2011).



1.9 Biocompatibility

Biocompatibility is the ability of a biomaterial to work, as intended, without causing any harm to the host (Ratner, 2001; Moharamzadeh *et al.* 2009; Wang and Zreiqat, 2010; Monsees, 2016). Therefore, in order to test biocompatibility of an implant or implant coating, the effects of the implant (or coating) on cell physiology and cytotoxicity should be tested (Monsees, 2016). This definition for biocompatibility suggests that the interaction between the host, implant material and the material's function must conform to one another (Wataha, 2001; Geetha *et al.* 2009; Duraccio *et al.* 2015). According to Zitter and Plenk (1987), the biocompatibility of metallic biomaterials is synonymous with its corrosion resistance, including not releasing harmful metal ions.

Microorganisms can interfere with osseointegration, as described above, thus, a dental biomaterial should have antimicrobial activity, because the oral cavity has many natural microbes. Huang *et al.* (2010) suggested the use of adapted implants that are antimicrobial or possess antimicrobial coatings, as this will reduce the quantity of bacterial adhesions on the implant surface.

1.10 Aims and objectives of this study

The aim of this thesis was to investigate if novel implant coatings could improve biocompatibility compared with the standard Ti₆Al₄V alloy.

This thesis has evaluated the following:

1. Adhesion of SaOS-2 human osteosarcoma cells to the implant surface; this was done by microscopic examination of the morphology and number of cells, after fluorescence labeling of actin fibers (phalloidin-TRITC) and nuclei (DAPI).
2. Cytotoxic effect of the dental implant material was done using fluorescence vital dyes (propidium iodide: dead cells; calcein-AM: alive cells) for single cell measurements.

3. Antimicrobial properties was done by measuring growth inhibition of several relevant bacteria species, namely *Staphylococcus aureus*, *Escherichia coli*, *Candida albicans* and *Streptococcus sanguinis*.



CHAPTER 2: Materials and Methods

2.1 Stock solutions and buffers

The stock solutions and buffers are shown in Table 2.1

Table 2.1: Preparation of stock solutions and buffers

Stock solution	Preparation
Hepes Buffer	Hepes buffer solution was prepared by dissolving 1301 mg of Hepes (final concentration of 10 mM) (Cat. no. H4034, Sigma-Aldrich, St. Louis, USA), 3944 mg of NaCl (final concentration 135 mM) (B & M Scientific cc, Cape Town), 105 mg of CaCl ₂ (1.2 mM) (Cat. no. AL1015, Alpha, Mumbai, India), 122 mg of MgCl ₂ (1.2 mM) (Merck, Modderfontein, Gauteng, South Africa), 186 mg of KCl (5 mM) (Cat. no. P9541, Sigma-Aldrich, Steinheim, Germany), 4000 mg of glucose (0.8%) (Merck, Modderfontein, Gauteng, South Africa) in 500 ml of reverse osmosis water and stored at 4°C for up to 4 months.
Bovine Serum Albumin (BSA, 1%)	A 1% solution of BSA was prepared by dissolving 200 mg of BSA powder (Cat. no. A1470-25G, Sigma-Aldrich, St. Louis, USA) in 20 ml of PBS (Cat. no. BR0014, Oxoid, Basingstoke, Hampshire, England). The dissolving process was facilitated by rotation for approximately 1 h at room temperature. The BSA solution was filtered using a syringe filter of 0.2 µm and stored, aliquoted, at 4°C until further use.
Propidium Iodide (PI) Stock Solution	A stock solution of 1 mg/ml (1.5 mM) of PI was prepared by dissolving 1 mg of PI (Cat. no. 81845, Sigma-Aldrich, St. Louis, USA) in 1 ml of reverse osmosis water; and stored, aliquoted in the dark, at -20°C until further use.
Calcein-AM Stock Solution	A 1 mg/ml stock solution of Calcein-AM was prepared by dissolving 1 mg of Calcein-AM (Cat. no. 17783-1MG, Sigma-Aldrich, St. Louis, USA) in 1 ml of DMSO (Cat. No. D2650, Sigma-Aldrich, St. Louis, USA). This solution was wrapped with aluminum foil and stored at -20°C until further use.

Phosphate Buffered Saline (PBS)	Dulbecco's PBS solution contained 0.15 M NaCl, 2.5 Mm KCl, 10 mM Na ₂ HPO ₄ and 18 mM Na ₂ HPO ₄ , PH 7.4. A PBS solution was prepared by dissolving one PBS tablet (Cat. no. BR0014G, Oxoid, Basingstoke, Hampshire, England) in 100 ml of reverse osmosis (RO) water, according to the manufacturer's instructions.
Phalloidin-TRITC	A stock solution of tetramethylrhodamine-isothiocyanate (TRITC)-phalloidin was prepared by dissolving 0.1 mg of phalloidin-TRITC (Cat. no. P1951, Sigma-Aldrich, St. Louis, USA) in 200 µl of methanol, and wrapped with aluminium foil to prevent exposure to direct light. The phalloidin-TRITC was stored in aliquots at -20°C until further use.
Triton X -100 (0.5%)	A 0.5% solution of Triton X-100 (4-(1,1,3,3-Tetramethylbutyl) phenyl-polyethylene glycol, <i>t</i> -Octylphenoxypolyethoxyethanol, Polyethylene glycoltert-octylphenyl ether) was prepared by dissolving 500µl of Triton X-100 (Cat. no. T8532, Sigma-Aldrich, St. Louis, USA) in 99.5 ml of PBS (Cat. no. BR0014, Oxoid, Basingstoke, Hampshire, England) and stored at room temperature until further use.
DAPI Stock Solution	A 5 mg/ml stock solution of DAPI (4', 6-diamidino-2-phenylindole dihydrochloride) was prepared by dissolving 5 mg of DAPI powder (Cat. no. D1306, Molecular Probes, Eugene, Oregon, USA) in 1 ml of reverse osmosis water and stored, aliquoted in the dark, at -20°C until further use.
Formaldehyde (4%)	A 4% solution of Formaldehyde was prepared by dissolving 40 ml of formaldehyde (Merck, Modderfontein, Gauteng, South Africa) in 60 ml of PBS and stored at room temperature until further use.
Crystal violet	A solution of crystal violet was prepared by dissolving 5 g of crystal violet powder (Cat. no. 25G, Saarchem (PTY) Ltd, Muldersdrift, South Africa) in 1 liter of reverse osmosis water and stored at room temperature until further use.

Lugol's Iodine	A solution of Lugol's iodine was prepared by dissolving 10 g of Lugol's iodine powder (B & M Scientific CC, Cape Town) and 20 g of potassium iodide (Cat. no. 10212, BDH Chemicals Ltd, Poole, England) in 1 liter of reverse osmosis water and stored at room temperature until further use.
Carbol Fuchsin	A 0.5 g/ml solution of carbol fuchsin was prepared by dissolving 0.5g of basic carbol fuchsin powder (Art. 4041, Merck, Darmstadt, Germany) in 1 ml of reverse osmosis water and stored at room temperature until further use.

2.2 Sterilisation of Ti₆Al₄V samples

All the samples used in this thesis were discs of the Ti₆Al₄V titanium alloy (8mm in the diameter and 2mm in height), which were produced by our co-operation partner Dr. eng. A. Vladescu, from the National Institute for Research and Development in Optoelectronics, Bucharest, Romania. These discs were all coated differently, with the exception of the uncoated Ti₆Al₄V. The coatings used were: hydroxyapatite 50W, silicon carbide 15W, magnesium oxide 50W (Sample 1), hydroxyapatite 50W, silicon carbide 15W, magnesium oxide 25W (Sample 2), hydroxyapatite 50W, titanium dioxide 25W, magnesium oxide 25W (Sample 3) and hydroxyapatite 50W, titanium dioxide 25W, magnesium oxide 50W (Sample 4). All metal samples were carefully cleaned and sterilized by immersion in a 70% ethanol solution for 30 minutes (Merck 70%, v/v in reverse osmosis water). Thereafter, they were exposed to ultraviolet (UV) light in a laminar flow hood (NuAire, USA) for 15 minutes on each side, and then stored in sealed sterile containers until further use. All discs were re-sterilized by UV light, as described, just prior to performing each experiment.

2.3 Sterilisation of cover glass slips coated with PLL

All the cover glass surfaces were cleaned with acidic alcohol, by submersion for 15 minutes. The acidic alcohol was prepared by adding 1 ml of 32% HCl (Saarchem, Gauteng, South Africa) to 31 ml of 70% ethanol and shaken a few times. Thereafter, the glass discs were washed several times with reverse osmosis water to

remove the acid. The glass slips were removed using forceps and placed onto clean paper towel at RT to dry them. Then, the glass cover slips were submerged in a 0.01% Poly-L-Lysine (Cat. no. P8920, Sigma-Aldrich, St. Louis, USA) solution for 5 minutes at RT. The glass slips were washed several times again with RO water and placed onto clean paper towel at RT over night. Afterwards, they were exposed to ultraviolet (UV) light in a laminar flow hood for 15 minutes on each side, and then stored in sealed sterile containers until further use. All glass slips were re-sterilized by UV light, as described, just prior to use.

2.4 Cell culture

A vial of osteoblast-like, human osteosarcoma, (SaOS-2) cells was purchased from the American Type Cell Culture Collection (ATCC HTB 85, Manassas, VA, USA). The cells were cultured in McCoy's 5A medium (Cat. no. BE12-168F, Lonza, Veriers, Belgium) supplemented with 15% fetal bovine serum (FBS) (Cat. No. SV30160.03, HyClone, South Logan, Utah) and 2.5% penicillin/streptomycin (Cat. no. DE17-602E, Lonza, Veriers, Belgium) in 75 cm² culture flasks. Culture flasks were placed in a humid incubator (NuAire, USA) at 37°C and 5% CO₂. The culture medium was replaced at least once every week. In addition, the fresh media was prepared at least once every two weeks and it was stored at 5°C.

2.4.1 Cell seeding and growth

The frozen human osteosarcoma cells (in cryo-vials) were removed from the storage freezer (-80°C) and then promptly thawed (approximately 2 minutes) in a 37°C water bath. The vial content was transferred to a 75cm² sterile tissue culture flask containing 20 ml complete growth medium (McCoy's 5A medium supplemented with 15% fetal bovine serum), under sterile conditions (Laminar Flow, NuAire, USA). The culture flask was placed under the inverted microscope to check for the presence of cells and then placed in an incubator at 37°C and 5% CO₂. The culture flask was incubated until 80-90% confluency was reached.

2.4.2 Subculturing of cells

When the cells reached 80-90% confluency, the cells were trypsinized. The culture growth medium was aspirated from the flasks with a pipette. Cells were then washed with 10 ml of sterile PBS for 1 minute. Thereafter, the PBS was replaced with 2 ml of 1X Trypsin- Ethylene Diamine Tetra Acetic acid (Cat. no. BE 17-161E, Lonza, Verviers, Belgium), gently shaken and then incubated at 37°C for about 5-7 minutes to detach the cells. After the incubation period, the flask was examined at 100X magnification to assess cell detachment. If the cells were not detached, the flask would be given two blows to its side to ensure cell detachment. Thereafter, the trypsin would be inactivated by adding 4 ml of complete growth medium to the flask. Cells were re-suspended by careful aspiration; this cell suspension was transferred to a 15 ml test tube (SLP, Gyeonggi-do, Korea) and centrifuged at 125 Xg for 5 minutes. After centrifugation, the supernatant was discarded, and the cell pellet was re-suspended in 1 ml of complete growth medium. Thereafter, 0.5 ml of the cell suspension was transferred into a new T-75 tissue culture flask containing 20 ml of fresh complete growth medium.

2.4.3 Cell counting

After trypsinisation, centrifugation and cell resuspension, 10 µl of trypan blue (Cat. no. T6146, Sigma-Aldrich, St. Louis, USA) was added to 10 µl cell suspensions in an Eppendorf cup (thereby give a dilution factor of 2). Subsequently, 10 µl of the trypan blue-cell suspension was transferred to a haemocytometer counting chamber (Marienfeld-Superior, Germany). Cells were counted under the microscope at 100X magnification; only clear, white cells were counted. The formula below was used to calculate the total number of cells in 1 ml of the cell suspension.

$\frac{\text{Total number of cells}}{\text{Number of chambers counted}} * 2 * 10000 = \text{cells/ml}$

Number of chambers counted

The number of cells to be plated on a 24 well plate was calculated using the formulae below, where C_1 is the concentration of cells as counted, C_2 is the

concentration of cells needed, V_1 is the volume of cells acquired (at concentration C_1) and V_2 is the volume of cells needed (at concentration C_2).

$$C_1V_1 = C_2V_2$$

2.4.4 Freezing cells

When cells reached 80-90% confluency, a portion of the cells were frozen following the same procedure as the sub culturing except that after centrifugation, the supernatant was removed and the pellet resuspended with either 1 ml or 3 ml of freezing medium (complete growth medium with 5% DMSO) (Cat. no. D2650, Sigma-Aldrich, St. Louis, USA) for T25 and T75 flasks (SLP, Gyeonggi-do, Korea), respectively, before transferring into either one or more cryovials. The cryovials were slowly cooled down via ice bath for 30 minutes. Afterwards, the cryovials were put into a styrofoam box, sealed and transferred with this box into -80°C , and then stored overnight. This step is important to prevent the development of icicles that could kill the cells. The next day, the styrofoam box was removed and the cells were stored at -80°C , or stored in liquid nitrogen, for future use.

2.5 Osteoblast-based assays

2.5.1 Fluorescence labeling of actin and nuclei

The fluorescence labeling of actin and nuclei was done according to Dalby *et al.*, 2002 and Monsees *et al.*, 2005.

The sterilized titanium discs were placed in separate wells of a sterile 24 well plate (Nest, China) and cover glass slips were put in separate wells of a sterile tissue culture dish 35 mm (SPL, Eumhyeon-ri 570, Naechon-myeon, Pocheon-si, Gyeonggi-do, Korea) under sterile conditions. Cells were carefully seeded as 60 μl (75, 500 cells/ml) drops on top of the disc surfaces and 100 μl (101, 800 cells/ml) drops on the glass slips. After either 60 or 120 minutes, enough medium was added to completely cover the sample discs and glass slips, respectively. Thereafter, the cells were incubated for either 24 hours or 72 hours (for the titanium discs) or different incubation times (1, 2, 4, 6, 12, 24 or 48 hours) for the glass discs. After

the appropriate incubation period, the medium was carefully removed and the wells were washed with 1 ml of PBS each. Cells were fixed with 4% formaldehyde (Merck, Modderfontein, Gauteng, South Africa) in PBS for 5 minutes at room temperature (RT). Thereafter, cells were permeabilized using 0.5% of Triton X-100 (Cat. no. M5655, Sigma-Aldrich, St. Louis, USA) in PBS for 6 minutes at RT. Subsequently, the cells were incubated with 1% of BSA (Cat. no. A1470, Sigma-Aldrich, St. Louis, USA) in PBS for 10 minutes at RT, to block non-specific interactions. Cells were washed with PBS, once more.

Phalloidin-TRITC (tetramethylrhodamine-isothiocyanate) was used for visualization of the actin fibers. Cells were incubated with 0.1 μM of phalloidin-TRITC (Cat. no. P1951, Sigma-Aldrich, St. Louis, USA) at room temperature for one hour. Cells were, then, washed three times with PBS.

DAPI (4',-6-Diamidino-2-phenylindole dihydrochloride) was used to fluorescently label the cell nuclei. Cells were additionally incubated with 1 $\mu\text{g}/\text{ml}$ of DAPI (Cat. no. D1306, Sigma-Aldrich, St. Louis, USA) for five minutes at RT. Thereafter, cells were washed three times with PBS. The excess buffer was drained from all the sample discs or the glass slips by using forceps prior to cell mounting.

For cell mounting, the titanium discs were carefully removed from the 24 well plates and placed upside down (cells at the bottom) in a drop (5 μl) of ProLong® Diamond Antifade Mountant (Cat. no P36961, Molecular Probes, Eugene, USA) into cover glass bottom dishes (SPL, Eumhyeon-ri 570, Naechon-myeon, Pocheon-si, Gyeonggi-do, Korea). Finally, the actin fibers and nuclei of the cells were viewed by fluorescence microscopy (Zeiss, Oberkochen, Germany) using an excitation wavelength of 535nm (emission at 617nm, red filaments); thereafter, all nuclei were visualized in the same field of view using an excitation wavelength of 365nm (emission at 445nm, blue nuclei). Both, 100X magnification and 400X magnification were used.

2.5.2 Cell Viability assays

Osteoblast-like SaOS-2 cells were seeded (19,000 cells/ml) onto the discs in 24 well cell culture plates and left for either 24 hours or 72 hours at 37°C and 5% CO₂. An 8% DMSO exposure and a complete medium exposure on cover slips were included as positive and negative controls, respectively. After the treatments, the culture medium was slowly aspirated from all wells to avoid detachment of cells (not all at the same time) under non sterile conditions.

Propidium Iodide–Calcein-AM staining was used for visualization of live and dead cells. Cells were incubated with 2.5 µg/ml of PI–Calcein-AM working dilution (Cat. no. 81845, Sigma-Aldrich, St. Louis, USA) (Cat. no. 17783-1MG, Sigma-Aldrich, St. Louis, USA) for 30 minutes at RT in the dark. Thereafter, the excess buffer was drained from all sample discs or cover glass slips prior to cell mounting.

For cell mounting, all the sample discs, as well as the positive and negative controls of the glass cover slips were carefully removed from the 24 well plates and then placed upside down (cell at the bottom) in a drop (5 µl) of ProLong® Diamond Antifade Mountant (Cat. no P36961, Molecular Probes, Eugene, USA) into cover glass bottom dishes (SPL, Eumhyeon-ri 570, Naechon-myeon, Pocheon-si, Gyeonggi-do, Korea). Lastly, the number of cells on the implant surface was evaluated immediately by fluorescence microscopy (Zeiss, Oberkochen, Germany) using excitation wavelengths of 535nm for PI and 493nm for calcein, and viewed at 100X magnification and 400X magnification. All dead cells were counted firstly at one field of view using a 617nm filter (viewed as red cells); thereafter, all live cells were counted in the same field of view using a 514nm filter (viewed as green cells).

Calcein-AM is hydrophobic which gives it the ability to cross the membranes of living cells. Once inside the cell, esterases can separate the AM group from the calcein. Thereafter, calcein cannot leave the cells, and it gives off green fluorescence when excited appropriately. On the other hand, PI is not hydrophobic. Therefore, PI cannot enter live cells to produce red fluorescence in them. Moreover, PI can enter dead cells because the cell membranes of dead cells are damaged. PI

enters the nucleus and binds the DNA; consequently the PI cannot leave the dead cells, giving them red fluorescence when excited appropriately.

2.6 Microorganism strains and culture conditions

All bacterial species, used for evaluating antimicrobial activity in this *in vitro* study, were obtained from the American Type Culture Collection (ATCC, Manassas, USA). Three species of facultative anaerobic microorganisms were cultured under aerobic conditions; namely, the Gram-positive bacterium *Staphylococcus aureus* (*S. aureus*) ATCC 8539, the Gram-negative bacterium *Escherichia coli* (*E. coli*) ATCC 25922 and *Candida albicans* (*C. albicans*) ATCC 90028. Additionally, one strain of facultative anaerobic bacterium was cultured under anaerobic conditions: the Gram-positive bacterium *Streptococcus sanguinis* (*S. sanguinis*) ATCC 10556.

The *S. aureus* and *E. coli* strains were cultured on a nutrient agar, namely Columbia blood agar base (Cat. no. CM0331, Oxoid Ltd, Basingstoke, Hampshire, England), using the streak method for a single colony isolation to ensure purity of the culture using a sterile inoculating loop. The fungal strain (*C. albicans*) was cultivated on yeast nitrogen base agar (YNBG, Cat. no. 239210) (Becton, Dickinson and Company Sparks, MD 21152) plates also using the streak method for a single colony isolation by sterile inoculation loop. These cultures were then incubated at 37°C, overnight under aerobic conditions.

The *S. sanguinis* strain was cultured on Columbia blood agar base (Cat. no. CM0331, Oxoid Ltd, Basingstoke, Hampshire, England), supplemented with 5% of horse blood (Ref. no. 08349, Medical Research Council, South African) using the streak method for a single colony isolation to ensure purity of the culture using an inoculation loop. Thereafter, the agar plates (containing *S. sanguinis*) were placed in an anaerobic jar together with sachets of AnaerobicGen™ 2.5L (*S. sanguinis* grows better in a microaerophilic environment) (Cat. no. AN0025A, Thermo Scientific, Oxoid Ltd, UK) and were incubated at 37°C overnight.

2.6.1 Preparation of agar plates

2.6.1.1 Columbia blood agar base

A Columbia blood agar base (CAB) solution was prepared by dissolving 39g of CAB powder (Cat. no. CM0331, Oxoid, Basingstoke, Hampshire, England) in one liter of reverse osmosis (RO) water, according to the manufacturer's instructions. This nutrient agar was completely dissolved by boiling in a microwave for 10 minutes. Thereafter, the nutrient agar was sterilized by autoclaving at 121°C for 15 minutes and then cooled to 50°C. Fresh horse blood would be added to this agar, to a concentration of 5% v/v, when preparing the CAB for culturing *S. sanguinis* only; this step would be omitted when preparing the CAB for culturing *E. coli* and *S. aureus*, though. Approximately 20 ml of the Columbia blood agar was poured into Petri dishes (90mm in diameter) (Ref. no. 07831, Lasec, South Africa) and left to cool and solidify at room temperature. These Petri dishes were inverted and stored at 4°C until further use.

2.6.1.2 Yeast nitrogen base agar supplemented with glucose

A 10X concentrated Difco™ yeast nitrogen base agar (YNBG) solution was prepared by dissolving 6.7g of YNBG powder (Cat. no 239210, Becton, Dickinson and Company Sparks, MD 21152), together with 5g of dextrose powder (Cat. no. 0155-17, Difco, USA) in 100 ml of RO water. Difco granulated bacteriological agar was prepared by dissolving 1.3g of granulated agar powder (Cat. no. 214530, Difco, USA) in 100 ml of RO water, according to the manufacturer's instructions. This granulated agar was completely dissolved by boiling in a microwave for 10 minutes. Thereafter, the granulated agar was sterilized by autoclaving at 121°C for 15 minutes and then cooled to 50°C. Afterwards, the solution of Difco™ yeast nitrogen base agar was filtered using a 0.45 µm disposable filter (Ref. no. 25NS, MSI filters, USA). Approximately 20 ml of the Difco™ yeast nitrogen base agar was poured into Petri dishes (90mm in diameter) and left to cool and solidify at room temperature. These Petri dishes were stored at 4°C until further use.

2.6.2 Gram staining and microscopy

After isolating the bacterial colonies, the Gram stain was used to confirm purity of the bacterial species used in this study, together with a light microscopic examination.

Glass slides were cleaned using 70% ethanol and dried using paper towel. Thereafter, one drop of saline was placed onto each slide, followed by a sweep of pure colonies from the bacterial isolates on the appropriate agar plates. The bacterial colonies, in saline, were then mixed together using a sterile inoculation loop. These bacterial colonies were then heat fixed onto the separate glass slides before each being flooded with crystal violet (primary stain) (Saarchem (PTY) Ltd, Muldersdrift, South Africa) for 30 second. The glass slides were then washed with under a stream of tap water for one minute; thereafter iodine solution (the mordant) (BDH Chemicals Ltd, Poole, England) was added to each slide for one minute, before being washed, once more, with a tap water stream for one minute. Afterwards, a 95% ethanol solution (used for decolorization) was added to each slide, and washed again for one minute with a tap water stream. Thereafter, carbol fuchsin (Merck, Darmstadt, Germany) was added (which acts as a counterstain) for one minute and the slides were washed again (tap water). The glass slides were air dried, and then one drop of immersion oil (Cat. no. MXA20234, Nikon, Japan) was placed on top of each stain. Finally, the slides were viewed under the microscope at 1000X magnification. Figure 3.10 shows typical photos of Gram-stained microorganism.

2.7 Antimicrobial susceptibility testing

2.7.1 Preparation of microorganism suspensions

The preparation of suspensions of all microorganism strains: *Staphylococcus aureus*, *Escherichia coli*, *Candida albicans* and *Streptococcus sanguinis* were carried out using a direct method, called the colony suspension method. Fresh colony isolates were transferred, using a sterile inoculation loop, into sterile glass tubes each containing 9 ml of reverse osmosis (RO) water. These tubes were then mixed using a Vortex mixer (15 seconds, pulsing) (Gemmy Industrial Corp, Taiwan) to prepare microbial cell suspensions. The microorganism suspensions were standardised to a McFarland standards (McF) turbidity equivalent of 0.5, using a Sensititre nephelometer (SN) (Magellan Bioscience, Diagnostic Systemic Ltd, USA). Fresh microbial suspensions were prepared for each experiment.

2.7.2 Disc diffusion assay (Kirby-Bauer assay)

A sterile cotton swab was dipped in the solution of microbial suspensions. The swab was gently squeezed against the inside of the tube to remove excess fluid, and appropriately inoculated onto either CAB (with or without horse blood) or YNBG agar plates. Thereafter, the sample discs (uncoated discs, hydroxyapatite 50W, silicon carbide 15W, magnesium oxide 50W sample, hydroxyapatite 50W, silicon carbide 15W, magnesium oxide 25W sample, HAP 50W, TiO₂ 25W, MgO 25W sample and HAP 50W, TiO₂ 25W, MgO 50W sample), as well as the respective positive controls, namely Cefuroxime 30µg (CXM; Mast diagnostics, Mast group Ltd, Merseyside, UK) in filter paper (for the bacteria) and Fluconazole 25µg (FCA; Oxoid Ltd, Wade Road, Basingstoke, Hants, RG24 8PW, UK) in filter paper (for *C. albicans*), were placed onto the inoculated plates using sterile forceps, and then appropriately incubated, overnight. After the incubation period, the susceptibility areas of the samples were visible as inhibition zones around the test discs. Subsequently, the inhibition zones were measured from the edge of the disk to the edge of the susceptibility area. All the Kirby-Bauer assays were done in duplicate.

2.8 Statistical Analysis

The statistical analysis was done using the MedCalc® software, Version 12.5.0.0. Either an independent t-test, a Welch test or a Mann-Whitney test was used, and a P-value lower than 0.05 was considered to be significant.



CHAPTER 3: Results

All the samples used in these experiments were discs consisting of Ti₆Al₄V (90% titanium, 6% aluminium, 4% vanadium) titanium alloy. Each sample disc was coated differently, and was labeled as follows: Sample 1 (hydroxyapatite 50W, silicon carbide 15W and magnesium oxide 50W), Sample 2 (hydroxyapatite 50W, silicon carbide 15W and magnesium oxide 25W), Sample 3 (hydroxyapatite 50W, titanium dioxide 25W and magnesium oxide 25W), Sample 4 (hydroxyapatite 50W, titanium dioxide 25W and magnesium oxide 50W) and an uncoated disc (C: standard Ti₆Al₄V). Additionally, different positive controls were used for each assay and they were specific to each assay used.

3.1 Osteoblast-based assays

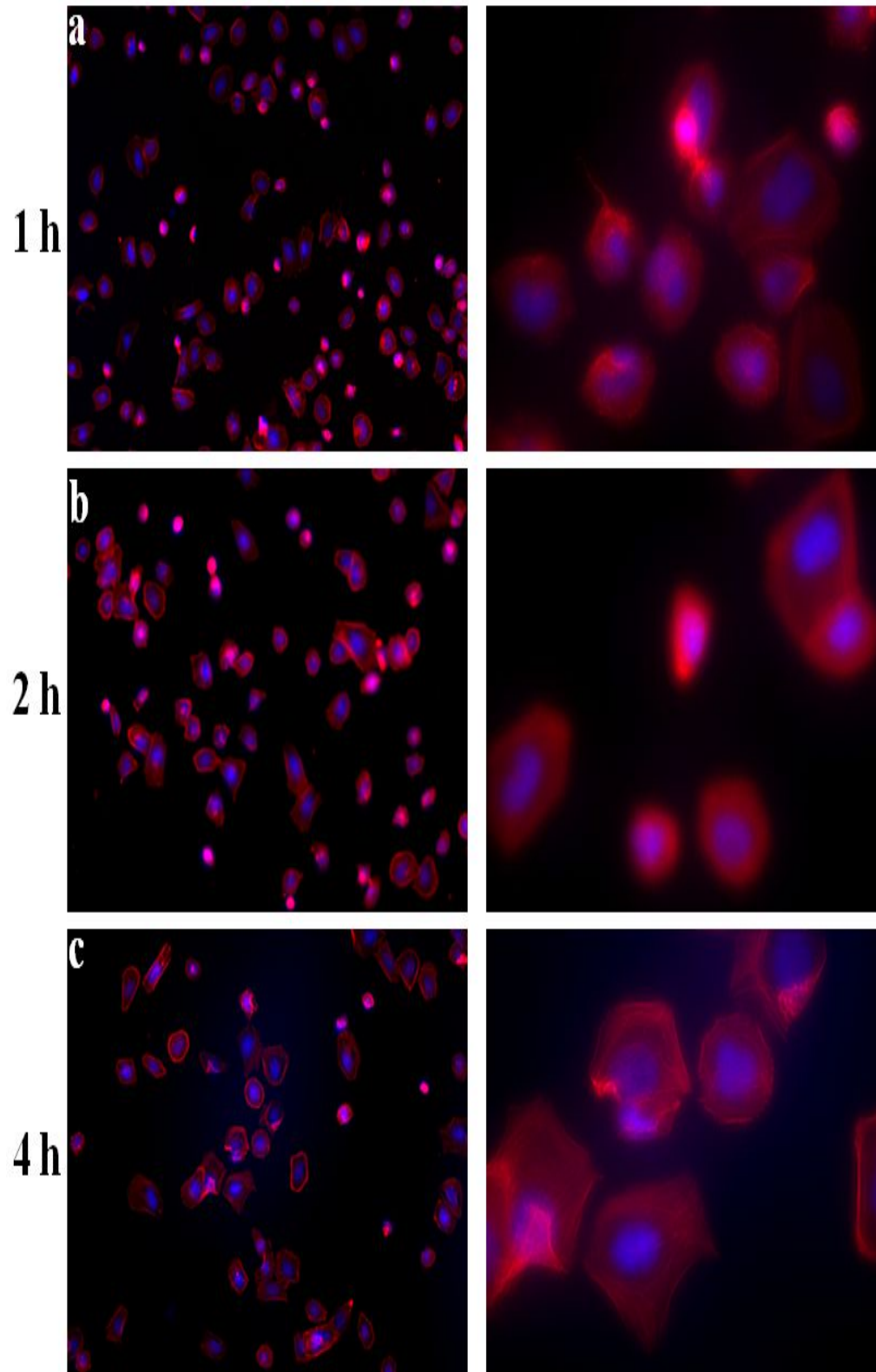
The human osteoblast-like SaOS-2 cells were seeded onto the upper surfaces of sterile Ti₆Al₄V discs (i.e. uncoated Ti₆Al₄V, or coated with either hydroxyapatite 50W, silicon carbide 15W and magnesium oxide 50W; hydroxyapatite 50W, silicon carbide 15W and magnesium oxide 25W; hydroxyapatite 50W, titanium dioxide 25W and magnesium oxide 25W or hydroxyapatite 50W, titanium dioxide 25W and magnesium oxide 50W), as well as sterile PLL-coated glass cover slips and were incubated for the appropriate times. The incubation periods for the adhesion assay were 1, 2, 4, 6, 12, 24 and 48 hours for the glass slips, but 24 hours and 72 hours for the implant samples. The cell viability assay had the same incubation period of 24 hours and 72 hours, respectively.

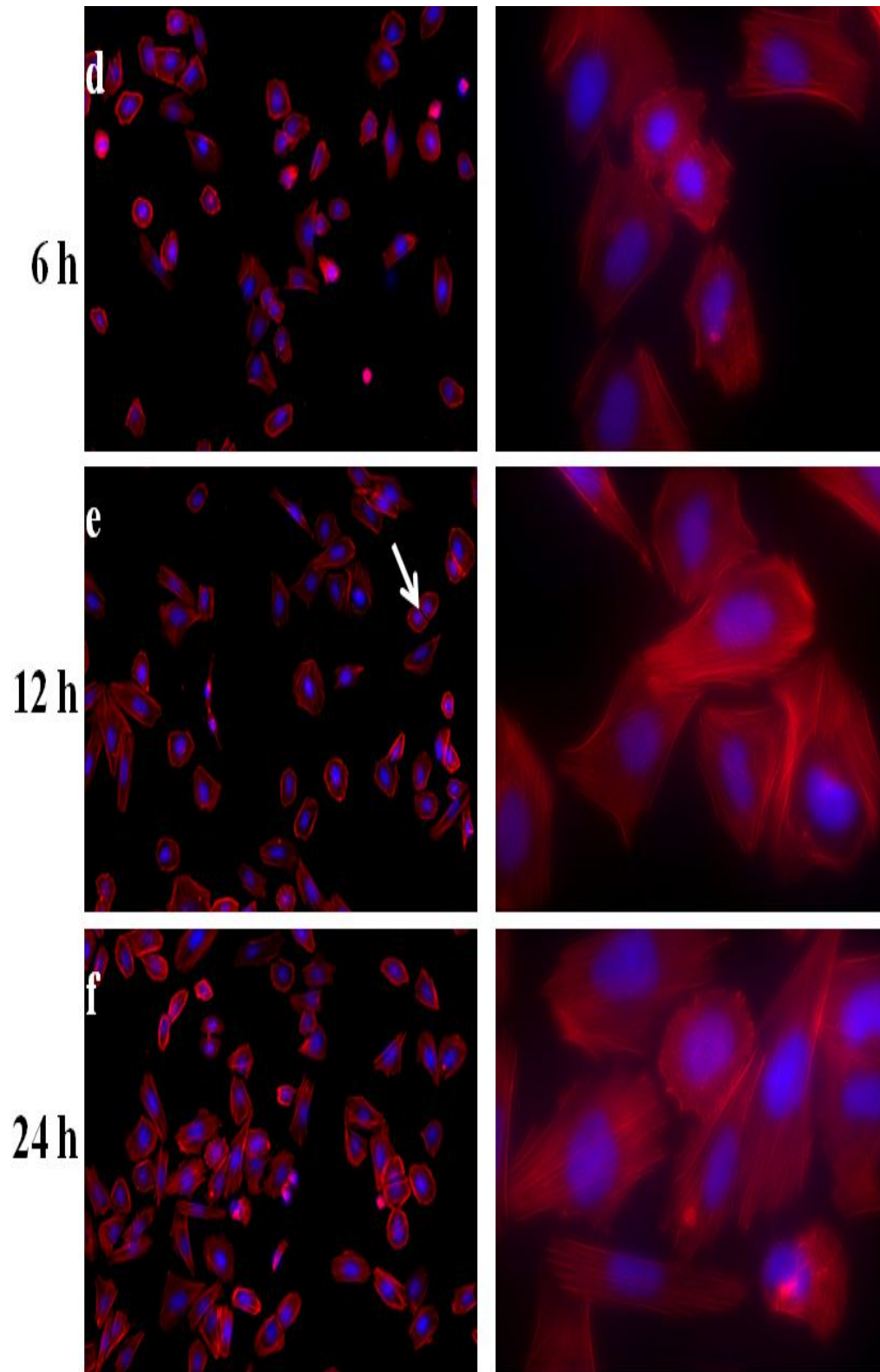
3.1.1 Cell morphology assessment

To investigate the initial adhesion of SaOS-2 cells onto the selected sample surfaces and the glass slips, cell adhesion, spreading, cytoskeleton filaments and nuclei were compared between cells growing on the different surfaces. In short, after the appropriate incubation periods, the actin fibers and nuclei were revealed by incubation with Phalloidin-TRITC and DAPI respectively, and were observed using fluorescence microscopy.

3.1.1.1 Cell morphology on PLL-coated glass.

At either one or two hours after seeding, the SaOS-2 cells were attached to the glass discs and showed a relatively rounded shape, but some cells exhibited weak spreading (Figure 3.1a and 3.1b). The actin stress fibers were not clearly observed inside the roundish cells after either 1 or 2 h of culture on the glass surfaces. Moreover, the nuclei of cells remained roundish (Figure 3.1a and 3.1b). After 4 or 6 hours of initial attachment, SaOS-2 cells showed good spreading on the glass slips. The spread cells (with proper morphology) were more numerous after 4 or 6 h attachment than after 1 or 2 h of attachment. Additionally, actin filaments of SaOS-2 cells were more spread and better defined after 4 or 6 h, since seeding, than after 1 or 2 h on the glass slips (Figure 3.1c and 3.1d). After 6 h of growth (and longer periods as well), most of the nuclei were a bit elongated and were arranged parallel to the long axes of the cells that they were a part of. There appear to be more SaOS-2 cells attached to the glass discs at 12 h post-seeding than at either 6 h, 4 h, 2 h or 1 h post-seeding. Furthermore, at 12 h post-seeding it is clear that some cells underwent mitosis, as revealed in Figure 3.1e. Osteosarcoma cells were more extended after 12 h growth than earlier incubation periods, and the subsequent incubation periods also showed cells with this morphology. At 24 or 48 hours after seeding, there were larger numbers of SaOS-2 cells than at shorter incubation times. Moreover, practically all the cells were properly spread after both 24 and 48 h (Figure 3.1f and 3.1g). The actin fibers were clearly observed inside the polygonal shaped cells on the glass surfaces after 12 h, 24 h or 48 h of growth.





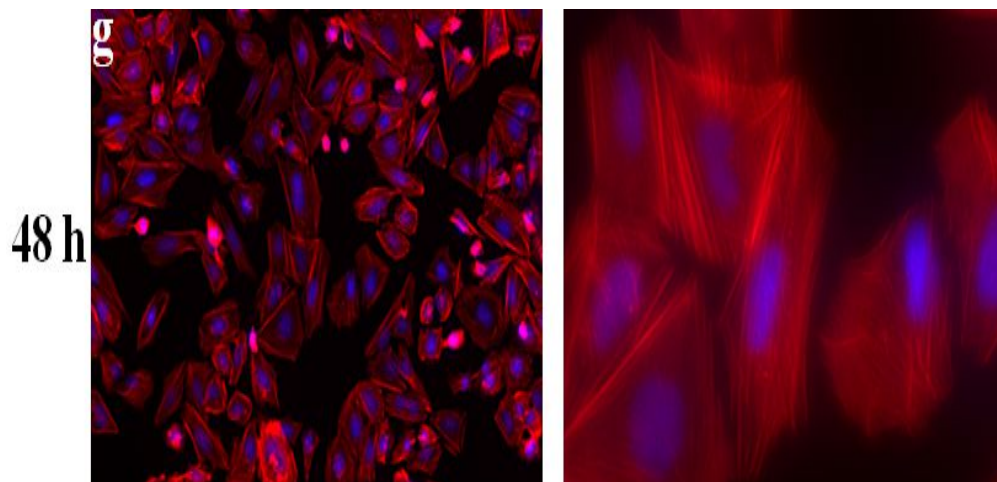
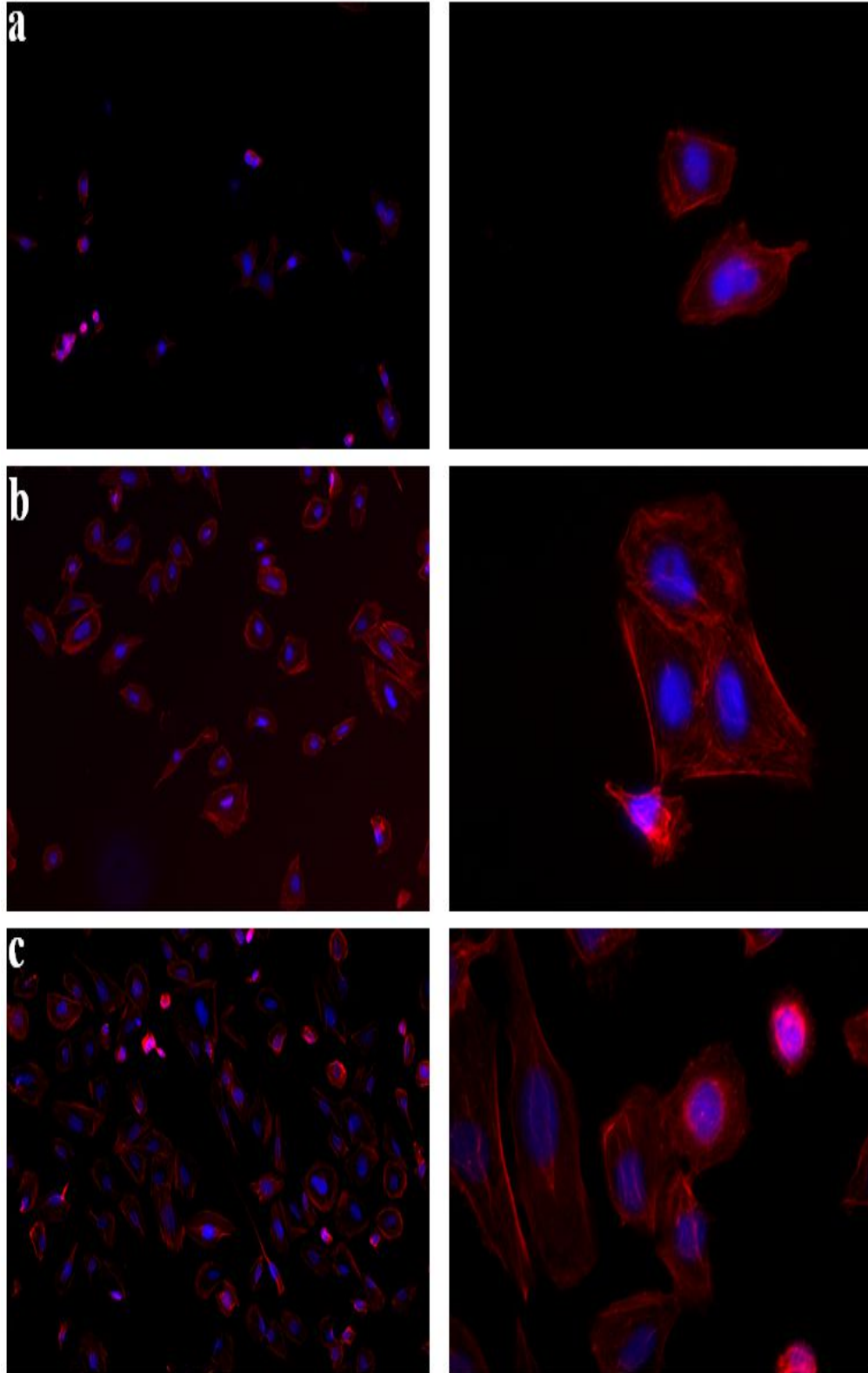


Figure 3.1: Fluorescence photomicrographs showing the cell morphology of SaOS-2 cells attached to glass discs at various times. The cells were incubated for 1 h (a), 2 h (b), 4 h (c), 6 h (d), 12 h (e), 24 h (f) and 48 h (g) and were labeled with Phalloidin-TRITC (red actin filaments) and DAPI (blue cell nuclei) before being viewed under a fluorescence microscope at 100X magnification (pictures on the left) and at 400X magnification (pictures on the right).

3.1.1.2 Cell attachment on coated Ti₆Al₄V discs.

After both 24 and 72 hours since seeding, our results showed that there were fewer attached cells on HAP 50W, SiC 15W, MgO 50W sample compared to HAP 50W, SiC 15W, MgO 25W sample, HAP 50W, TiO₂ 25W, MgO 25W sample or HAP 50W, TiO₂ 25W, MgO 50W sample and the uncoated Ti₆Al₄V sample (see Figure 3.2a and 3.3a). The SaOS-2 cells attached to HAP 50W, SiC 15W and MgO 50W coating showed spreading, but the actin fibers were not clearly defined (as displayed in Figure 3.2a and 3.3a). In addition, most of the cell nuclei on HAP 50W, SiC 15W, MgO 50W coating, HAP 50W, SiC 15W, MgO 25W coating, HAP 50W, TiO₂ 25W, MgO 25W coating or HAP 50W, TiO₂ 25W, MgO 50W coating and the uncoated sample were elongated and were parallel to the long axes of the cells that they were a part of (as shown in Figure 3.2 and 3.3). The cells on HAP 50W, SiC 15W, MgO 25W surface were more numerous than those on HAP 50W, SiC 15W, MgO 50W surface at both 24 h and 72 hour post-seeding, and showed good spreading. Most of the cytoskeleton fibers of the spread cells on HAP 50W, SiC 15W, MgO 25W surface were linear, but there were some fibers that had a waved shape (see Figure 3.2b and 3.3b). The osteosarcoma cells on HAP 50W, TiO₂ 25W, MgO 25W surface or HAP 50W, TiO₂ 25W and MgO 50W surface had

even larger numbers than those on HAP 50W, SiC 15W and MgO 50W surface or HAP 50W, SiC 15W and MgO 25W surface (see Table 3.1). Furthermore, the actin filaments were more linear orientated on HAP 50W, TiO₂ 25W and MgO 25W sample or HAP 50W, TiO₂ 25W and MgO 50W sample than those on either HAP 50W, SiC 15W and MgO 50W sample or HAP 50W, SiC 15W and MgO 25W sample (Figures 3.2c, 3.2d, 3.3c and 3.3d). The cultured SaOS-2 cells on HAP 50W, TiO₂ 25W, MgO 25W sample and HAP 50W, TiO₂ 25W, MgO 50W sample at 24 hours were similar in morphology to the cells on the glass surfaces after 24 h since seeding. Additionally, after 72 hours the SaOS-2 cells on both HAP 50W, TiO₂ 25W, MgO 25W sample and HAP 50W, TiO₂ 25W, MgO 50W sample were similar in morphology to the cells on the glass discs after 48 hours since seeding. The SaOS-2 cells grown on the uncoated Ti₆Al₄V surfaces were well attached and displayed good spreading. Our results showed that the uncoated discs appeared to have greater numbers of the attached SaOS-2 cells than HAP 50W, SiC 15W, MgO 50W coating, similar numbers of cells to HAP 50W, SiC 15W, MgO 25W coating, and smaller numbers of cells than both HAP 50W, TiO₂ 25W, MgO 25W coating and HAP 50W, TiO₂ 25W MgO 50W coating (Figure 3.2). At 24 h after seeding, it is clear that some cells underwent mitosis (as revealed in Figure 3.2e). The spread cells exhibited distinguishable actin fibers that were linear on the uncoated samples after both 24 hours and 72 hours of culture (Figure 3.2e and 3.3e). Moreover, the cultured cells on the uncoated and HAP 50W, SiC 15W and MgO 25W surfaces at 24 h were similar in morphology to the cultivated cells on the glass discs at 6-12 h after seeding. The attached cells on the Ti₆Al₄V sample after 72 hours were similar in morphology to the cultured cells on the glass surfaces at 24 h, whereas the cells on HAP 50W, SiC 15W and MgO 25W surface after 72 hours were similar to the cells on glass after 12 h post-seeding.



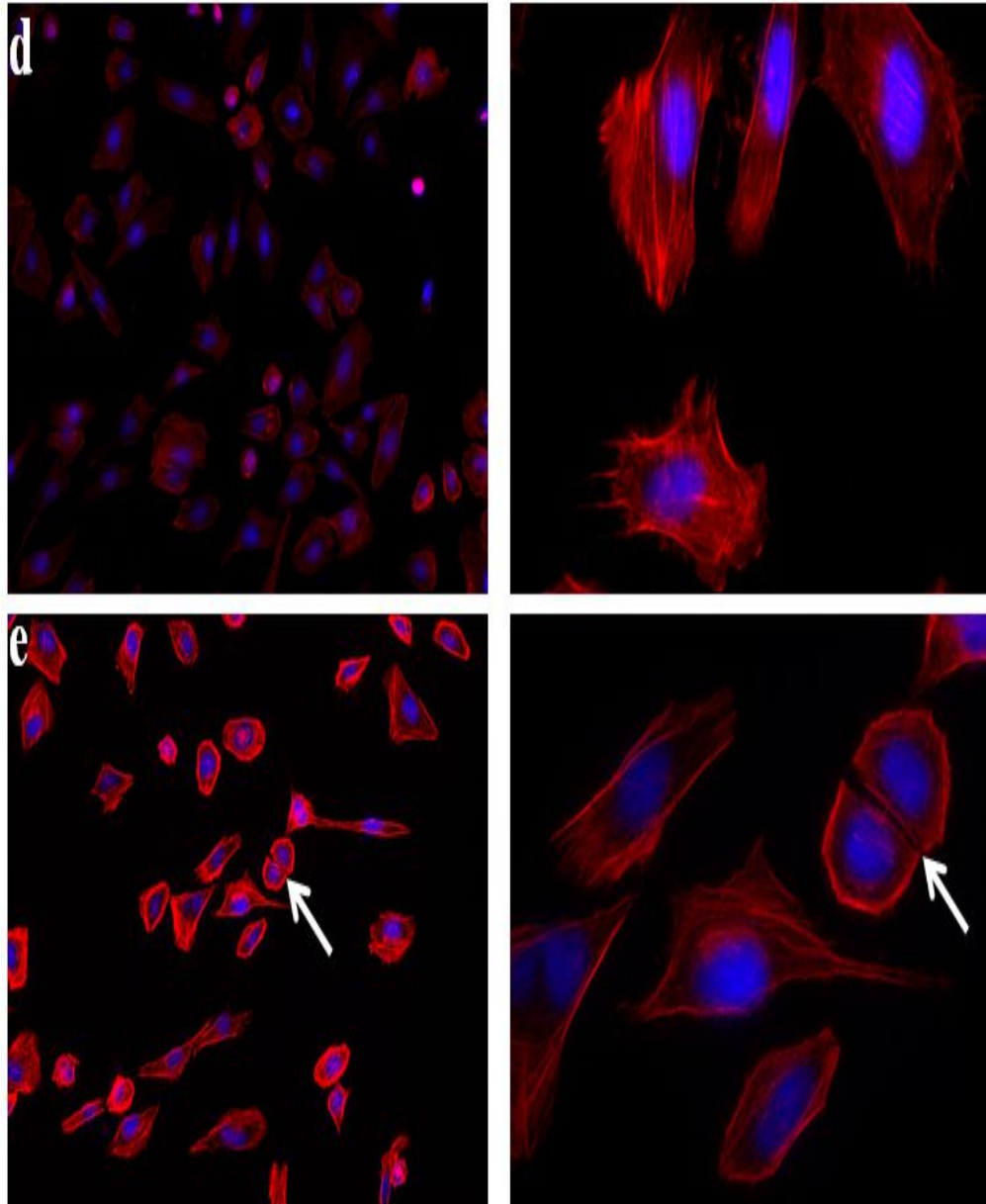
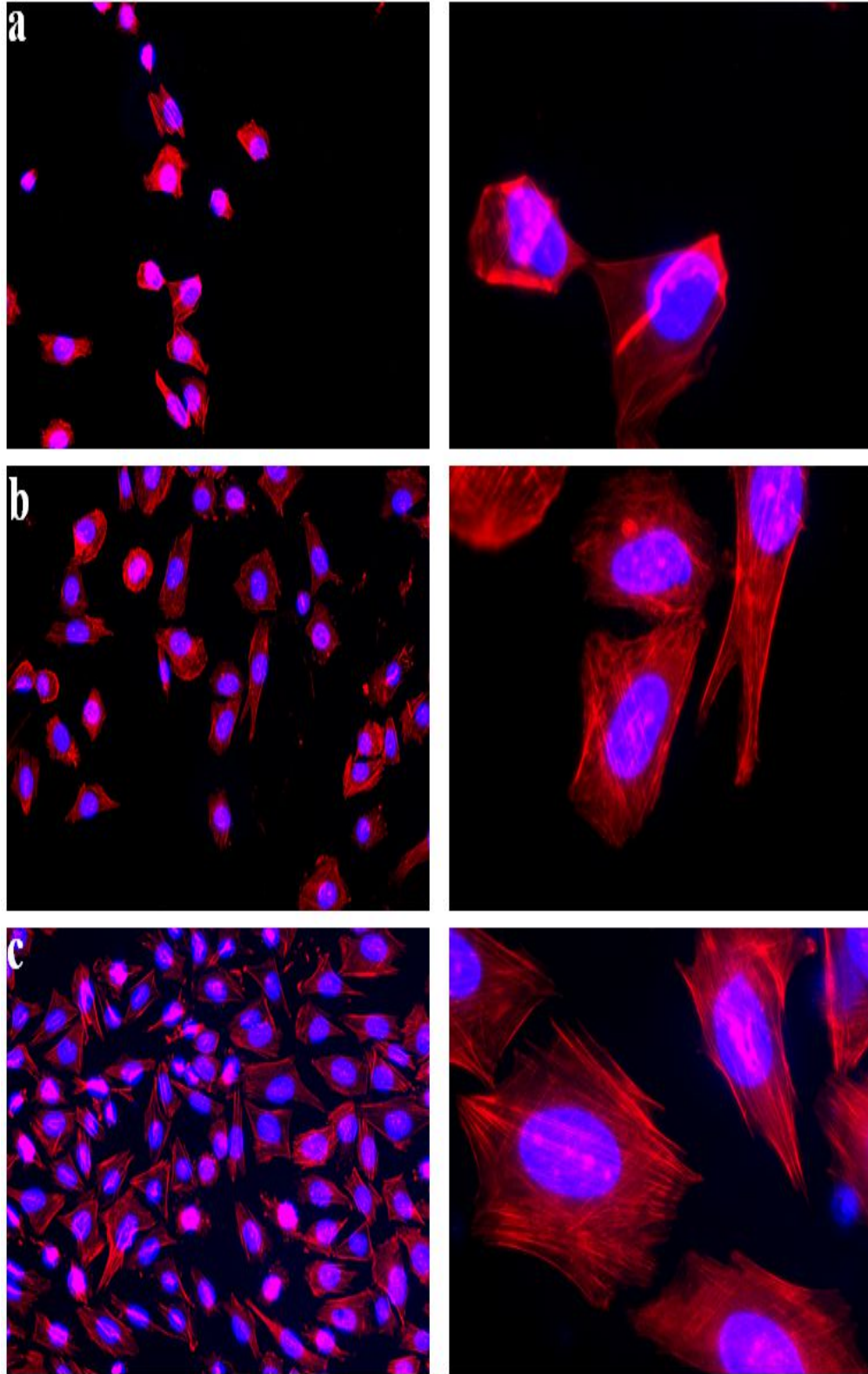


Figure 3.2: Fluorescence photomicrographs showing the cell morphology of SaOS-2 cells grown on the implant samples for 24 hours. SaOS-2 cells were seeded onto HAP 50W, SiC 15W and MgO 50W sample (a), HAP 50W, SiC 15W and MgO 25W sample (b), HAP 50W, TiO₂ 25W and MgO 25W sample (c) and HAP 50W, TiO₂ 25W and MgO 50W sample (d) as well as the uncoated Ti₆Al₄V (e) sample surfaces and were double fluorescence labeled for actin fibers (red) with Phalloidin-TRITC and cell nuclei (blue) with DAPI. Finally the cells were viewed under a fluorescence microscope at 100X magnification (pictures on the left) and at 400X magnification (pictures on the right).



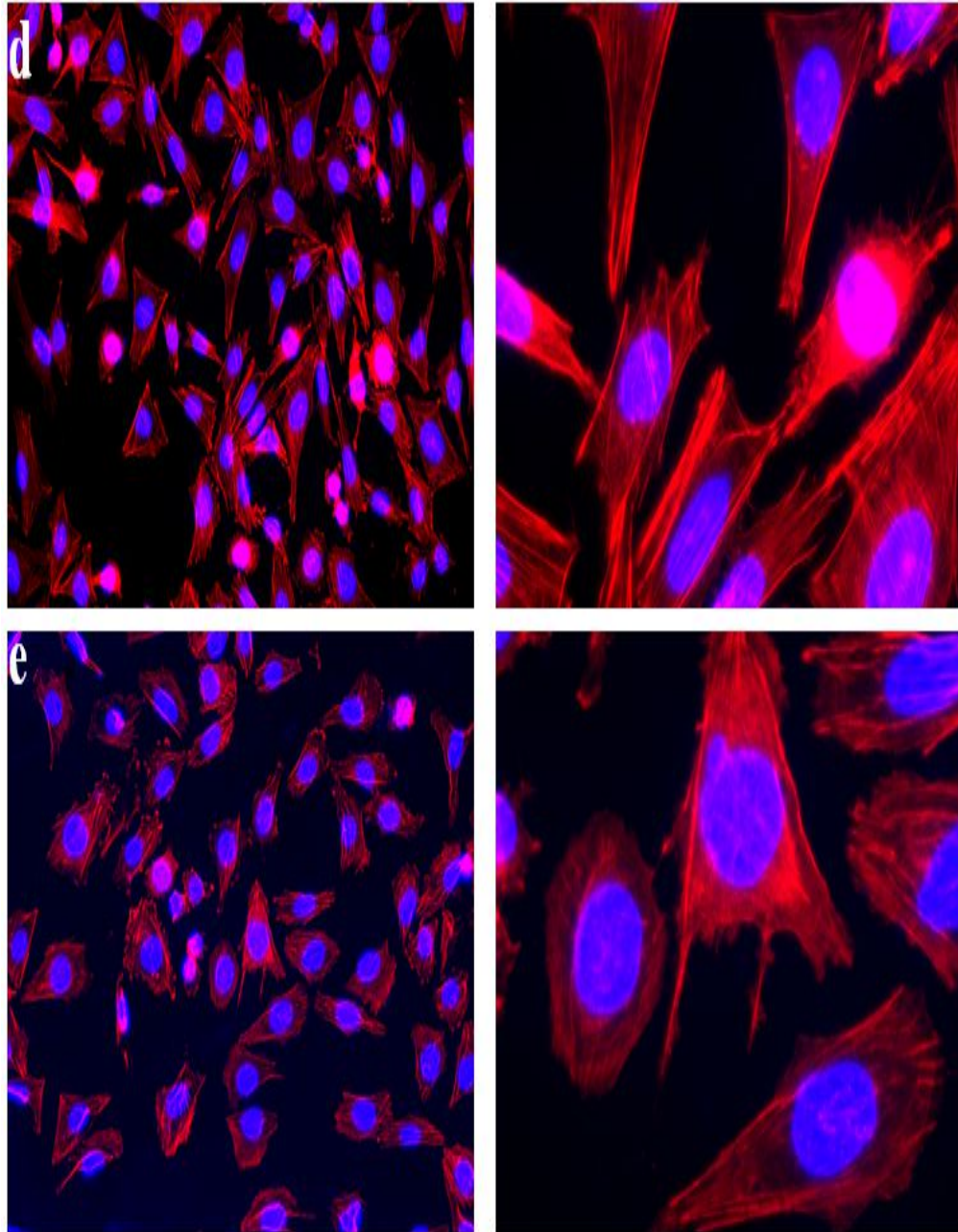


Figure 3.3: Fluorescence photomicrographs showing the cell morphology of SaOS-2 cells grown on the implant samples for 72 hours. SaOS-2 cells were seeded onto HAP 50W, SiC 15W, MgO 50W sample (a), HAP 50W, SiC 15W, MgO 25W (b), HAP 50W, TiO₂ 25W, MgO 25W sample (c) and HAP 50W, TiO₂ 25W, MgO 50W sample (d) as well as the uncoated Ti₆Al₄V (e) sample surfaces and were double fluorescence labeled for actin fibers (red) with Phalloidin-TRITC and cell nuclei (blue) with DAPI. Finally the cells were viewed under a fluorescence microscope at 100X magnification (pictures on the left) and at 400X magnification (pictures on the right).

Table 3.1: Table showing the cell densities calculated from the phalloidin-TRITC and DAPI photomicrographs. Results are presented as mean \pm standard deviation; n=3 for 24h results and n=5 for 72h results; *P< 0.05 when compare to Ti₆Al₄V.

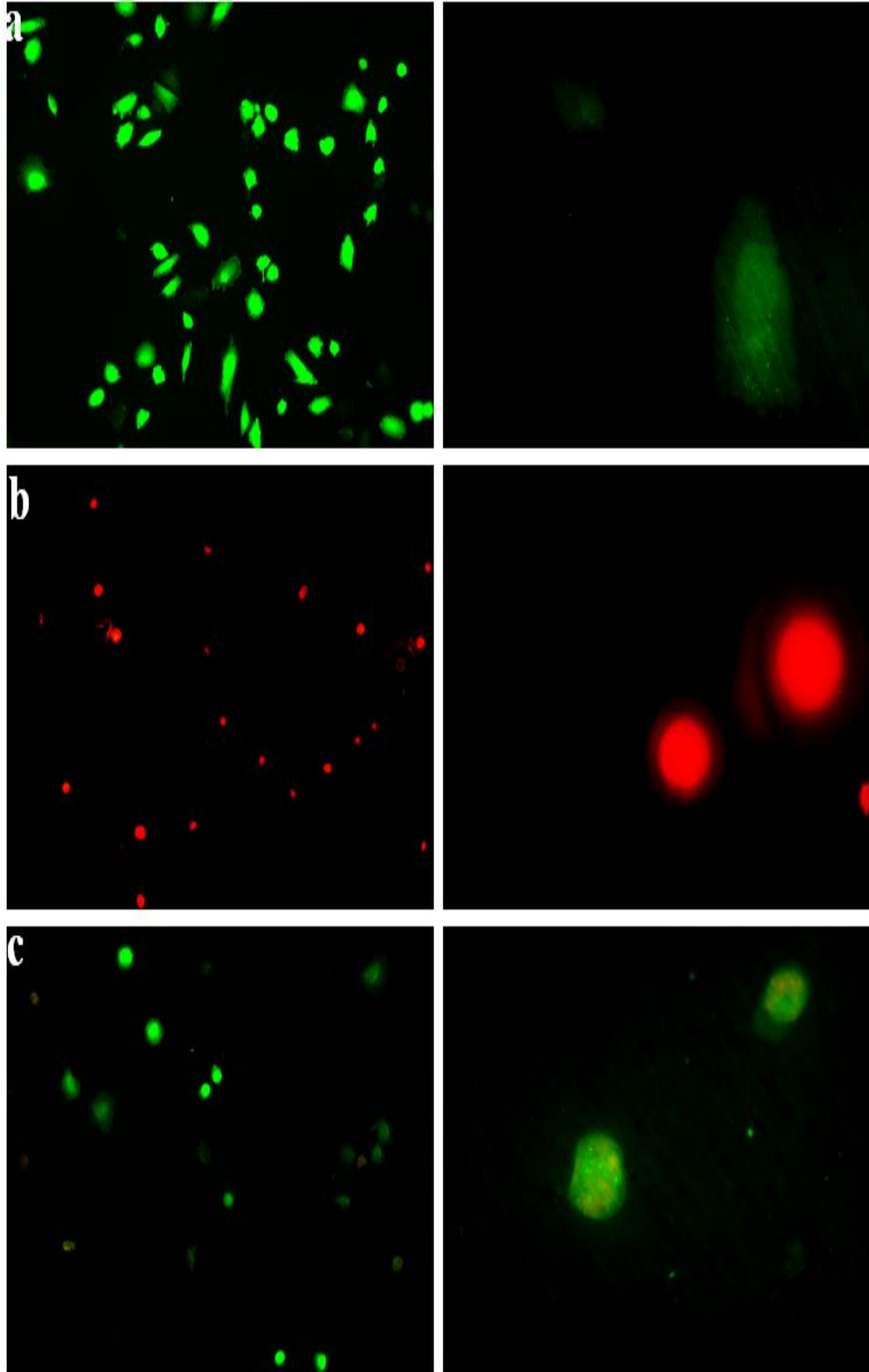
Samples	24 Hour Relative Cell Density	72 Hour Relative Cell Density
Ti ₆ Al ₄ V	36.67 \pm 5.51	65.6 \pm 12.54
HAP 50W, SiC 15W, MgO 50W	17.33 \pm 3.21	20 \pm 6.96*
HAP 50W, SiC 15W, MgO 25W	34 \pm 6.24	36 \pm 8.86*
HAP 50W, TiO ₂ 25W, MgO 25W	72.33 \pm 22.68	72.2 \pm 16.69
HAP 50W, TiO ₂ 25W, MgO 50W	62.33 \pm 5.77	67.8 \pm 11.12

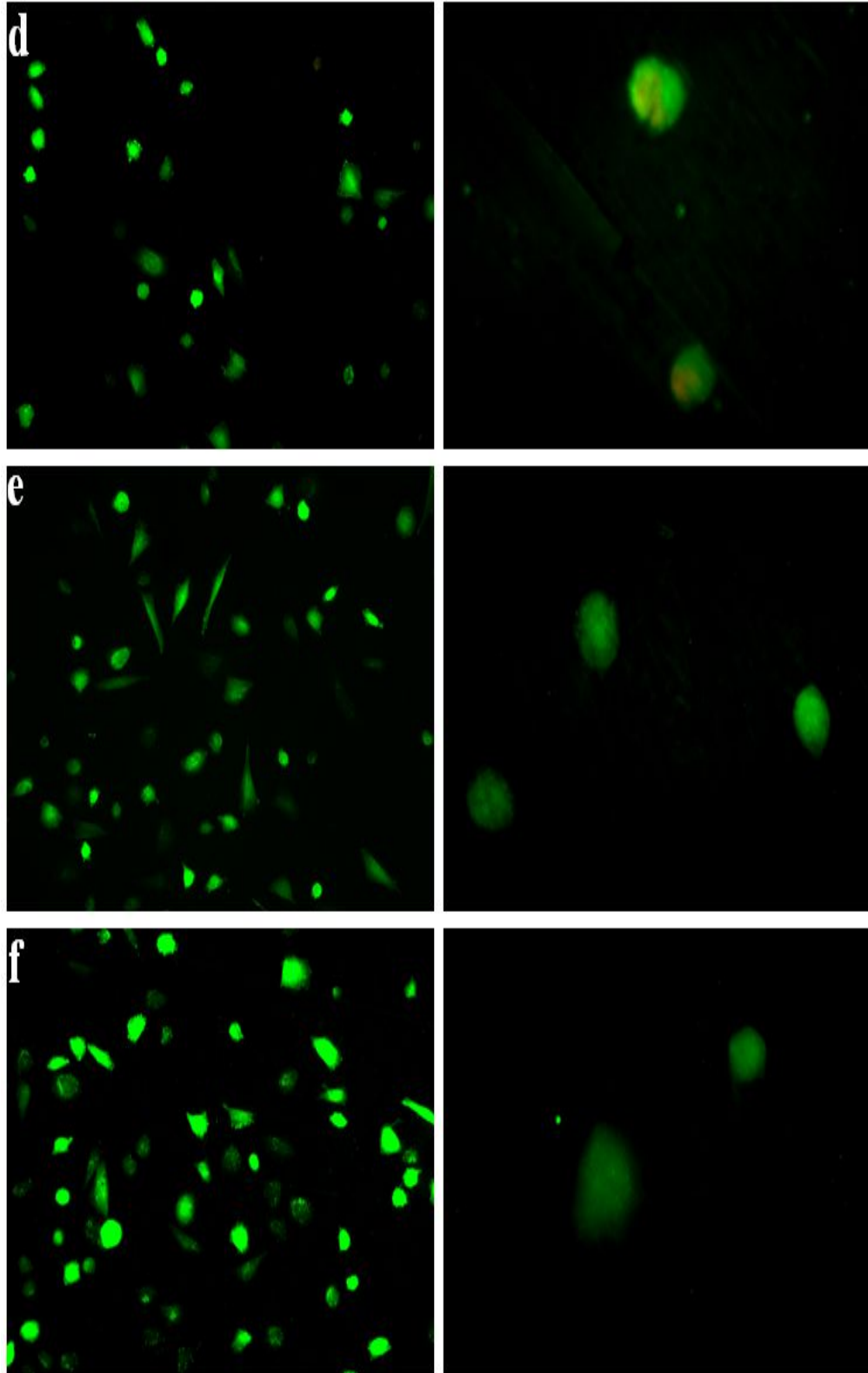
3.1.2 Cell viability assay on coated Ti₆Al₄V discs

Our results showed that the cultured SaOS-2 cells' viabilities were significantly poorer on hydroxyapatite 50W, silicon carbide 15W and magnesium oxide 50W (83.19% and 72.18%, respectively) and hydroxyapatite 50W, silicon carbide 15W and magnesium oxide 25W (91.96% and 94.17%, respectively) coated surfaces than on the uncoated Ti₆Al₄V surface after 24 hours and 72 hours of incubation (see Figure 3.5, Figure 3.8, Table 3.2 and Table 3.3). Additionally, SaOS-2 cell viability on hydroxyapatite 50W, titanium dioxide 25W and magnesium oxide 25W (100% and 99.31%) and hydroxyapatite 50W, titanium dioxide 25W and magnesium oxide 50W (98.19% and 98.19%) coated samples was not significantly different compared to uncoated Ti₆Al₄V (99.19% and 98.74%), respectively, after the same time (Figure 3.5, Figure 3.8, Table 3.2 and Table 3.3). Moreover, cell viability after both 24 hours and 72 hours was significantly different on hydroxyapatite 50W, silicon carbide 15W and magnesium oxide 50W (P=0.0028 and P=0.0029, respectively) and hydroxyapatite 50W, silicon carbide 15W and magnesium oxide 25W (P=0.0037 and P=0.0312, respectively) samples compared to the Ti₆Al₄V alloy. On the other hand, after 24 hours and 72 hours the cell viability on hydroxyapatite 50W, titanium dioxide 25W and magnesium oxide 25W (P=0.2073 and P=0.6065) and hydroxyapatite 50W, titanium dioxide 25W and magnesium

oxide 50W (P=0.2576 and P=0.5794) samples was not significantly different compared to Ti₆Al₄V (Figure 3.5 and Figure 3.8).

Twenty four-hour live cell density (live cell density is the number of vital cells per field of view) on hydroxyapatite 50W, silicon carbide 15W and magnesium oxide 50W (P=0.0001) and hydroxyapatite 50W, silicon carbide 15W and magnesium oxide 25W (P=0.0004) coated samples was significantly lower than on the Ti₆Al₄V sample. The cell densities on both hydroxyapatite 50W, titanium dioxide 25W and magnesium oxide 25W (P=0.0025) and hydroxyapatite 50W, titanium dioxide 25W and magnesium oxide 50W (P=0.0127) coated surfaces were higher than the Ti₆Al₄V alloy, and were significantly different to Ti₆Al₄V (Figure 3.6). Furthermore, the cell densities on hydroxyapatite 50W, silicon carbide 15W and magnesium oxide 50W (P=<0.0001) and hydroxyapatite 50W, silicon carbide 15W and magnesium oxide 25W (P=0.0442) coatings were also significantly different to those on Ti₆Al₄V, but were not significantly different on hydroxyapatite 50W, titanium dioxide 25W and magnesium oxide 25W (P=0.6872) and hydroxyapatite 50W, titanium dioxide 25W and magnesium oxide 50W (P=0.1732) coatings compared to the Ti₆Al₄V sample after 72 hours (Figure 3.9).





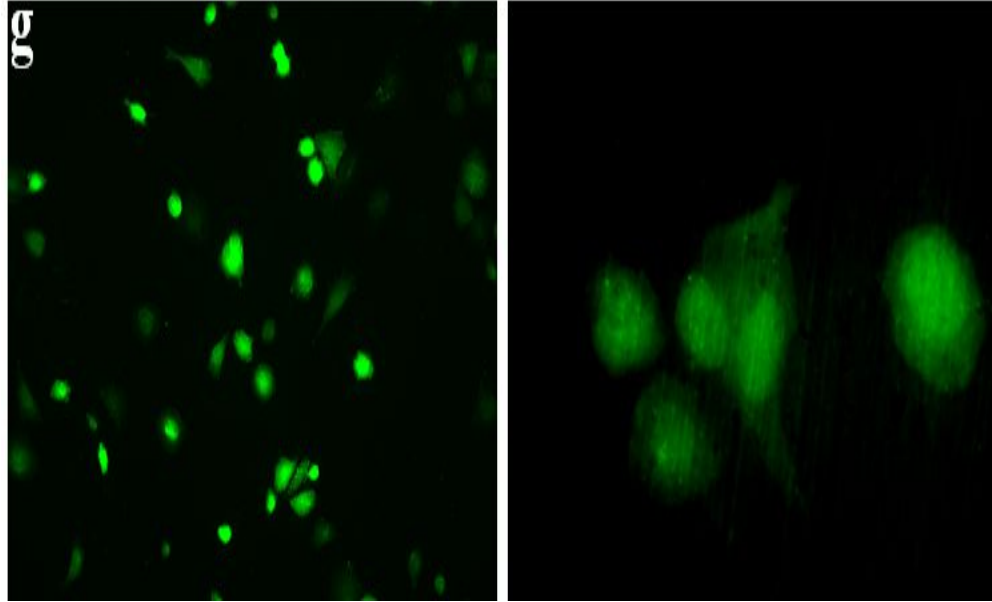


Figure 3.4: Fluorescence photomicrographs of the live/dead cell results of cells cultured on the implant samples or the controls for 24 hours. SaOS-2 cells were seeded onto the various surfaces and were double fluorescence labeled for dead cells (red) with propidium iodide and live cells (green) with calcein-AM. Thereafter, the cells were seen under a fluorescence microscope at 100X magnification (pictures on the left) and at 400X magnification (pictures on the right). Photo a: cells on glass coated with Poly-L-Lysine (NC); Photo b: cells on NC with 8% DMSO; Photo c: HAP 50W, SiC 15W, MgO 50W; Photo d: HAP 50W, SiC 15W, MgO 25W; Photo e: HAP 50W, TiO₂ 25W, MgO 25W and Photo f: HAP 50W, TiO₂ 25W, MgO 50W as well as Photo g: Ti₆Al₄V (uncoated titanium disc).

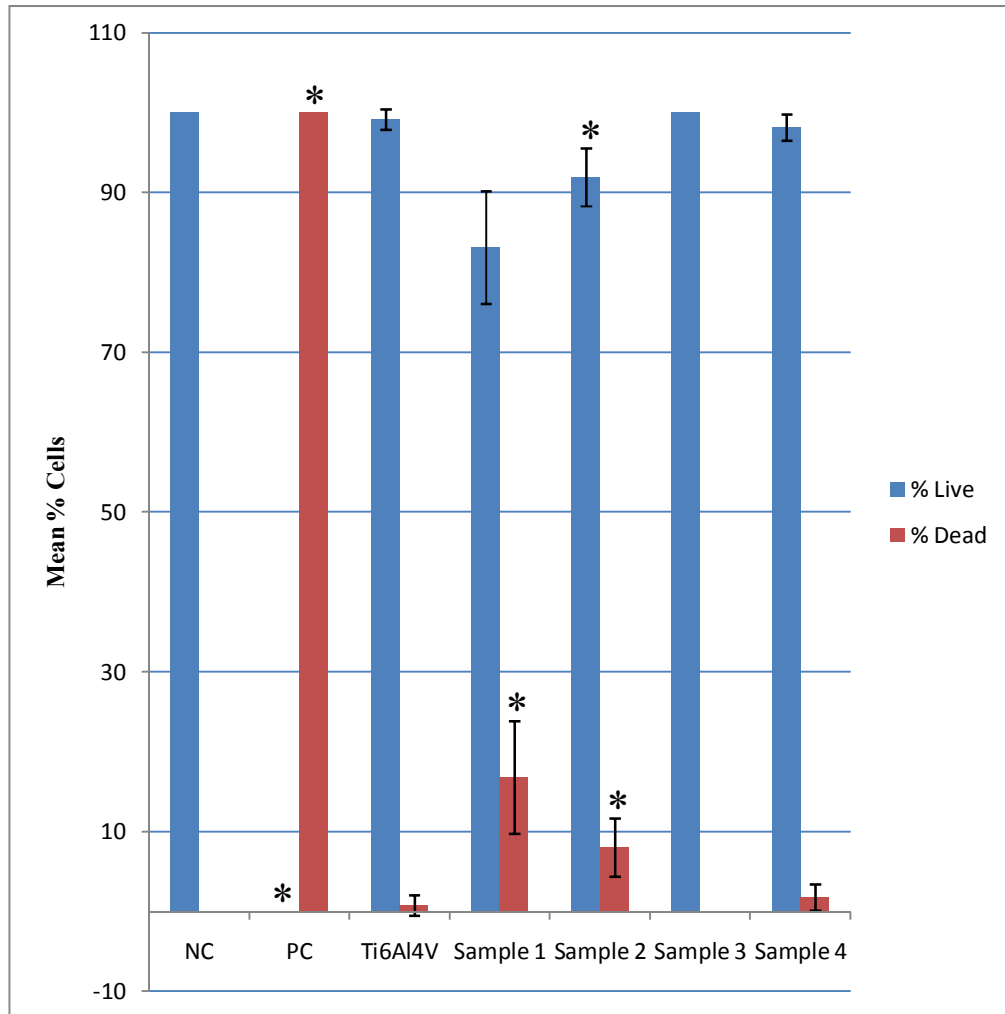


Figure 3.5: Graph showing the percentage of live or dead SaOS-2 cells 24h after seeding on the implant samples. SaOS-2 cells were seeded onto the various surfaces and were double fluorescence labeled for dead cells (red) with propidium iodide and live cells (green) with calcein-AM. Sample NC: glass coated with Poly-L-Lysine (negative control); Sample PC: NC with 8% DMSO (positive control); Sample Ti₆Al₄V: uncoated titanium disc (Ti₆Al₄V); Sample 1: HAP 50W, SiC 15W, MgO 50W; Sample 2: HAP 50W, SiC 15W, MgO 25W; Sample 3: HAP 50W, TiO₂ 25W, MgO 25W; Sample 4: HAP 50W, TiO₂ 25W, MgO 50W. Values are the mean ± standard deviation; n=6; *P< 0.05 when compare to Ti₆Al₄V.

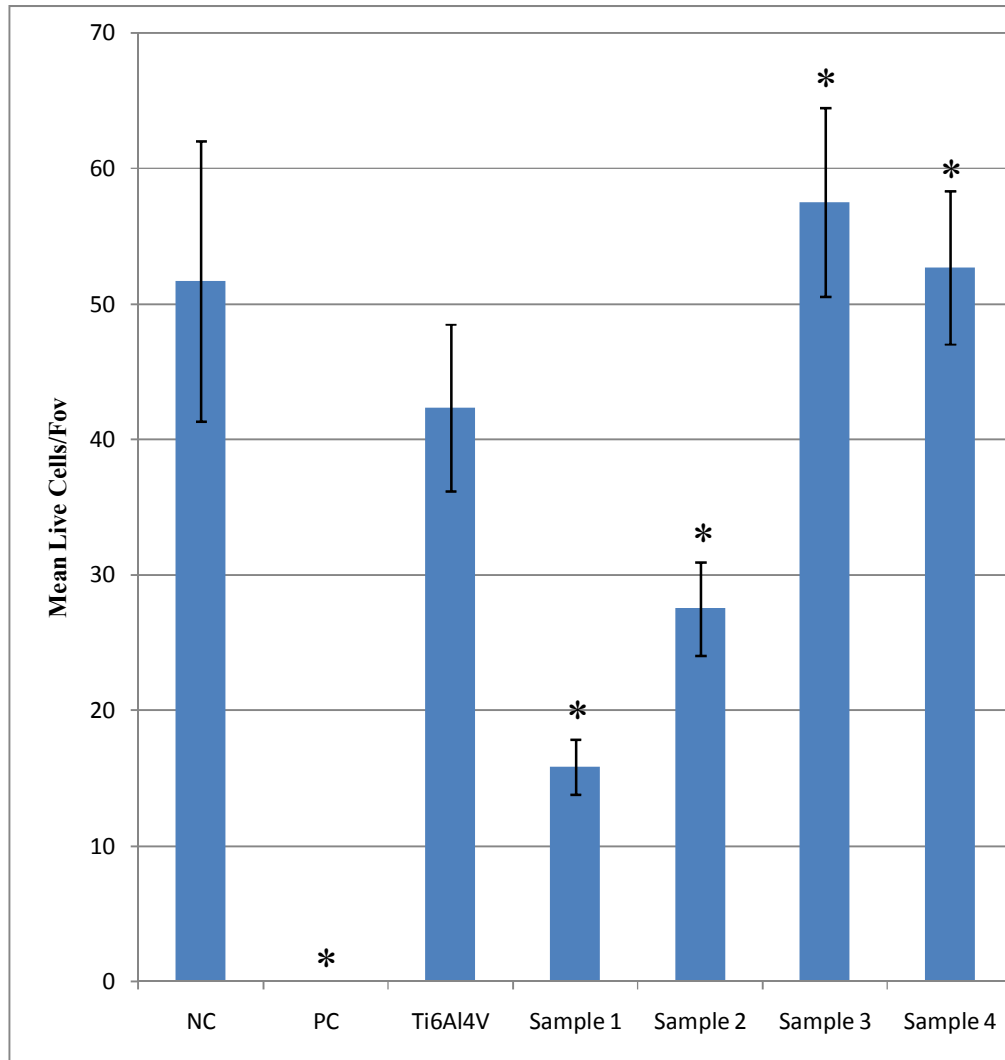
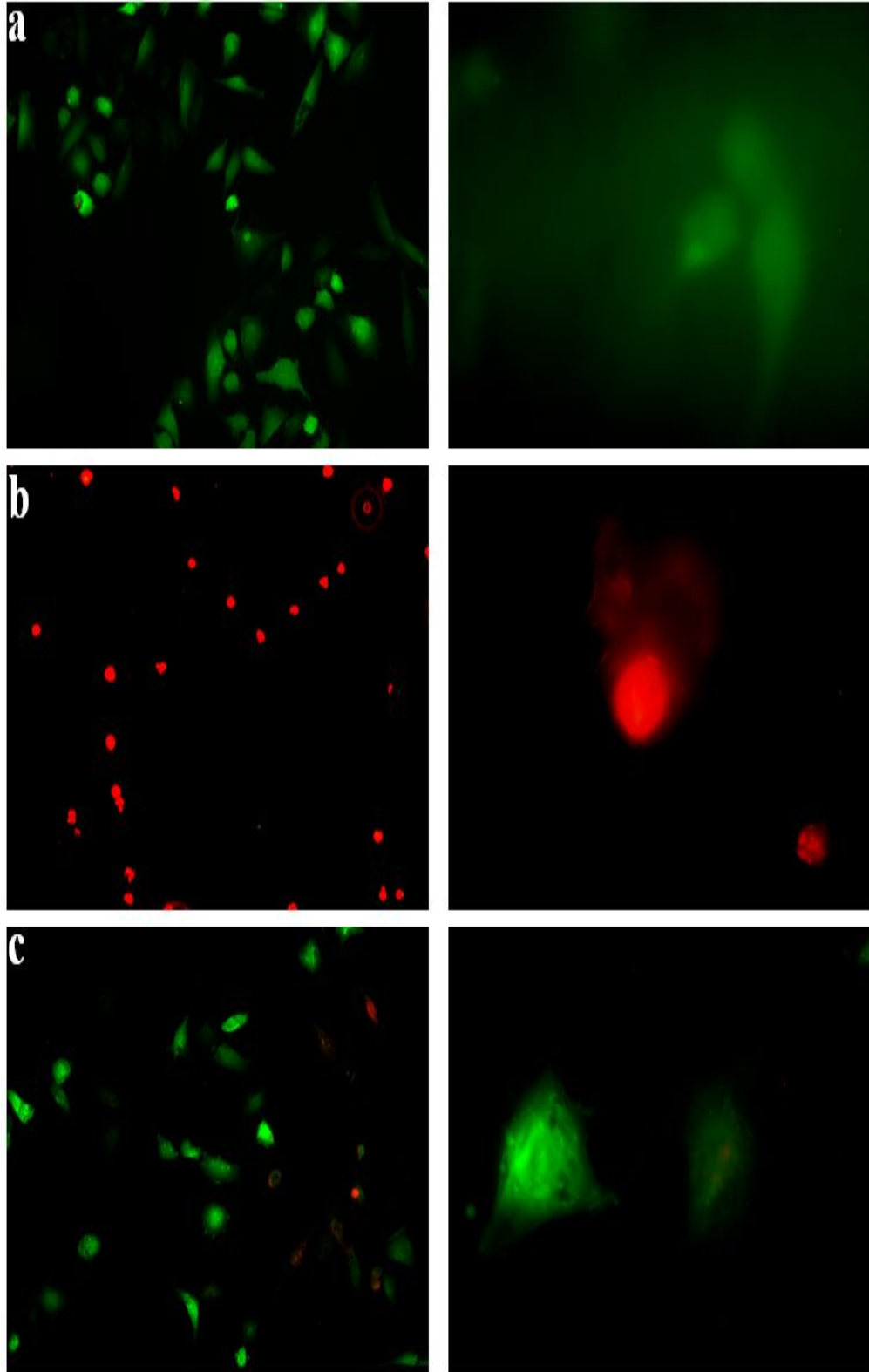
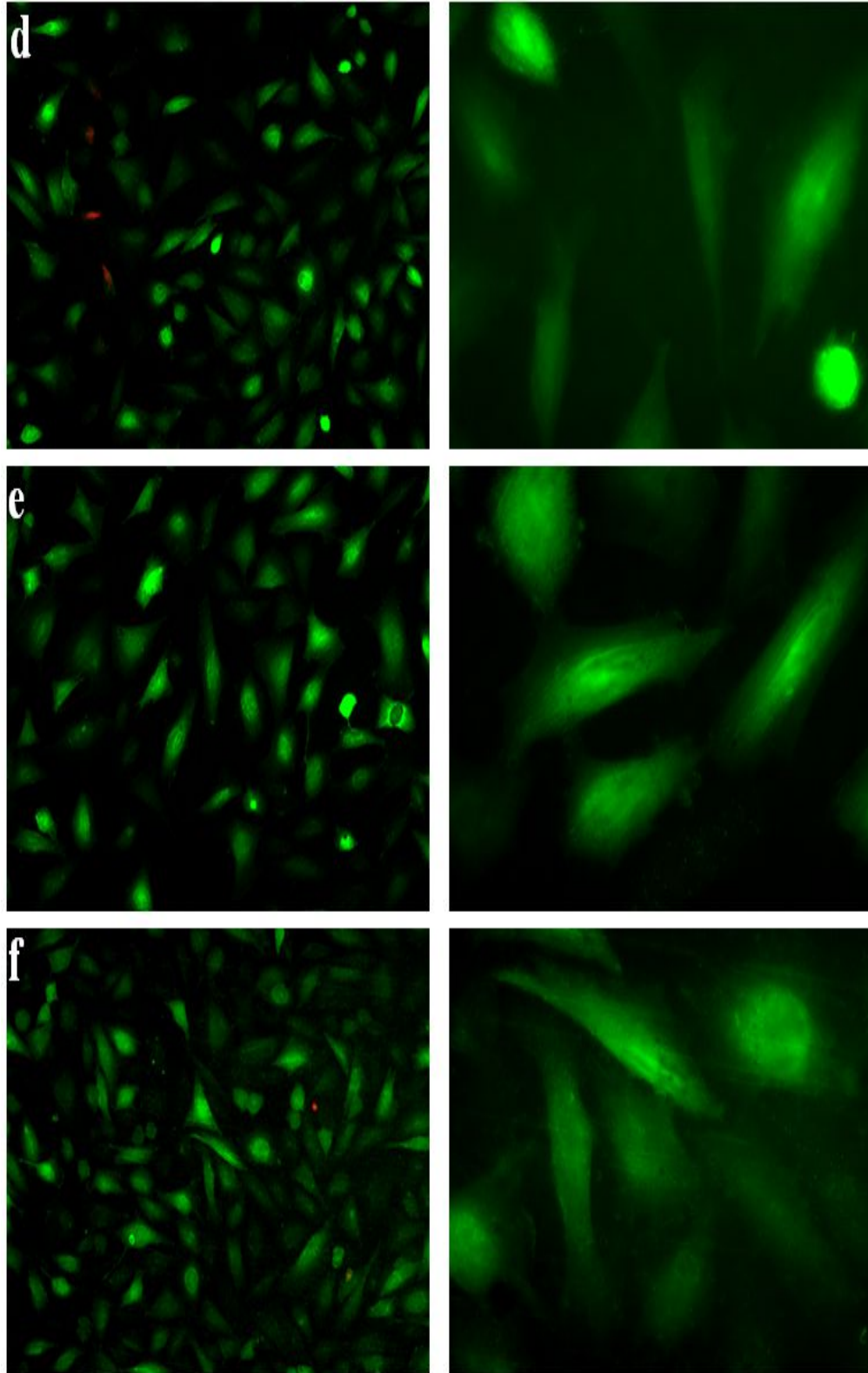


Figure 3.6: Graph showing the relative live cell density of cells cultured on the implant samples or the controls for 24 hours. SaOS-2 cells were seeded onto the various surfaces. Sample NC: glass coated with Poly-L-Lysine (negative control); Sample PC: NC with 8% DMSO (positive control); Sample Ti₆Al₄V: uncoated titanium disc (Ti₆Al₄V); Sample 1: HAP 50W, SiC 15W, MgO 50W; Sample 2: HAP 50W, SiC 15W, MgO 25W; Sample 3: HAP 50W, TiO₂ 25W, MgO 25W; Sample 4: HAP 50W, TiO₂ 25W, MgO 50W. Values are the mean ± standard deviation; n=6; *P< 0.05 when compare to Ti₆Al₄V.





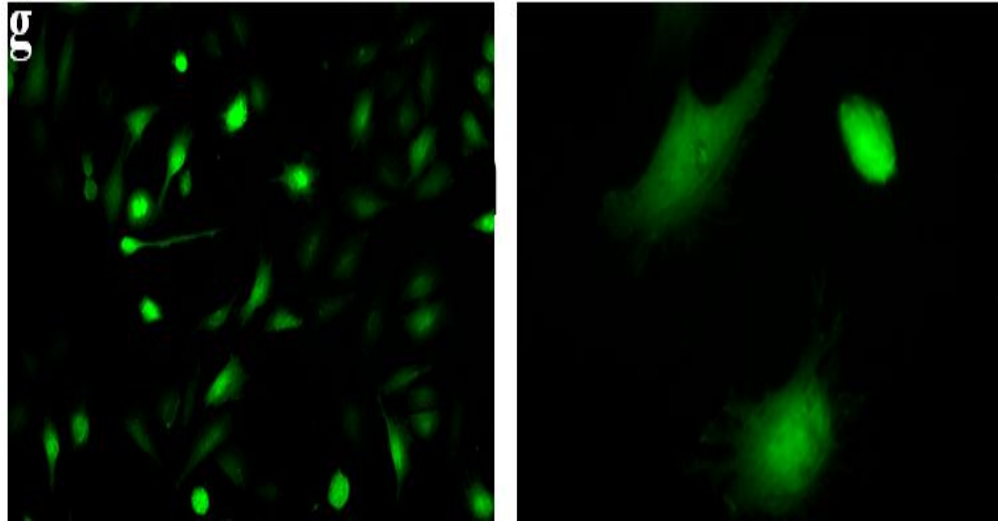


Figure 3.7: Fluorescence photomicrographs of the live/dead cell results of cells cultured on the implant samples or the controls for 72 hours. SaOS-2 cells were seeded onto the various surfaces and were double fluorescence labeled for dead cells (red) with propidium iodide and live cells (green) with calcein-AM. Thereafter, the cells were seen under a fluorescence microscope at 100X magnification (pictures on the left) and at 400X magnification (pictures on the right). Photo a: cells on glass coated with Poly-L-Lysine (NC); Photo b: cells on NC with 8% DMSO; Photo c: HAP 50W, SiC 15W, MgO 50W; Photo d: HAP 50W, SiC 15W, MgO 25W; Photo e: HAP 50W, TiO₂ 25W, MgO 25W and Photo f: HAP 50W, TiO₂ 25W, MgO 50W as well as Photo g: Ti₆Al₄V (uncoated titanium disc).

UNIVERSITY of the
WESTERN CAPE

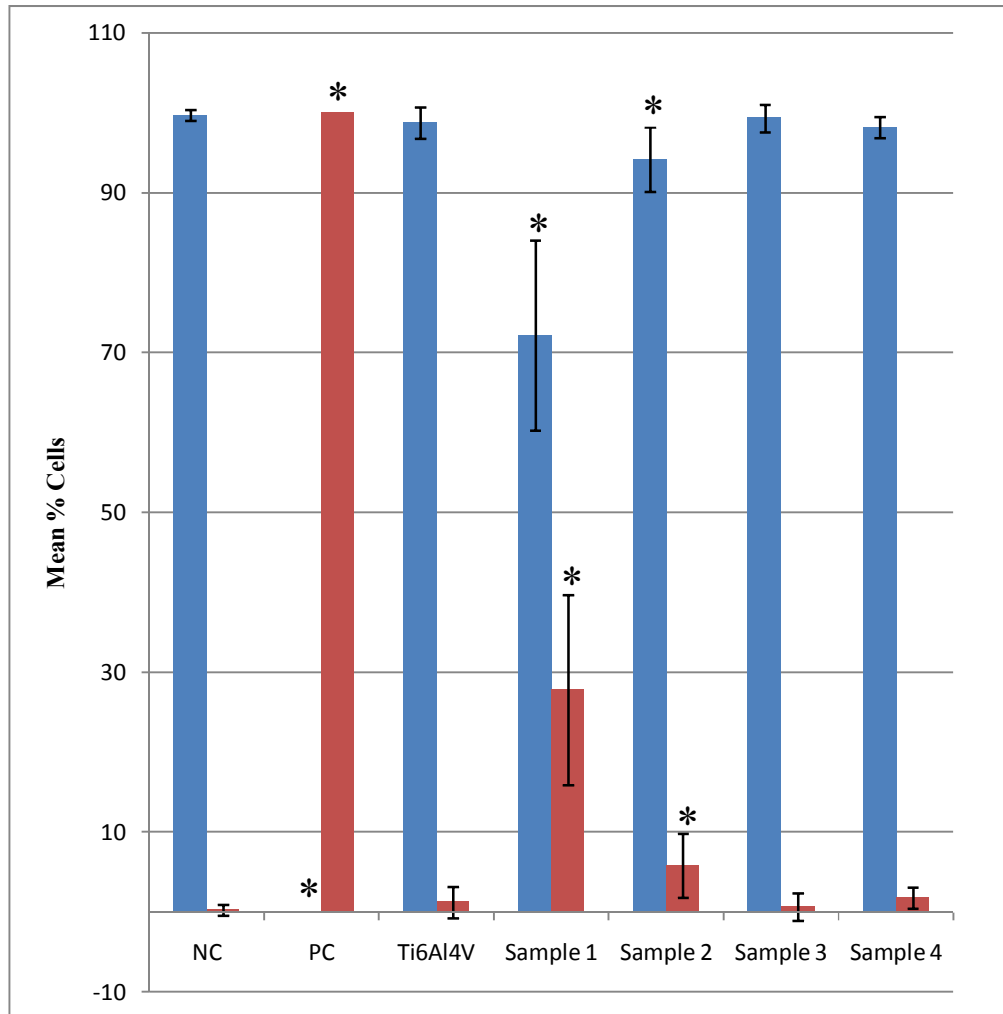


Figure 3.8: Graph showing the percentage of live or dead SaOS-2 cells 72h after seeding on the implant samples. SaOS-2 cells were seeded onto the various surfaces and were double fluorescence labeled for dead cells (red) with propidium iodide and live cells (green) with calcein-AM. Sample NC: glass coated with Poly-L-Lysine (negative control); Sample PC: NC with 8% DMSO (positive control); Sample Ti₆Al₄V: uncoated titanium disc (Ti₆Al₄V); Sample 1: HAP 50W, SiC 15W, MgO 50W; Sample 2: HAP 50W, SiC 15W, MgO 25W; Sample 3: HAP 50W, TiO₂ 25W, MgO 25W; Sample 4: HAP 50W, TiO₂ 25W, MgO 50W. Values are the mean ± standard deviation; n=6; *P< 0.05 when compare to Ti₆Al₄V.

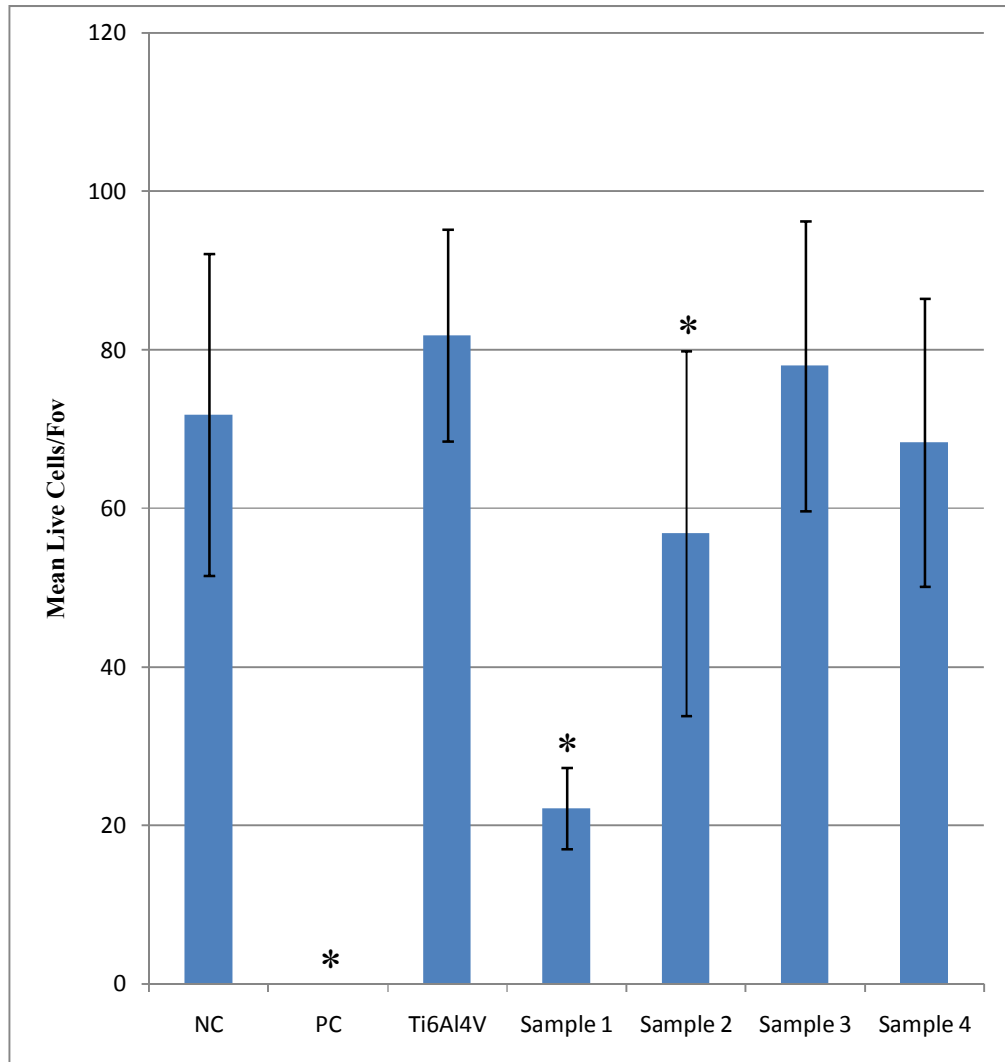


Figure 3.9: Graph showing the relative live cell density of cells cultured on the implant samples or the controls for 72 hours. SaOS-2 cells were seeded onto the various surfaces. Sample NC: glass coated with Poly-L-Lysine (negative control); Sample PC: NC with 8% DMSO (positive control); Sample Ti₆Al₄V: uncoated titanium disc (Ti₆Al₄V); Sample 1: HAP 50W, SiC 15W, MgO 50W; Sample 2: HAP 50W, SiC 15W, MgO 25W; Sample 3: HAP 50W, TiO₂ 25W, MgO 25W; Sample 4: HAP 50W, TiO₂ 25W, MgO 50W. Values are the mean ± standard deviation, n=6; *P< 0.05 when compare to Ti₆Al₄V.

Table 3.2: Table showing the percentage of live and dead cells on the implant samples and controls after 24 hours of cell culture. Results were calculated from PI and Calcein-AM staining data and are presented as mean \pm standard deviation; n=6; *P< 0.05 when compare to Ti₆Al₄V.

24 hours	% Live	% Dead	Relative Live Cell Density
NC	100 \pm 0	0 \pm 0	51.67 \pm 10.35
PC	0 \pm 0*	100 \pm 0*	0 \pm 0*
Ti ₆ Al ₄ V	99.19 \pm 1.26	0.81 \pm 1.26	42.33 \pm 6.15
HAP 50W, SiC 15W, MgO 50W	83.19 \pm 7.04*	16.81 \pm 7.04*	15.83 \pm 2.04*
HAP 50W, SiC 15W, MgO 25W	91.96 \pm 3.63*	8.04 \pm 3.63*	27.5 \pm 3.45*
HAP 50W, TiO ₂ 25W, MgO 25W	100 \pm 0	0 \pm 0	57.5 \pm 6.98*
HAP 50W, TiO ₂ 25W, MgO 50W	98.19 \pm 1.61	1.81 \pm 1.61	52.67 \pm 5.64*

Table 3.3: Table showing the percentage of live and dead cells on the implant samples and controls after 72 hours of cell culture. Results were calculated from PI and Calcein-AM staining data and are presented as mean \pm standard deviation; n=6; *P< 0.05 when compare to Ti₆Al₄V.

72 hours	% Live	% Dead	Relative Live Cell Density
NC	99.72 \pm 0.68	0.28 \pm 0.68	71.83 \pm 20.34
PC	0 \pm 0*	100 \pm 0*	0 \pm 0*
Ti ₆ Al ₄ V	98.74 \pm 1.96	1.26 \pm 1.96	81.83 \pm 13.35
HAP 50W, SiC 15W, MgO 50W	72.18 \pm 11.86*	27.82 \pm 11.86*	22.17 \pm 5.15*
HAP 50W, SiC 15W, MgO 25W	94.17 \pm 4.02*	5.83 \pm 4.02*	56.83 \pm 23.03*
HAP 50W, TiO ₂ 25W, MgO 25W	99.31 \pm 1.70	0.69 \pm 1.70	78 \pm 18.30
HAP 50W, TiO ₂ 25W, MgO 50W	98.19 \pm 1.32	1.81 \pm 1.32	68.33 \pm 18.17

3.2 Microbiology tests

After isolating the bacterial colonies, the Gram stain was used to confirm purity of the bacterial species used in this study, together with a light microscopic examination. Figure 3.10 shows Gram stains of the microbes used in this thesis.

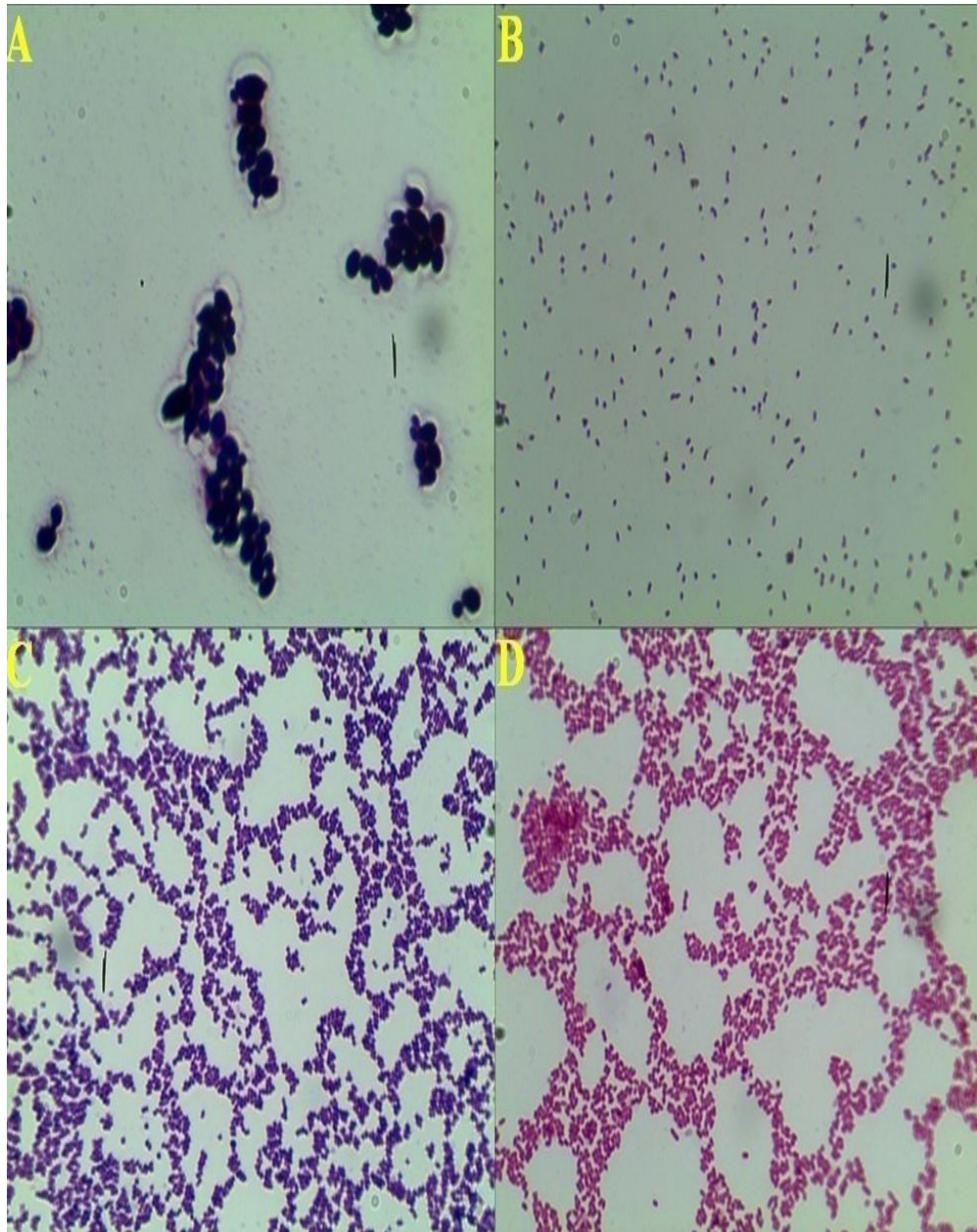


Figure 3.10: Gram staining photos: A, *C. albicans* (ATCC 90028). B, *S. sanguinis* (ATCC 10556). C, *S. aureus* (ATCC 8539). D, *E. coli* (ATCC 25922).

3.2.1 *Candida albicans* susceptibility results

Candida albicans was resistant to all samples tested (including the uncoated disc), but was susceptible to the positive control (a paper disc loaded with 25 µg fluconazole), refer to Figure 3.11. Our results showed that the inhibition zones of *C. albicans* were 0mm in diameter for all samples tested (refer to Table 3.4). Nonetheless, as shown in Table 3.4, the inhibition zone of *C. albicans* was 48mm in diameter for fluconazole.

It should be noted that *C. albicans* colonies were observed making direct contact with all samples tested. Furthermore, the apparent clear zones seen in Figure 3.11 are artifacts due to movement of the agar plates and discs.



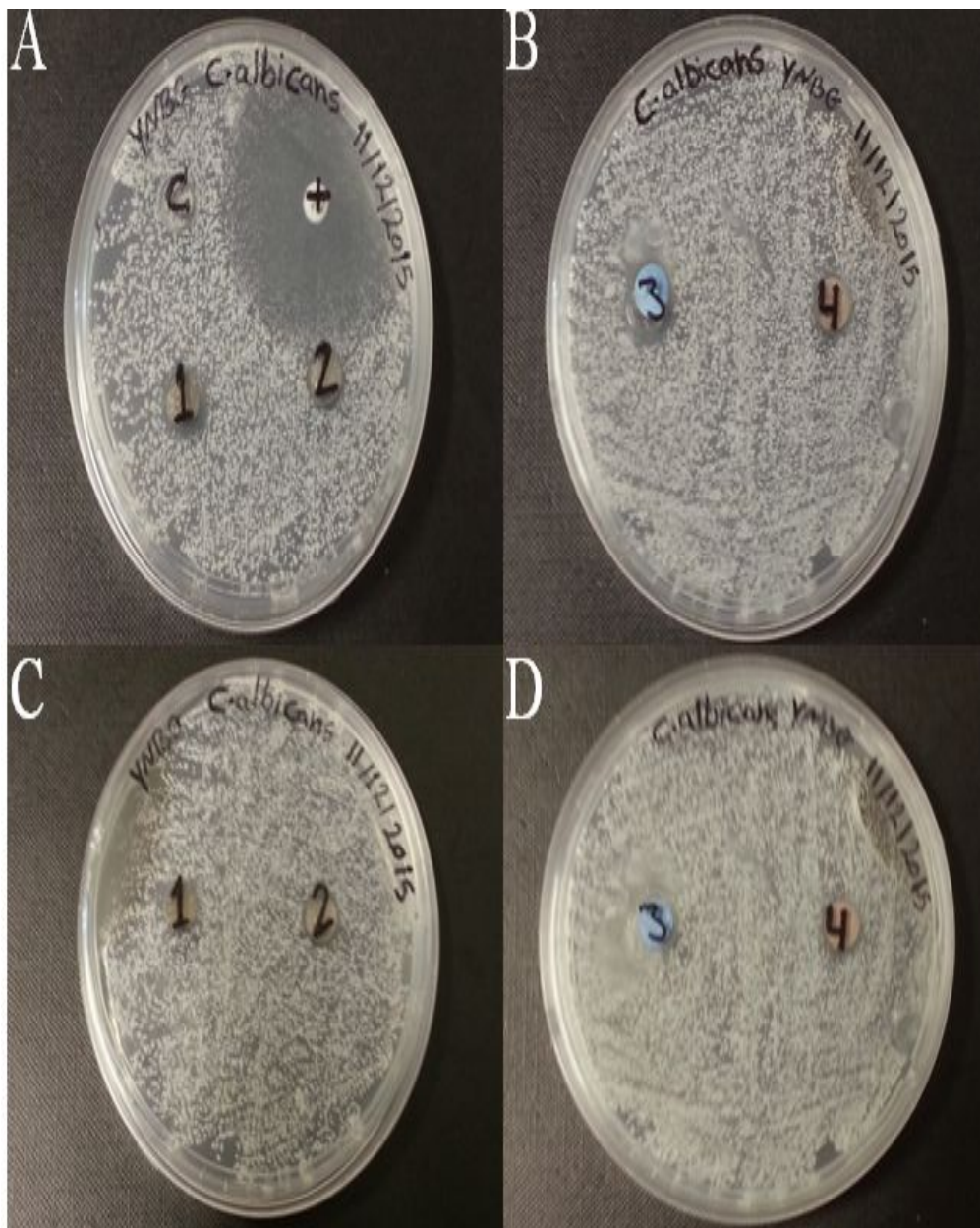


Figure 3.11: Photographs of Petri dishes, showing inhibition of *Candida albicans* growth on YNBG medium in the presence of samples and a control. Plate A, c: uncoated titanium disc; pc (+): fluconazole filter paper disc (positive control); 1: HAP 50W, SiC 15W, MgO 50W; 2: HAP 50W, SiC 15W, MgO 25W. Plate B, 3: HAP 50W, TiO₂ 25W, MgO 25W; 4: HAP 50W, TiO₂ 25W, MgO 50W. Plate C, 1: HAP 50W, SiC 15W, MgO 50W; 2: HAP 50W, SiC 15W, MgO 25W. Plate D, 3: HAP 50W, TiO₂ 25W, MgO 25W; 4: HAP 50W, TiO₂ 25W, MgO 50W. *Candida albicans* was resistant to all samples tested, as well as the uncoated disc. However, *C. albicans* was susceptible to the positive control (FCA25µg).

3.2.2 *Streptococcus sanguinis* susceptibility results

The results for *S. sanguinis* showed inhibition zones of 0mm in diameter for all samples assayed; with the exception of the 30 µg cefuroxime positive control (see Figure 3.12), which showed an inhibition zone of 40mm in diameter (see Table 3.4). Consequently, *S. sanguinis* showed resistance to each of the samples.

It should be noted that *S. sanguinis* colonies were observed making direct contact with all samples tested.



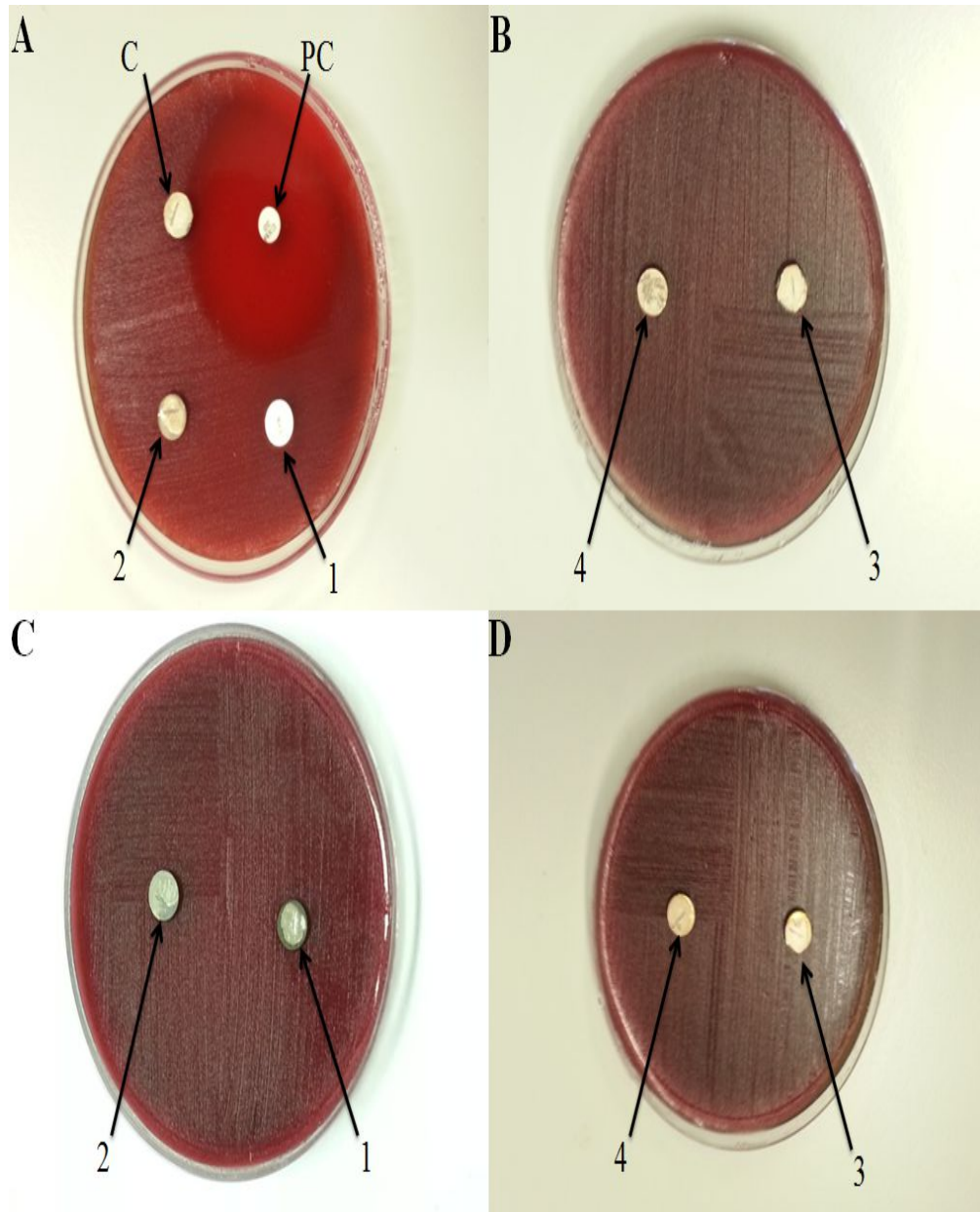
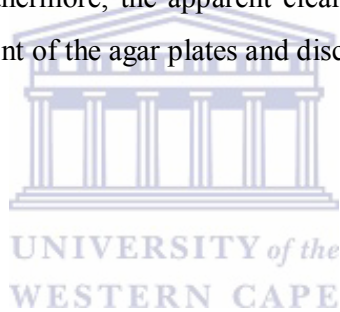


Figure 3.12: Photographs of Petri dishes, showing inhibition of *Streptococcus sanguinis* growth on CAB medium in the presence of samples and a control. Plate A, c: uncoated titanium disc; pc (+): cefuroxime filter paper disc (positive control); 1: HAP 50W, SiC 15W, MgO 50W; 2: HAP 50W, SiC 15W, MgO 25W. Plate B, 3: HAP 50W, TiO₂ 25W, MgO 25W; 4: HAP 50W, TiO₂ 25W, MgO 50W. Plate C, 1: HAP 50W, SiC 15W, MgO 50W; 2: HAP 50W, SiC 15W, MgO 25W. Plate D, 3: HAP 50W, TiO₂ 25W, MgO 25W; 4: HAP 50W, TiO₂ 25W, MgO 50W. *Streptococcus sanguinis* was resistant to all samples tested, as well as the uncoated disc. However, *S. sanguinis* was susceptible to the positive control (CXM 30µg).

3.2.3 *Staphylococcus aureus* susceptibility results

The *S. aureus* experiments showed no inhibition zones (0mm in diameter) for any of the samples tested (as shown in Table 3.4 and Figure 3.13). On the other hand, the growth inhibition zone diameter was 31mm for the positive control (30 µg cefuroxime) (as displayed in Table 3.4). Therefore, *S. aureus* was resistant to hydroxyapatite 50W, silicon carbide 15W, magnesium oxide 50W sample, hydroxyapatite 50W, silicon carbide 15W and magnesium oxide 25W sample, hydroxyapatite 50W, Titanium dioxide 25W, magnesium oxide 25W sample, hydroxyapatite 50W, Titanium dioxide 25W, magnesium oxide 50W sample and the uncoated sample.

It should be noted that *S. aureus* colonies were observed making direct contact with all samples tested. Furthermore, the apparent clear zones seen in Figure 3.13 are artifacts due to movement of the agar plates and discs.



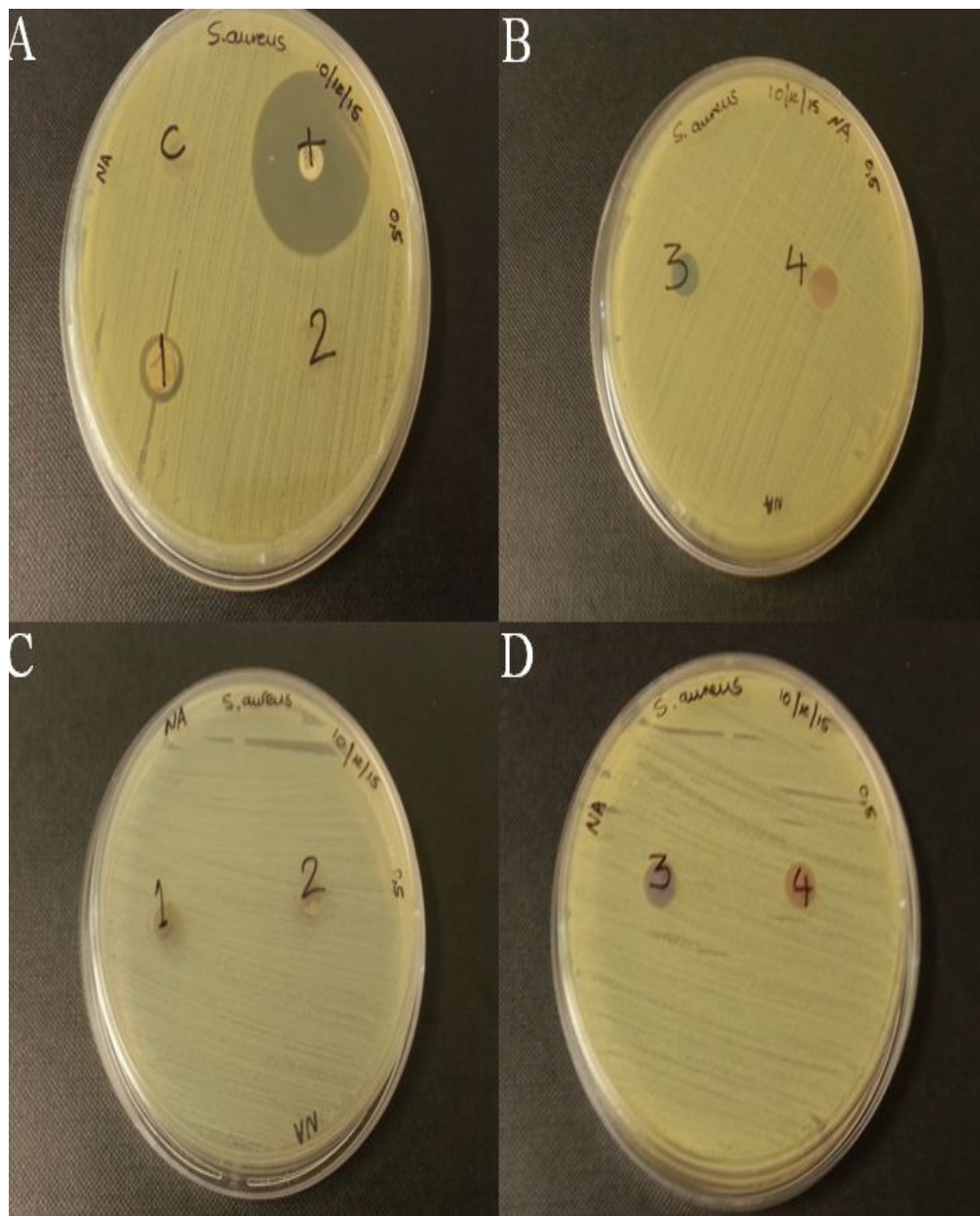


Figure 3.13: Photographs of Petri dishes, showing inhibition of *Staphylococcus aureus* growth on CAB medium in the presence of samples and a control. Plate A, c: uncoated titanium disc; pc (+): cefuroxime filter paper disc (positive control); 1: HAP 50W, SiC 15W, MgO 50W; 2: HAP 50W, SiC 15W, MgO 25W. Plate B, 3: HAP 50W, TiO₂ 25W, MgO 25W; 4: HAP 50W, TiO₂ 25W, MgO 50W. Plate C, 1: HAP 50W, SiC 15W, MgO 50W; 2: HAP 50W, SiC 15W, MgO 25W. Plate D, 3: HAP 50W, TiO₂ 25W, MgO 25W; 4: HAP 50W, TiO₂ 25W, MgO 50W. *Staphylococcus aureus* was resistant to all samples tested, as well as the uncoated disc. However, *S. aureus* was susceptible to the positive control (CXM 30µg).

3.2.4 *Escherichia coli* susceptibility results

Escherichia coli was resistant to all the samples assayed in this thesis, except for the positive control (30 µg cefuroxime). The diameter of the *E. coli* growth inhibition zones were 0mm for all the samples tested, including the uncoated discs (revealed in Table 3.4 and Figure 3.14). However, *E. coli*'s inhibition zone was 25mm in diameter for cefuroxime (as shown in Table 3.4).

It should be noted that *E. coli* colonies were observed making direct contact with all samples tested.



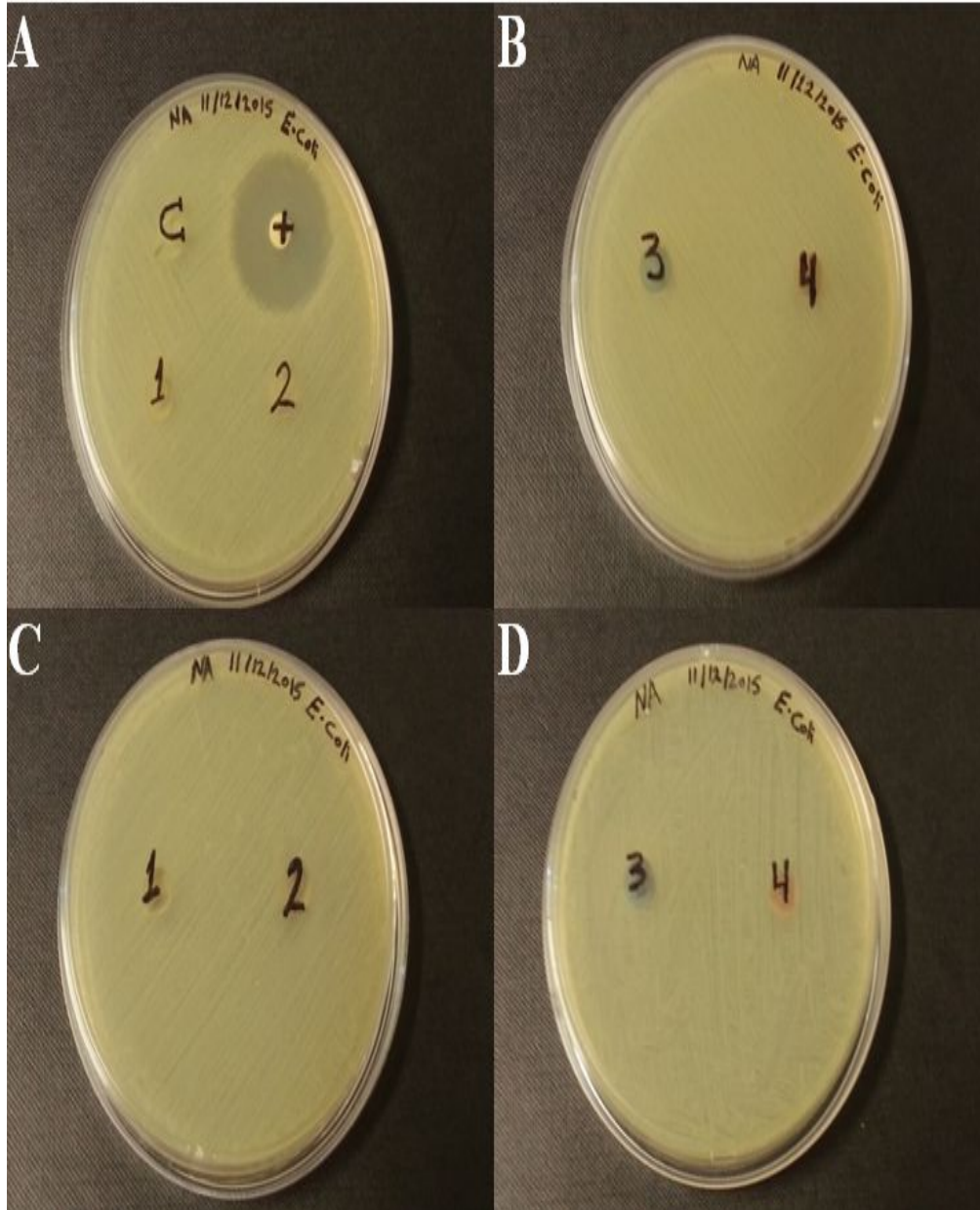


Figure 3.14: Photographs of Petri dishes, showing inhibition of *Escherichia coli* growth on CAB medium in the presence of samples and a control. Plate A, c: uncoated titanium disc; pc (+): cefuroxime filter paper disc (positive control); 1: HAP 50W, SiC 15W, MgO 50W; 2: HAP 50W, SiC 15W, MgO 25W. Plate B, 3: HAP 50W, TiO₂ 25W, MgO 25W; 4: HAP 50W, TiO₂ 25W, MgO 50W. Plate C, 1: HAP 50W, SiC 15W, MgO 50W; 2: HAP 50W, SiC 15W, MgO 25W. Plate D, 3: HAP 50W, TiO₂ 25W, MgO 25W; 4: HAP 50W, TiO₂ 25W, MgO 50W. *Escherichia coli* was resistant to all samples tested, as well as the uncoated disc. However, *E. coli* was susceptible to the positive control (CXM 30µg).

Table 3.4: Inhibition zone diameters of sample discs against *C. albicans*, *S. sanguinis*, *S. aureus* and *E. coli*.

Microbe	Test sample zone of inhibition (mm)					
	HAP 50W, SiC 15W, MgO 50W	HAP 50W, SiC 15W, MgO 25W	HAP 50W, TiO ₂ 25W, MgO 25W	HAP 50W, TiO ₂ 25W, MgO 50W	C	Pos Control
<i>C. albicans</i>	0	0	0	0	0	48
<i>S. sanguinis</i>	0	0	0	0	0	40
<i>S. aureus</i>	0	0	0	0	0	31
<i>E. coli</i>	0	0	0	0	0	25



CHAPTER 4: Discussion

4.1 Osteoblast-based assays

Human osteosarcoma (SaOS-2) cells were used as a model for osteoblasts *in vitro*, to measure the endpoints of cell adhesion and cell viability in cells exposed either to the new sample coatings or to uncoated Ti₆Al₄V. The new implant coatings were deposited onto the surfaces of Ti₆Al₄V alloy discs, because this is the most common biomaterial used in both orthopedic and dental implants (Al-Sanabani *et al.* 2013; Boyd *et al.* 2015).

When titanium is exposed to air, a thin titanium dioxide layer is immediately formed on their surfaces (Bruschi *et al.* 2015; Mandracci *et al.* 2016; Monsees, 2016). In addition, man-made TiO₂ coatings can also be deposited onto implant surfaces by various techniques; the most widely used being plasma spray, low pressure chemical vapor deposition and magnetron sputtering (Mandracci *et al.* 2016). The application of titanium dioxide (TiO₂) coatings to titanium dental implant surfaces has been studied in recent years with the intension of increasing osseointegration or to prevent bacterial attachment onto the implant surfaces (Mandracci *et al.* 2016).

Due to their good bioactivity and biocompatibility, other compounds, such as hydroxyapatite ceramics, have also been tested as biomaterial implant coatings in order to enhance bone implant contact (Al-Sanabani *et al.* 2013; Bruschi *et al.* 2015; Mandracci *et al.* 2016). Moreover, hydroxyapatite (HAP) is an inorganic compound used to produce bone-like coatings due to it being a major compound found in bone (Cruz *et al.* 2016). Metal implant surfaces can be coated with hydroxyapatite by using different techniques such as the micro-arc-oxidation (MAO), plasma spray, magnetron sputtering, sol-gel and pulsed laser deposition (Azem *et al.* 2014; Bruschi *et al.* 2015; Vladescu *et al.* 2015; Mandracci *et al.* 2016). Despite the benefits of hydroxyapatite coatings, there are some disadvantages that restrict the use of HAP in biomedical applications (Azem *et al.* 2014). Hydroxyapatite has poor mechanical properties, low corrosion resistance, a high dissolution rate between the HAP coating and metallic substrate, they are

brittle, have low tensile strength and fracture toughness (Azem *et al.* 2014; Family *et al.* 2012).

Silicon carbide (SiC) is a compound that can be used for coatings in biomedical applications due to its good resistance to harsh mechanical and chemical environments, low dissolution rate and high mechanical properties (Azem *et al.* 2014). Furthermore, SiC coatings are chemically inert and are expected to have good biocompatibility. The magnetron sputtering technique is used to deposit the SiC coatings onto metal implants (Azem *et al.* 2014). Although silicon carbide also has other attractive mechanical properties, SiC has not been used as the bulk material of load bearing bone implants (Will *et al.* 2010).

This work tested the biocompatibility of novel implant coatings that were prepared using radio frequency magnetron sputtering onto the Ti₆Al₄V alloy with three cathodes. All the implant coatings tested contain hydroxyapatite (50W) and magnesium oxide (either 25W or 50W), as well as either silicon carbide (15W) or titanium dioxide (25W). Different wattages applied during magnetron sputtering will result in different elemental composition of the final coating. The higher the wattage, the more of the specific element/compound will be deposited on the surface.

The cell attachment results from this thesis indicate that SaOS-2 cells did not have proper morphology on hydroxyapatite 50W, silicon carbide 15W and magnesium oxide 50W sample (refer to Figure 3.2a and 3.3a) and that their cell numbers were lower than those on hydroxyapatite 50W, silicon carbide 15W and magnesium oxide 25W sample. The relative live cell density on HAP 50W, SiC 15W and MgO 50W surface showed significantly lower density than on HAP 50W, SiC 15W and MgO 25W surface after 24 hours and 72 hours of incubation, respectively (see Figure 3.6, Figure 3.9, Table 3.2 and Table 3.3). Additionally, the cell density results of both HAP 50W, SiC 15W, MgO 50W and HAP 50W, SiC 15W, MgO 25W samples showed significantly lower numbers than uncoated Ti₆Al₄V sample after the same incubation times (Figure 3.6, Figure 3.9, Table 3.2 and Table 3.3).

The cells on hydroxyapatite 50W, silicon carbide 15W and magnesium oxide 25W sample were spread over larger areas and their actin fibers were more extended than those on hydroxyapatite 50W, silicon carbide 15W and magnesium oxide 50W sample. Both the Samples 1 (hydroxyapatite 50W, silicon carbide 15W, magnesium oxide 50W) and 2 (hydroxyapatite 50W, silicon carbide 15W, magnesium oxide 25W), contained the same compounds of hydroxyapatite 50W and silicon carbide 15W. In addition, the Sample 1 and Sample 2 had different wattages of magnesium oxide, which were 50W for Sample 1 and 25W for Sample 2. Therefore, magnetron sputtering with higher wattages of magnesium oxide led to a surface coating that seems to be detrimental to biocompatibility as measured by cell morphology and viability. Furthermore, lower wattages of magnesium oxide, with silicon carbide but without TiO₂, showed similar morphology to, but lower cell density than Ti₆Al₄V.

In the current study, the cell morphology results of hydroxyapatite 50W, titanium dioxide 25W, magnesium oxide 25W and hydroxyapatite 50W, titanium dioxide 25W, Magnesium oxide 50W samples were similar to each other as well as to Ti₆Al₄V (as shown in Figures 3.2 and 3.3). The cell population on hydroxyapatite 50W, titanium dioxide 25W, magnesium oxide 25W surface showed significantly higher density than on hydroxyapatite 50W, titanium dioxide 25W, magnesium oxide 50W surface after 24 hours and 72 hours, respectively (Figure 3.6, Figure 3.9, Table 3.2 and Table 3.3). Likewise, the cell numbers on both hydroxyapatite 50W, titanium dioxide 25W, magnesium oxide 25W coating and hydroxyapatite 50W, titanium dioxide 25W, magnesium oxide 50W coating showed significantly higher density than the standard Ti₆Al₄V alloy after 24 hours of incubation (see Figure 3.6 and Table 3.2). On the other hand, after 72 hours the cell density on hydroxyapatite 50W, titanium dioxide 25W, magnesium oxide 25W sample and hydroxyapatite 50W, titanium dioxide 25W, magnesium oxide 50W sample did not show any significant difference compared to Ti₆Al₄V (Figure 3.9 and Table 3.3). During the first 24 hours of incubation, the cells that attached to uncoated Ti₆Al₄V were fewer and they may have reproduced slower than the cells on HAP 50W, TiO₂ 25W, MgO 25W sample and HAP 50W, TiO₂ 25W, MgO 50W sample.

On the other hand, the cells on the uncoated Ti₆Al₄V sample seems to divide faster in between 24 hours and 72 hours of incubation than cells on hydroxyapatite 50W, titanium dioxide 25W, magnesium oxide 25W and hydroxyapatite 50W, titanium dioxide 25W, magnesium oxide 50W samples did, probably because there was not enough space on Sample 3 (HAP 50W, TiO₂ 25W and MgO 25W) and Sample 4 (HAP 50W, TiO₂ 25W and MgO 50W) to divide in. The cells on hydroxyapatite 50W, titanium dioxide 25W, magnesium oxide 25W and hydroxyapatite 50W, titanium dioxide 25W, magnesium oxide 50W surfaces possibly produced more extracellular matrix than the cells on the uncoated surface, because the cells on Sample 3 (HAP 50W, TiO₂ 25W and MgO 25W) and Sample 4 (HAP 50W, TiO₂ 25W and MgO 50W) surfaces reached confluency quicker than those on the uncoated surface. This means that they had more time to produce the ECM. Therefore, HAP 50W, TiO₂ 25W, MgO 25W coating and HAP 50W, TiO₂ 25W, MgO 50W coating probably may improve and accelerate the osseointegration, and hence the biocompatibility. Moreover, Sample 3 and Sample 4 were composed of the same compounds of hydroxyapatite 50W and titanium dioxide 25W, but their magnesium oxide content were in different wattages, which were 25W for Sample 3 and 50W for Sample 4. Accordingly, lower wattages of magnesium oxide could most likely lead to improved cell morphology and increase cell density.

On the other hand, although the adherent cells on HAP 50W, SiC 15W and MgO 50W sample were few, as well as not having proper morphology, the cells on HAP 50W, TiO₂ 25W and MgO 50W sample were larger in number and were more spread than those on HAP 50W, SiC 15W and MgO 50W sample. After both 24 hours and 72 hours of incubation, SaOS-2 cell density on HAP 50W, TiO₂ 25W and MgO 50W surface demonstrated significantly higher numbers than on HAP 50W, SiC 15W and MgO 50W surface, respectively. Sample 1 and Sample 4 have the same compounds, but they have one difference: Sample 1 contained silicon carbide, whereas Sample 4 contained titanium dioxide instead. Thus, titanium dioxide could improve attachment of cells compared to silicon carbide. The Sample 2 (HAP 50W, SiC 15W and MgO 25W) versus Sample 3 (HAP 50W, TiO₂ 25W and MgO 25W)

results were in agreement with the Sample 1 (HAP 50W, SiC 15W and MgO 50W) versus Sample 4 (HAP 50W, TiO₂ 25W and MgO 50W) results in this regard; as Sample 2 had fewer, poorer spread cells with significantly lower cell density after 24 hours than Sample 3. Once more, Sample 2 and Sample 3 were the same but for Sample 2 containing SiC, whereas Sample 3 contained TiO₂.

Additionally, the SaOS-2 cell attachment results on the uncoated Ti₆Al₄V surface were demonstrated better biocompatibility and their cell morphology was more spread than those on HAP 50W, SiC 15W and MgO 50W sample (Figure 3.2e and Figure 3.3e). A hydroxyapatite 50W, silicon carbide 15W and magnesium oxide 25W sample was as good as the uncoated sample with regards to cell attachment. Therefore, HAP 50W, SiC 15W and MgO 50W sample and HAP 50W, SiC 15W and MgO 25W sample did not improve cell morphology or density. Moreover, HAP 50W, TiO₂ 25W and MgO 25W sample and HAP 50W, TiO₂ 25W and MgO 50W sample have improved cell attachment compared to the uncoated metal alloy. Hence, titanium dioxide appeared to counteract the detrimental effects of magnesium oxide on cell adhesion.

Titanium alloys usually have a titanium dioxide layer on their surfaces, which forms when the titanium surfaces are exposed to air or water (Shibata and Tanimoto, 2015). This titanium dioxide layer is hydrophilic; which means that a drop of water placed onto such a surface would have a contact angle of less than 90° (Shibata and Tanimoto, 2015). When a titanium implant is placed inside a surgical site, the sodium and phosphate ions, of biological fluids, concentrate at the TiO₂ layer (Shibata and Tanimoto, 2015). The high concentrations of sodium and phosphate at the TiO₂ layer promote adsorption of extracellular matrix (ECM) proteins at that site (Shibata and Tanimoto, 2015). According to Shibata and Tanimoto (2015), bone cells have specific receptors that bind to ECM proteins to stimulate the formation of focal adhesion points by those cells. Furthermore, the focal adhesion contacts of cells have the ability to attach those cells to the titanium surface. This process could explain how the titanium dioxide (TiO₂) retained cell

adhesion on Sample 4 (hydroxyapatite 50W, titanium dioxide 25W, magnesium oxide 50W), despite the harmful effects of magnesium oxide.

According to Monsees (2016), cytotoxicity assays are important to evaluate the biocompatibility of novel implant coatings. The cytotoxicity in this thesis was assessed by fluorescence labeling, using propidium iodide (PI) for dead cells (red fluorescence) and calcein-AM for live cells (green fluorescence). After either 24 hours or 72 hours of incubation, live and dead cells were directly viewed and photographed under a fluorescence microscope. Thereafter, live and dead cells were counted on the photomicrographs.

The results obtained from the cell viability assay indicate that cells seeded on hydroxyapatite 50W, silicon carbide 15W and magnesium oxide 50W surface showed significantly lower viability than cells grown on uncoated Ti_6Al_4V after 24 hours and 72 hours of incubation. Additionally, SaOS-2 cell viability on hydroxyapatite 50W, silicon carbide 15W and magnesium oxide 25W surface showed significantly higher percentages than on hydroxyapatite 50W, silicon carbide 15W and magnesium oxide 50W surface after both 24 hours and 72 hours, respectively; but was significantly lower than on the Ti_6Al_4V sample after the same incubation times. As was already established, Sample 1 and Sample 2 had different wattages of MgO (50W and 25W, respectively) and the same wattages of SiC. Hence, the magnesium oxide and silicon carbide coatings could exert a detrimental effect to the osteosarcoma cells. Moreover, silicon carbide would produce the same results between Sample 1 and Sample 2 (because they had the same wattages), but magnesium oxide may account for the drop in cell viability. The results obtained from HAP 50W, TiO_2 25W and MgO 25W coating and HAP 50W, TiO_2 25W and MgO 50W coating were in agreement with HAP 50W, SiC 15W and MgO 50W result and HAP 50W, SiC 15W and MgO 25W result. Furthermore, the coatings with the low concentration of magnesium oxide produced higher cell viability than, the coatings with the high concentration of magnesium oxide.

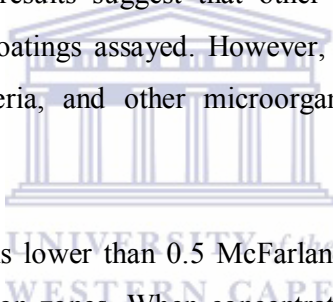
On the other hand, after 24 hours of incubation the percentage of cell viability on hydroxyapatite 50W, silicon carbide 15W and magnesium oxide 50W (Sample 1) coating surface was significantly lower than on hydroxyapatite 50W, titanium dioxide 25W, magnesium oxide 50W (Sample 4) coating surface. The only difference between Sample 1 and Sample 4 was that Sample 1 had silicon carbide whereas Sample 4 had titanium dioxide. The Sample 2 and Sample 3 results were in agreement with the Sample 1 and Sample 4 results (Sample 3 had significantly higher viability than Sample 2, and Sample 2 contained SiC whereas Sample 3 contained TiO₂). Moreover, the cell viability on hydroxyapatite 50W, silicon carbide 15W and magnesium oxide 50W sample was also significantly different compared to hydroxyapatite 50W, titanium dioxide 25W, magnesium oxide 50W sample after 72 hours. Consequently, the titanium dioxide coatings (Sample 4 and Sample 3) could increase the SaOS-2 cell viability compared to SiC coatings (Sample 1 and Sample 2). In addition, the SiC coatings showed no improvement in cell viability, because they reduced cell viability. Therefore, the SiC coatings were not as good as Ti₆Al₄V in terms of biocompatibility.

The results in this thesis indicated that the magnesium oxide and silicon carbide coatings did not improve cell morphology, cell density or cell viability. Therefore, the novel implant coatings containing MgO and SiC did not improve the biocompatibility compared to standard Ti₆Al₄V alloy. On the other hand, titanium dioxide appears to neutralise the apparent harmful effects of magnesium oxide on cell adhesion, morphology and viability. Moreover, the titanium dioxide coatings actually improved the biocompatibility of the Ti₆Al₄V alloy by accelerating initial cell adhesion.

4.2 Antimicrobial susceptibility testing

The agar disc diffusion technique was used to test the potential antimicrobial properties of novel implant coatings against *Candida albicans*, *Streptococcus sanguinis*, *Staphylococcus aureus* and *Escherichia coli*. These microorganisms were selected for this study because they can be present in the oral cavity and may, subsequently, cause implant failure and related infections.

The present study found that the inhibition zones of the microorganisms tested were 0mm in diameter for all the sample coatings as well as uncoated Ti₆Al₄V. The photographs of Petri dishes appear to show small zones of inhibition around some of the samples (e.g. Figure 3.12 A), but these zones did not actually indicate antimicrobial activity, since they were not present before the photos were taken. As mentioned in Chapter 3, these zones only appeared when the plates were moved. On the other hand, the positive controls (30µg cefuroxime for the bacteria and 25µg fluconazole for *Candida albicans*, both antimicrobials in filter paper) showed clear growth inhibition zones for all microbial strains tested. Therefore, the positive control results prove that the Kirby-Bauer assay worked and that the new implant coatings truly had no proven antimicrobial properties (at least against the four microbes tested). Our results suggest that other microorganisms could also be resistant to the novel coatings assayed. However, this study has only tested four commonly found bacteria, and other microorganism strains might instead be susceptible.



Microbial concentrations lower than 0.5 McFarland standard were also used, and also showed no inhibition zones. When concentrations lower than 0.5 McFarland standard were used, too few microbial colonies were present to see the potential edge of the growth inhibition zones for most of microorganisms tested.

Earlier studies, conducted by Stanić *et al.* (2011) and by Iqbal *et al.* (2014), showed that pure hydroxyapatite (HAP) had no proven antimicrobial activity. All of the dental implant coatings tested in this thesis also contained hydroxyapatite, but with other compounds (magnesium oxide and either silicon carbide or titanium dioxide) added as well. The studies, by Stanić *et al.* (2011) and Iqbal *et al.* (2014), also used the Kirby-Bauer assay and both tested HAP nanoparticles doped with silver, but Iqbal *et al.* (2014), added zinc as well. Nonetheless, these research groups included controls of pure HAP nanoparticles, which showed no antimicrobial activity, just like the novel HAP coatings tested here. Stanić *et al.* (2011) used *Staphylococcus*

aureus and *Escherichia coli* in their assays, whereas Iqbal *et al.* (2014) used both of these as well as *Candida albicans*, making our results comparable.

In contrast to Stanić *et al.* (2011) and to Iqbal *et al.* (2014), Tin-Oo *et al.* (2007) reported that HAP did have antimicrobial activity, but they used a different assay (namely, the Miles and Misra method). When hydroxyapatite was used by Tin-Oo *et al.* (2007), it was a powder dissolved in a broth, which was subsequently inoculated with a bacterial suspension. Hydroxyapatite powder has a higher surface area-to-volume ratio than a HAP powder compressed into discs does (as used by both Stanić *et al.* 2011 and Iqbal *et al.* 2014). A hydroxyapatite powder would produce more interaction between the HAP and bacteria than a compressed disc would. Thus, the Miles and Misra method, as used by Tin-Oo *et al.* (2007), is likely more sensitive to antimicrobial activity than the disc diffusion method. Additionally, Tin-Oo *et al.* (2007) employed *Streptococcus mutans* to test antimicrobial activity of their samples, which we speculate may have been more susceptible to HAP than either *Staphylococcus aureus*, *Escherichia coli* or *Candida albicans*.

In another study, by Ahmad and Sardar, (2013), a titanium dioxide (TiO₂) nanoparticle solution showed antimicrobial activity against *E. coli*. Their study utilized the well diffusion method, where wells were cut out of inoculated agar plates followed by addition of TiO₂ samples into the holes as drops of TiO₂ suspensions. TiO₂ nanoparticles were dissolved in distilled water such that they likely became more soluble in the agar than an equivalent TiO₂ disc would have been, as would be used in the Kirby-Bauer assay. Subsequently, the TiO₂ suspensions could probably travel further through the agar than they would from equivalent discs. Therefore, nanoparticles suspensions could likely increase growth inhibitory activity of TiO₂; thus producing (larger) inhibition zones.

Additionally, a study by Sundrarajan *et al.* (2012), also tested the antimicrobial activity of nanoparticles (MgO) using a well diffusion assay, also against *E. coli*, as well as *S. aureus*. Sundrarajan *et al.* (2012), discovered that smaller sized MgO

nanoparticles produced larger bacterial growth inhibition zones than the bigger sized MgO nanoparticles did. This discovery supports the argument that more soluble particles would produce larger growth inhibition zones, since smaller nanoparticles would be more soluble in the agar than bigger nanoparticles. Additionally, smaller nanoparticles could penetrate bacterial walls more easily than bigger nanoparticles, which would then interfere with the cells' reproduction.

In the present study, samples of the Ti₆Al₄V alloy were coated either with hydroxyapatite, silicon carbide and magnesium oxide; or with hydroxyapatite, titanium dioxide and magnesium oxide (in two different elemental compositions due to different applied wattages during the magnetron sputtering process). The novel implant coatings were unable to inhibit microbial growth in Kirby-Bauer assays, probably because they were likely insoluble in the agar. Additionally, the new sample coatings used in this study were not in nanoparticle powder form, which would have a high surface area-to-volume ratio; the implant coatings Sample 1 (hydroxyapatite 50W, silicon carbide 15W and magnesium oxide 50W), Sample 2 (hydroxyapatite 50W, silicon carbide 15W and magnesium oxide 25W), Sample 3 (hydroxyapatite 50W, titanium dioxide 25W, magnesium oxide 25W) and Sample 4 (hydroxyapatite 50W, titanium dioxide 25W, magnesium oxide 50W) have much lower surface areas instead. Hence, both of these factors (i.e. high surface area and solubility) likely contributed to Tin-Oo *et al.* (2007), Ahmad and Sardar (2013), and Sundrarajan *et al.* (2012) finding antimicrobial activity of their respective nanoparticles; whereas Sample 1, Sample 2, Sample 3 and Sample 4 did not show antimicrobial properties, despite the fact that Sample 1, Sample 2, Sample 3 and Sample 4 contained some of the same compounds that the mentioned authors tested. Moreover, when HAP nanoparticles were compressed into discs, they showed no antimicrobial activity, because they did not have a high surface areas or solubility either (like Sample 1, Sample 2, Sample 3 and Sample 4). This agrees with the proposed explanation presented here.

CHAPTER 5: Conclusion

- In conclusion, the results obtained from this study indicate that on coatings containing HAP and either silicon carbide or titanium oxide, the higher the concentration of additional magnesium oxide, the worse the coatings are for osseointegration, and therefore biocompatibility.
- On the other hand, the coatings that contained both magnesium oxide and titanium dioxide could improve osseointegration compared to the MgO coatings without titanium dioxide.
- Moreover, the coatings containing titanium dioxide were better for biocompatibility than the SiC coatings were. Hence, the coatings that contained SiC were worse for biocompatibility than the coatings that contained TiO₂.
- After 24 hours, the cell densities on Sample 3 (hydroxyapatite 50W, titanium dioxide 25W, magnesium oxide 25W) and Sample 4 (hydroxyapatite 50W, titanium dioxide 25W, magnesium oxide 50W) were significantly higher than on the uncoated Ti₆Al₄V sample. Consequently, the coatings containing both titanium dioxide and magnesium oxide could improve osseointegration compared to the uncoated Ti₆Al₄V alloy.
- None of the novel implant coatings tested in this study showed either antibacterial or antimycotic activity. The disc diffusion assay, which relies on solubility to work, was used here to test the antimicrobial activity of these coatings. Therefore, the implant coatings probably were insoluble in agar.
- It is recommended that other assays be carried out on the novel implant coatings tested here, such as more bone-specific assays, scanning electron microscopy, alkaline phosphatase activity of osteoblast-like cells, a TREK sensititre assay, etc.

- Including titanium dioxide in coatings could also be recommended for future implants.



CHAPTER 6: References

Abraham CM (2014). A brief historical perspective on dental implants, their surface coatings and treatments. *The Open Dentistry Journal*, 8: 50–55.

Ahmad R, Sardar M (2013). TiO₂ nanoparticles as an antibacterial agents against *E. coli*. *International Journal of Innovative Research in Science, Engineering and Technology*, 2: 3569–3574.

Akcali A, Huck O, Tenenbaum H, Davideau JL, Buduneli N (2013). Periodontal diseases and stress: a brief review. *Journal of Oral Rehabilitation*, 40: 60–68

Ali SMF, Tanwir F (2012). Oral microbial habitat a dynamic entity. *Journal of Oral Biology and Craniofacial Research*, 2: 181–187.

Al-Makki AAA (2006). A comparative study to evaluate patient satisfaction with conventional dentures and implant retained overdentures. *Master Thesis, University of the Western Cape, South Africa*: 70.

Al-Sanabani JS, Madfa AA, Al-Sanabani FA (2013). Application of calcium phosphate materials in dentistry. *International journal of biomaterials*, 2013: 1–12.

Anselme K (2000). Osteoblast adhesion on biomaterials. *Biomaterials*, 21: 667–681.

Atbayga AMA (2013). In vitro anti-bacterial activity of titanium oxide nanocomposites containing benzalkonium chloride and chlorhexidine gluconate. *Master Thesis, University of the Cape Peninsula of Technology, South Africa*: 63.

Azem FA, Kiss A, Birlik I, Braic V, Luculescu C, Vladescu A (2014). The corrosion and bioactivity behavior of SiC doped hydroxyapatite for dental applications. *Ceramics International*, 40: 15881–15887.

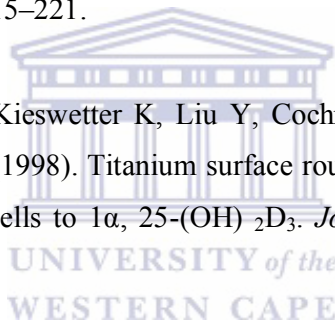
Ballo AM, Omar O, Xia W, Palmquist A (2011). *Dental Implant Surfaces-physicochemical Properties, biological performance and trends*. Implant dentistry– A rapidly evolving practice, InTech: 19–56.

Bang Lee H, Khang G, Ho Lee J (2000). *Polymeric Biomaterials*. The biomedical engineering handbook. 2nd edition, Boca Raton, Bronzino JD: CRC Press LLC.

Bik EM, Long CD, Armitage GC, Loomer P, Emerson J, Mongodin EF, Relman, DA (2010). Bacterial diversity in the oral cavity of 10 healthy individuals. *The ISME Journal*, 4: 962–974.

Bodic F, Hamel L, Lerouxel E, Baslé MF, Chappard D (2005). Bone loss and teeth. *Joint Bone Spine*, 72: 215–221.

Boyan BD, Batzer R, Kieswetter K, Liu Y, Cochran DL, Szmuckler-Moncler S, Dean DD, Schwartz Z (1998). Titanium surface roughness alters responsiveness of MG63 osteoblast-like cells to $1\alpha, 25\text{-(OH)}_2\text{D}_3$. *Journal of Biomedical Materials Research*, 39: 77–85.



Boyd AR, Rutledge L, Randolph LD, Meenan BJ (2015). Strontium-substituted hydroxyapatite coatings deposited via a co-deposition sputter technique. *Materials Science and Engineering: C*, 46: 290–300.

Brånemark PI (1983). Osseointegration and its experimental background. *Journal of Prosthetic Dentistry*, 50: 399–410.

Brånemark R, Brånemark PI, Rydevik B, Myers RR (2001). Osseointegration in skeletal reconstruction and rehabilitation: a review. *Journal of Rehabilitation Research and Development*, 38: 175–182.

Bruschi M, Steinmüller-Nethl D, Goriwoda W, Rasse M (2015). Composition and modifications of dental implant surfaces. *Journal of Oral Implant*, 2015: 1–14.

Carey JC, Michael Cohen M, Curry CJR, Devriendt K, Holmes LB, Verloes A (2009). Elements of morphology: Standard terminology for the lips, mouth, and oral region. *American Journal of Medical Genetics Part A*, 149: 77–92.

Chen CM, Cheng CT, Lin CS, Lin SC, Chiang CC, Luo CA, Tseng CS (2014). Biomechanical effects of bone-implant fitness and screw breakage on the stability and stress performance of the nonstemmed hip system. *Clinical Biomechanics*, 29: 161–169.

Chowdhury MRH, Bhuiyan MI, Saha A, Mosleh IM, Mondol S, Ahmed CS (2014). Identification and analysis of potential targets in *Streptococcus sanguinis* using computer aided protein data analysis. *Advances and Applications in Bioinformatics and Chemistry*, 7: 45–54.

Chug A, Shukla S, Mahesh L, Jadwani S (2013). Osseointegration-molecular events at the bone-implant interface: A review. *Journal of Oral and Maxillofacial Surgery, Medicine, and Pathology*, 25: 1–4.

Clarke B (2008). Normal bone anatomy and physiology. *Clinical journal of the American Society of Nephrology*, 3: S131–S139.

Costa F, Carvalho IF, Montelaro RC, Gomes P, Martins MCL (2011). Covalent immobilization of antimicrobial peptides (AMPs) onto biomaterial surfaces. *Acta Biomaterialia*, 7: 1431–1440.

Craddock HL (2010). Consequences of tooth loss: 2. Dentist considerations-restorative problems and implications. *Dental Update*, 37: 28–32.

Cruz MAE, Ruiz GC, Faria AN, Zancanela DC, Pereira LS, Ciancaglini P, Ramos AP (2016). Calcium carbonate hybrid coating promotes the formation of

biomimetic hydroxyapatite on titanium surfaces. *Applied Surface Science*, 370: 459–468.

Dalby MJ, DI Silvio L, Harper EJ, Bonfield W (2002). In vitro adhesion and biocompatibility of osteoblast-like cells to poly(methylmethacrylate) and poly(ethylmethacrylate) bone cements. *Journal of Materials Science: Materials in Medicine*, 13: 311–314.

Dale BA, Fredericks LP (2005). Antimicrobial peptides in the oral environment: expression and function in health and disease. *Current Issues Molecular Biology*, 7: 119–133.

Davies JE (2003). Understanding peri-implant endosseous healing. *Journal of Dental Education*, 67: 932–949.

Duraccio D, Mussano F, Faga MG (2015). Biomaterials for dental implants: current and future trends. *Journal of Materials Science*, 50: 4779–4812.

Elashi B (2015). The antimicrobial and antifungal efficacy of indigenous plant extracts against *Streptococcus mutans*, *Escherichia coli* and *Candida albicans*. *Master Thesis, University of the Western Cape, South Africa*: 72.

Elias CN, Lima JHC, Valiev R, Meyers MA (2008). Biomedical applications of titanium and its alloys. *Jom*, 60: 46–49.

Elisa CN (2011). *Factors affecting the success of dental implants*. Implant dentistry—A rapidly evolving practice. InTech: 544.

Eslami H, Hashjin MS, Tahriri M, Bakhshi F (2010). Synthesis and characterization of nanocrystalline hydroxyapatite obtained by the wet chemical technique. *Materials Science-Poland*, 28: 5–13.

FadiI-allah SA, Quahtany M, El-Shenawy NS (2013). Surface modification of titanium Plate with anodic oxidation and its application in bone growth. *Journal of biomaterials and Nanobiotechnology*, 4: 74–83.

Family R, Solati-Hashjin M, Nik SN, Nemati A (2012). Surface modification for titanium implants by hydroxyapatite nanocomposite. *Caspian Journal of Internal Medicine*, 3: 460–465.

Felgueiras H (2014). Synthesis and grafting of bioactive polymers to create biomimetic surfaces which can control the host response: Study of the biological mechanisms from the origin of the observed activity. *PhD Thesis, University of the Paris-Nord-Paris XIII*: 198.

Fulmer MT, Ison IC, Hankermayer CR, Constantz BR, Ross J (2002). Measurements of the solubilities and dissolution rates of several hydroxyapatites. *Biomaterials*, 23: 751–755.

Gallardo-Moreno AM, Pacha-Olivenza MA, Saldaña L, Pérez-Giraldo C, Bruque JM, Vilaboa N, González-Martín ML (2009). In vitro biocompatibility and bacterial adhesion of physico-chemically modified Ti6Al4V surface by means of UV irradiation. *Acta Biomaterialia*, 5: 181–192.

Geetha M, Singh AK, Asokamani R, Gogia AK (2009). Ti based biomaterials, the ultimate choice for orthopaedic implants-a review. *Progress in Materials Science*, 54: 397–425.

Glendor Ulf (2009). Aetiology and risk factors related to traumatic dental injuries – a review of the literature. *Dental Traumatology*, 25: 19–31.

Gray H, Standring S, Ellis H, Berkovitz BKB (2005). Gray's anatomy: the anatomical basis of clinical practice. 39th edition, Edinburgh, Elsevier Churchill Livingstone: 1627.

Han MJ, Chung CH, Choi HC (2002). A study on surface alternation of implant screws after function. *Journal of Korean Academy of Prosthodontics*, 40: 275–286.

<http://www.sweetwatersmile.com/Dental-Bridge-Fairhope-AL-9.html> Accessed on August 2015.

http://www.studiodentisticobizioli.it/1/protesi_dentarie_2281138.html Accessed on July 2015.

<http://painlesspetedentist.com/services/removable-partial-dentures/> Accessed on July 2015.

<http://rydedentalcare.com.au/restoratedentistry/dental-extractions/> Accessed on July 2015.

<http://www.bethesdadentalimplantcenter.com/wp-content/uploads/2014/03/dental-implant-procedure.jpg> Accessed on August 2015.

<http://www.bournedentalpractice.co.uk/implant-treatment.asp> Accessed on July 2015.

<http://www.dentalimplantcostarica.com/replacing-multiple-teeth-with-dental-implants/> Accessed on July 2015.

<http://www.gratefuldental.com/services/dental-implants/> Accessed on July 2015.

http://www.vsmpto-tirus.co.uk/products_from_stock.php Accessed on July 2015.

<http://www.webmd.com/oral-health/picture-of-the-teeth> Accessed on May 2015.

Huang HL, Chang YY, Lai MC, Lin CR, Lai CH, Shieh TM (2010). Antibacterial TaN-Ag coatings on titanium dental implants. *Surface and Coatings Technology*, 205: 1636–1641.

Iqbal N, Kadir MRA, Mahmood NH, Salim N, Froemming GR, Balaji HR, Kamarul T (2014). Characterization, antibacterial and in vitro compatibility of zinc–silver doped hydroxyapatite nanoparticles prepared through microwave synthesis. *Ceramics International*, 40: 4507–4513.

Javed F, Romanos GE (2010). The role of primary stability for successful immediate loading of dental implants. A literature review. *Journal of Dentistry*, 38: 612–620.

Jayesh RS, Dhinakarsamy V (2015). Osseointegration. *Journal of Pharmacy and Bioallied Sciences*, 7: S226–S229.

Kabir MA, Hussain MA, Ahmad Z (2012). *Candida albicans*: a model organism for studying fungal pathogens. *International Scholarly Research Network Microbiology*, 2012: 1–15.

Karamian E, Motamedi MRK, Khandan A, Soltani P, Maghsoudi S (2014). An in vitro evaluation of novel NHA/zircon plasma coating on 316L stainless steel dental implant. *Progress in Natural Science: Materials International*, 24: 150–156.

Kargupta R, Bok S, Darr CM, Crist BD, Gangopadhyay K, Gangopadhyay S, Sengupta S (2014). Coatings and surface modifications imparting antimicrobial activity to orthopedic implants. *Wiley Interdisciplinary Reviews: Nanomedicine and Nanobiotechnology*, 6: 475–495.

Kim J, Amar S (2006). Periodontal disease and systemic conditions: a bidirectional relationship. *Odontology*, 94: 10–21.

Kim MH, Park K, Choi KH, Kim SH, Kim SE, Jeong CM, Huh JB (2015). Cell adhesion and in vivo osseointegration of sandblasted/acid etched/anodized dental implants. *International Journal of Molecular Science*, 16: 10324–10336.

Kim RW, Kim HS, Choe HC, Son MK, Chung CH (2011). Microscopic analysis of fractured dental implant surface after clinical use. *Procedia Engineering*, 10: 1955–1960.

Kini U, Nandeesh BN (2012). *Physiology of bone formation, remodeling, and metabolism*. In Radionuclide and hybrid bone imaging. Berlin, Springer Berlin Heidelberg: 29–57.

Ladhani S, Konana OS, Mwarumba S, English MC (2004). Bacteraemia due to *Staphylococcus aureus*. *Archives of Disease in Childhood*, 89: 568–571.

Lee BH, Koshizaki N (2008). Nanostructured hydroxyapatite/TiO₂ composite coating applied to commercially pure titanium by a co-sputtering technique. *Nanotechnology*, 19: 415303.

Leung KY (2008). Anti-bacteria plasma-treated metallic surface for orthopaedics use. *Master Thesis, University of the Hong Kong, China*: 155.

Linkow LI (2010). The legends of implant dentistry with the history of transplantology and implantology. New Delhi, India, Jaypee Brothers Medical Publishers (P) Ltd: 320.

Liu X, Chu PK, Ding C (2004). Surface modification of titanium, titanium alloys, and related materials for biomedical applications. *Materials Science and Engineering R: Reports*, 47: 49–121.

Macha D, Koppolu P, Swapna LA, Bathini C (2014). Osseointegration in implants: a review. *Journal of Research Advancement in Dentistry*, 3: 67–72.

Majumdar P, Singh SB, Chakraborty M (2008). Elastic modulus of biomedical titanium alloys by nano-indentation and ultrasonic techniques—A comparative study. *Materials Science and Engineering: A*, 489: 419–425.

Malhotra S, Hegde MN, Shetty C (2014). Bioceramic technology in endodontics. *British Journal of Medicine and Medical Research*, 4: 2446–2454.

Mandracci P, Mussano F, Rivolo P, Carossa S (2016). Surface treatments and functional coatings for biocompatibility improvement and bacterial adhesion reduction in dental implantology. *Coatings*, 6: 1–22.

Marcotte H, Lavoie MC (1998). Oral microbial ecology and the role of salivary immunoglobulin A. *Microbiology and Molecular Biology Reviews*, 62: 71–109.

Martin TJ, Sims NA (2005). Osteoclast-derived activity in the coupling of bone formation to resorption. *Trends in Molecular Medicine*, 11: 76–81.

Matsuo K, Irie N (2008). Osteoclast–osteoblast communication. *Archives of Biochemistry and Biophysics*, 473: 201–209.

Mayer FL, Wilson D, Hube B (2013). *Candida albicans* pathogenicity mechanisms. *Virulence*, 4: 119–128.

Meng, G. (2014). Effect of biofilm on the mechanical properties and repair strength of denture acrylic. *Master Thesis, University of the Illinois, Chicago*: 59.

Misch CE (2014). *Rationale for dental implants*. Dental implant Prosthetics. 2nd edition, St. Louis, Missouri, Elsevier Mosby: 1–25.

Moharamzadeh K, Brook IM, Van Noort R (2009). Biocompatibility of Resin-based dental materials. *Materials*, 2: 514–548.

Monsees TK (2016). Biocompatibility and anti-microbiological activity characterization of novel coatings for dental implants: A primer for non-biologists. *Frontiers in Materials*, 3: 1–6.

Monsees TK, Barth K, Tippelt S, Heidel K, Gorbunov A, Pompe W, Funk RHW (2005). Effects of different titanium alloys and nanosize surface patterning on adhesion, differentiation, and orientation of osteoblast-like cells. *Cells Tissues Organs*, 180: 81–95.

Muddugangadhar BC, Amarnath GS, Tripathi S, Dikshit S (2011). Biomaterials for dental implants: an overview. *International Journal of Oral Implantology and Clinical Research*, 2: 13–24.

Nandal S, Ghalaut P, Shekhawat H, Nagar P (2014). Osseointegration in dental implants: a literature review. *Indian Journal of Applied Research*, 4: 411–413.

Natto ZS, Aladmawy M, Alasqah M, Papas A (2014). Factors contributing to tooth loss among the elderly: a cross sectional study. *Singapore Dental Journal*, 35: 17–22.

Nelson SJ, Ash MM (2010) Wheeler's dental anatomy, physiology and occlusion. 9th edition, St. Louis, Missouri, Elsevier: 1–307.

Nippon dental university department of oral implantology (1994). Osseointegrated implant a manual. 1th edition, St. Louis, I Shiyaku Euro America: 159.

Oshida Y, Tuna EB, Aktören O, Gençay K (2010). Dental implant systems. *International Journal of Molecular Sciences*, 11: 1580–1678.

Osman RB, Swain MV (2015). A critical review of dental implant materials with an emphasis on titanium versus zirconia. *Materials*, 8: 932–958.

Özcan M, Hämmerle C (2012). Titanium as a reconstruction and implant material in dentistry: Advantages and pitfalls. *Materials*, 5: 1528–1545.

Özkurt Z, Kazazoğlu E (2011). Zirconia dental implants: a literature review. *Journal of Oral Implantology*, 37: 367–376.

Patel NR, Gohil PP (2012). A Review on biomaterials: Scope, applications and human anatomy significance. *International Journal of Emerging Technology and Advanced Engineering*, 2: 91–101.

Pektaş Ö (2012). Design and mechanical analysis of a new dental implant that would mimic natural tooth with a periodontal ligament. *Master Thesis, University of the Middle East Technical, Turkey*: 177.

Pihlstrom BL, Michalowicz BS, Johnson NW (2005). Periodontal diseases. *The Lancet*, 366: 1809–1820.

Porter JA, Von Fraunhofer JA (2005). Success or failure of dental implants? A literature review with treatment considerations. *Journal of the Academy of General Dentistry*, 53: 423–432.

Pye AD, Lockhart DEA, Dawson MP, Murray CA, Smith AJ (2009). A review of dental implants and infection. *Journal of Hospital Infection*, 72: 104–110.

Ratner BD (2001). Replacing and renewing: Synthetic materials, biomimetics, and tissue engineering in implant dentistry. *Journal of Dental Education*, 65: 1340–1347.

Revilla-López G, Bertran O, Casanovas J, Turon P, Puiggali J, Alemán C (2016). Effects of hydroxyapatite (0001) Ca²⁺/Mg²⁺ substitution on adsorbed d-ribose ring puckering. *RSC Advances*, 6: 69634–69640.

Saini M, Singh Y, Arora P, Arora V, Jain K (2015). Implant biomaterials: a comprehensive review. *World Journal of Clinical Cases*, 3: 52–57.

Sakka S, Baroudi K, Nassani MZ (2012). Factors associated with early and late failure of dental implants. *Journal of Investigative and Clinical Dentistry*, 3: 258–261.

Shibata Y, Tanimoto Y (2015). A review of improved fixation methods for dental implants. Part I: Surface optimization for rapid osseointegration. *Journal of Prosthodontic Research*, 59: 20–33.

Soboyejo WO, Nemetski B, Allameh S, Marcantonio N, Mercer C, Ricci J (2002). Interactions between MC3T3-E1 cells and textured Ti6Al4V surfaces. *Journal of Biomedical Materials Research*, 62: 56–72.

Stanić V, Janačković D, Dimitrijević S, Tanasković SB, Mitrić M, Pavlović MS, Raičević S (2011). Synthesis of antimicrobial monophase silver-doped hydroxyapatite nanopowders for bone tissue engineering. *Applied Surface Science*, 257: 4510–4518.

Strnad G, Chirila N (2015). Corrosion rate of sand blasted and acid etched Ti6Al4V for dental implants. *Procedia Technology*, 19: 909–915.

Sundrarajan M, Suresh J, Gandhi RR (2012). A comparative study on antibacterial properties of MgO nanoparticles prepared under different calcination temperature. *Digest Journal of Nanomaterials and Biostructures*, 7: 983–989.

Thamaraiselvi TV, Rajeswari S (2004). Biological evaluation of bioceramic materials-a review. *Trends Biomater Artif Organs*, 18: 9–17.

Tin-Oo MM, Gopalakrishnan V, Samsuddin AR, Al Salihi KA, Shamsuria O (2007). Antibacterial property of locally produced hydroxyapatite. *Archives of Orofacial Sciences*, 2: 41–44.

Vladescu A, Birlik I, Braic V, Toparli M, Celik E, Azem FA (2014). Enhancement of the mechanical properties of hydroxyapatite by SiC addition. *Journal of the mechanical behavior of biomedical materials*, 40: 362–368.

Vladescu A, Braic M, Azem FA, Titorencu I, Braic V, Pruna V, Birlik I (2015). Effect of the deposition temperature on corrosion resistance and biocompatibility of the hydroxyapatite coatings. *Applied Surface Science*, 354: 373–379.

Wang G, Zreiqat, H (2010). Functional coatings or films for hard-tissue applications. *Materials*, 7: 3994–4050.

Wataha JC (2001). Principles of biocompatibility for dental practitioners. *The Journal of Prosthetic Dentistry*, 86: 203–209.

Weatherholt AM, Fuchs RK, Warden SJ (2012). Specialized connective tissue: bone, the structural framework of the upper extremity. *Journal of Hand Therapy*, 25: 123–132.

West NX, Joiner A (2014). Enamel mineral loss. *Journal of Dentistry*, 42: S2–S11.

Will J, Hoppe A, Müller FA, Raya CT, Fernández JM, Greil P (2010). Bioactivation of biomorphous silicon carbide bone implants. *Acta biomaterialia*, 6: 4488–4494.

Wood MR, Vermilyea SG (2004). A review of selected dental literature on evidence-based treatment planning for dental implants: report of the committee on research in fixed prosthodontics of the academy of fixed prosthodontics. *The Journal of Prosthetic Dentistry*, 92: 447–462.

Yoshinari M, Matsuzaka K, Inoue T, Oda Y, Shimono M (2002). Bio-functionalization of titanium surface for dental implants. *Materials Transactions*, 43: 2494–2501.

Zha X (2011). Image processing of optical coherence tomography for image guided dental drilling. *Master Thesis, University of the Delft Technology, Delft*: 91.

Zhang D, Zheng L (2015). *Dental implants*. Emerging trends in oral health sciences and dentistry. InTech: 265–286.

Zitter H, Plenk H (1987). The electrochemical behavior of metallic implant materials as an indicator of their biocompatibility. *Journal of Biomedical Materials Research*, 21: 881–896.

